Imperial College London
Department of Chemical Engineering

Applications of ATR-FTIR Spectroscopic Imaging to Proteins

Stefanie E. Glassford
October 2013

Supervised by Sergei G. Kazarian and Bernadette Byrne

Submitted in part fulfilment of the requirements for the degree of Doctor of Philosophy in Chemical Engineering of Imperial College London and the Diploma of Imperial College London.

I would like to dedicate this thesis to my parents, David and Laura Glassford.

Declaration

This thesis is a description of the work carried out in the Department of Chemical Engineering at Imperial College London between October 2010 and October 2013 under the supervision of Professor Sergei Kazarian and Dr Bernadette Byrne. Except where acknowledged, the material is the original work of the author and no part of it has been submitted for a degree at any other university.

Abstract

Protein aggregation and crystallisation play an important role in the development of biopharmaceuticals and for structural proteomics but both processes are still poorly understood. There is a demand for new methods to screen the extensive range of conditions that promote crystallisation and aggregation as well as provide insight into the behaviour of the proteins.

Attenuated Total Reflection (ATR) – Fourier Transform Infrared (FTIR) spectroscopic imaging is a powerful analytical tool which can be applied to study proteins. This technique combines ATR-FTIR spectroscopy with an infrared array detector allowing for both spatial and chemical information to be obtained from the sample. There are a range of imaging fields of view and spatial resolution possible with ATR-FTIR spectroscopic imaging and this presents multiple opportunities for the study of proteins.

The purpose of this research was to further develop the application of ATR-FTIR spectroscopic imaging within the field of protein studies. ATR-FTIR imaging has been applied to study the effects of different conditions for microbatch protein crystallisation in a high throughput manner, where many samples can be analysed at the same time on the surface of a Macro ATR crystal by building a wax grid with multiple wells for different samples. Additionally, Micro ATR-FTIR imaging was combined with hanging drop protein crystallisation for high spatial resolution imaging of the growth of protein crystals. The surface properties of Silicon ATR crystals were modified to create a gradient of hydrophobicity allowing the effect of different surface properties on protein adsorption and crystallisation to be studied *in situ*. The development of these approaches will advance the use of spectroscopic imaging within the field of biopharmaceuticals, where it is has the potential to help the optimisation of both biopharmaceutical drug discovery processes and structural proteomics studies.

Acknowledgements

The work presented in this thesis would not have been possible without the aid and support of my supervisors, Professor Sergei Kazarian and Dr Bernadette Byrne. To Professor Kazarian, I owe special thanks for his advice and encouragement throughout, as well as for allowing my participation in many exciting opportunities during my time in his group. I also thank my collaborating academic Professor Paul Luckham.

My experience at Imperial College would not have been half as fruitful if it wasn't for the useful discussions and friendship with the members, both past and present, of the Vibrational Spectroscopy and Chemical Imaging group; Alina, Satoko, Ian, Patrick, James, Jen, Kirsty, Andrew and Tiphaine. Notably, thanks to Dr Andrew Chan for his help during my first two years. Also my coffee group; Joanna, Jeeves, Ali, Carlos, Michael, Andrew, Sascha, Puja, thank you for keeping me revived with caffeine, biscuits and for enduring my baking creations without complaint and perfectly on time at 10.30 am. In addition, I thank Flaminia Cavallo for her friendship; I'll miss our lunches in the V&A courtyard.

A special mention goes to the wardening team at Wilkinson Hall; Arash, Will, Oli, Diogo and Kat who became my London family. I loved every minute, even the gory parts and I'm sure that is entirely because of them. Also despite living in distant places, Lisa and Colette, your friendship has been invaluable to me and I hope we continue to email and plan trips for many years to come.

I would like to thank Ed Johnson for being there to listen, look after me and above all, for bringing so much happiness into my life and always making me smile. Finally and most importantly, thank you to my family; my mother Laura, father David and brothers Jonathan and David as well as my extended family in Scotland. Especially my parents, everything that I am is because of you, and I will never be able to thank you enough.

Table of Content

List of Figures

List of Tables

Abbreviations

Abbreviation	Description
AD	Anomalous dispersion
AFM	Atomic force microscopy
a.u.	Arbitrary units
ATR	Attenuated total reflection
BSA	Bovine serum albumin
CD	Circular dichroism
FID	Free interface diffusion
FPA	Focal plane array
FTIR	Fourier Transform infrared
FWHH	Full width half height
Ge	Germanium
HTP	High throughput
IgG	Immunoglobulin
IRE	Internal reflection element
IR	Infrared
MCT	Mercury-Cadmium-Telluride
MIP	Molecularly imprinted polymer
NA	Numerical aperture
NMR	Nuclear magnetic resonance
NTA	Nitrilotriacetic acid
PDMS	Polydimethylsiloxane
PEG	Polyethylene Glycol
PMIRRAS	Polarization modulation infrared absorption spectroscopy
OTS	Octyltrichlorosilane
SAM	Self assembled monolayer
SEC	Size-exclusion chromatography
SEIRAS	Surface enhanced infrared absorption spectroscopy
SEM	Scanning electron microscopy
Si	Silicon
SNR	Signal-to-noise ratio
VL	Visible light
ZnSe	Zinc selenide

Nomenclature

Symbol	Meaning
λ	Wavelength (cm)
δ	Optical path difference (cm)
ε	Molar absorptivity ($l.mol^{-1}.m^{-1}$)
θ_i	Angle of incidence (°)
Θ_{crit}	Critical angle (°)
A	Absorbance
c	Molar concentration ($mol.l^{-1}$)
d_p	Depth of penetration (m)
d_e	Effective depth of penetration (m)
I_0	Incident intensity of light
I	Transmitted intensity of light
l	Pathlength (m)
n	Refractive index
n_1	Refractive index of IRE
n_2	Refractive index of sample
N	Number of scans
NA	Numerical aperture
2r	Distance between two objects for them to be just resolved (m)
T	Transmittance
$\tilde{\nu}$	Wavenumber (cm^{-1})

Publications and Conferences

Publications

S. E. Glassford, B. Byrne, S. G. Kazarian, Recent applications of ATR FTIR spectroscopy and imaging to proteins, BBA-Proteins and Proteomics 1834 (2013) 2849-2858.

S.E. Glassford, L. Govada, N.E. Chayen, B. Byrne, S.G. Kazarian, Micro ATR FTIR imaging of hanging drop protein crystallisation, Vibrational Spectroscopy 63 (2012) 492-498.

S. Glassford, K.L.A. Chan, B. Byrne, S.G. Kazarian, Chemical imaging of protein adsorption and crystallization on a wettability gradient surface, Langmuir 28 (2012) 3174-3179.

Conferences

IRDG (200th) Christmas Meeting, UCL, London, December 2012, Poster title: Chemical imaging of proteins on a wettability gradient surface.

1st Brazilian Biophotonics Winter School, Sao Jose dos Campos, July 2012, Poster Title: Chemical imaging of proteins on a wettability gradient surface.

FT-IR Spectroscopic Imaging: New Trends and Emerging Applications, Society of Applied Spectroscopy, Imperial College London, June 2012.

Awards

Department of Chemical Engineering PhD Research Symposium 2nd Place Presentation Prize (Industrial and academic panel and Student vote), Shedding new light on proteins: ATR-FTIR spectroscopic imaging of protein crystallisation, July 2013.

Department of Chemical Engineering PhD Symposium, Student vote poster prize, Chemical Imaging of Proteins on a wettability gradient surface, March 2012.

Exhibitions

Imperial Festival, Chemical Photography, May 2013.
Imperial Festival, Chemical Photography, May 2012.
All Russia Science Festival, Moscow, Chemical Photography, October 2011.
After Hours: Science Uncovered at Natural History Museum, London, September 2011.
Royal Society Summer Science Exhibition, Chemical Photography, June 2010.

Chapter 1 - Introduction

I. Background

Our understanding of protein structure and function has advanced dramatically over the last 20 years or so, at least in part, as a result of the time and effort spent on structural proteomic projects (Chandonia and Brenner, 2006). Obtaining high-resolution 3D protein structures is essential to gain insights into the mechanism of action of these important molecules, as well as to provide a potential framework for rational and targeted drug design. X-ray diffraction is the most commonly used method for determination of high resolution structures but obtaining well-diffracting protein crystals can be both difficult and time consuming (Bolanos Garcia et al., 2009). As more and more structures are solved the remaining uncharacterised proteins tend to be those that are the most challenging to work with including multi-subunit complexes, unstructured proteins (Uversky, 2002), and integral membrane proteins (Bill et al., 2011). Methods to provide efficient high-throughput screening of conditions likely to yield diffracting protein crystals would greatly facilitate studies on the more challenging protein molecules. In addition although X-ray crystallographic studies can reveal much, such studies produce static snapshots of protein molecules and lack dynamic information key to understand the conformational changes associated with function.

Many of the most challenging types of proteins are prone to aggregation and unfolding as a result of the conditions used for isolation and final preparation (Gutmann et al., 2007). Similar problems are known to occur in the case of biopharmaceuticals such as therapeutic antibodies and antibody fragments (Shukla, 2005, Dengl et al., 2013). Whilst it is likely that increases in protein concentration along with exposure to extremes of pH, temperature and ion concentration can result in protein aggregation during processing (Arosio et al., 2011), the effects of the surfaces that proteins encounter during isolation are far less well understood (Gerontas et al., 2013, Matheus et al., 2006). A much better understanding of the effects of surfaces on protein behaviour has major implications for the development of biomedical materials, clinical diagnostics and cellular adhesion (Ma et al., 2007, Nakanishi et al., 2001, Chittur, 1998). One prominent field is the study of the effect of surface properties on proteins which has major implications in the development of medical devices and implants (Ma et al., 2007, Mei et al., 2005). The ability to understand the role that a particular surface has on a protein conformation, in situ would be extremely valuable.

Infrared spectroscopy, in particular attenuated total reflection (ATR) Fourier transform infrared (FTIR) spectroscopy and when coupled with a focal plane array detector for ATR-FTIR imaging, has significant potential as an analytical technique to facilitate both protein crystallisation studies and

investigations on the effect of surface properties on protein behaviour as well as other key questions related to protein structure and function.

II. Objectives

The full potential of ATR-FTIR spectroscopic imaging as a means of studying proteins is yet to be realised; therefore, the main objective of this thesis was to develop the applications of ATR-FTIR spectroscopic imaging within this field.

More specifically, the main objectives can be summarised as follows:

- The challenge of using ATR-FTIR spectroscopy with a diamond ATR crystal is possible band shifts associated with the effects of anomalous dispersion. This could have repercussions for the analysis of the amide bands in protein measurements. It is thought that by increasing the angle of incidence of IR light to a sample, the effects of anomalous dispersion can be reduced. One aim of this thesis was to carry out a study to determine if these band shifts could be indeed overcome through the use of ATR-FTIR spectroscopic imaging with variable angles of incidence.

- ATR-FTIR spectroscopic imaging, with its ability to provide both spatial and chemical information from samples, can be applied to protein crystallisation studies. One of the main objectives of this thesis was to further develop its application within this area by expanding the use of Macro ATR-FTIR imaging to study a greater number of protein samples simultaneously, providing a method of high throughput screening for successful crystallisation conditions.

- Also within the potential applications of spectroscopic imaging to protein crystallisation studies, one aim was to combine the use of Micro ATR-FTIR spectroscopic imaging with hanging drop protein crystallisation. This would provide the opportunity to measure the growth of protein crystals with a higher spatial resolution and could be applied to proteins that are challenging to crystallise to the standard required for X-ray diffraction experiments.

- ATR-FTIR spectroscopic imaging is well suited to measure relatively thin surface layers of a sample and is also inherently suited to high throughput applications. Another objective of this thesis was to investigate the combination of gradient surface chemistry formed on the surface of an ATR element and ATR-FTIR spectroscopic imaging to study the effect of different surface properties on protein adsorption and crystallisation.

III. **Outline of thesis**

The work in this thesis presents the applications of ATR-FTIR spectroscopic imaging to different areas within the field of protein studies. Chapter 2 provides a detailed literature review of the main challenges within this field and introduces the fundamentals of both ATR-FTIR spectroscopy and ATR-FTIR spectroscopic imaging. It also discusses the suitability of the technique to help overcome some of the challenges faced in protein studies. Chapter 3 provides a brief introduction and explanation of the main experimental equipment used to carry out this work.

The main experimental results are presented in Chapters 4 – 7. The application of ATR-FTIR spectroscopic imaging with variable angles of incidence using a diamond Golden Gate accessory to overcome the effects of anomalous dispersion is discussed first in Chapter 4 as this had some implications on the choice of internal reflection element used for the rest of the work in the thesis. Chapter 5 is divided into two parts showing the application of ATR-FTIR spectroscopic imaging to protein crystallisation. The first part demonstrates the use of Macro ATR-FTIR spectroscopic imaging for high throughput studies of microbatch protein crystallisation and the second part shows the development of Micro ATR-FTIR imaging combined with hanging drop protein crystallisation for *in situ* studies of protein crystallisation growth with high spatial resolution.

The combination of gradient surface chemistry with ATR-FTIR spectroscopic imaging was achieved for high throughput studies on the effect of surface hydrophobicity on protein adsorption and crystallisation. This work is presented in Chapter 6 of the thesis.

The conclusions from each of the different studies in this thesis are discussed separately at the end of each chapter. However, a summary of the main conclusions obtained from the work of this thesis are presented in the final chapter along with a discussion on recommendations for future work within this field.

Chapter 2 - Literature Review

I. Overview

The use of recombinant expressed proteins as drugs is a rapidly emerging field known as Biopharmaceuticals. This requires knowledge of the function of the protein which can be determined from its structure. The majority of target proteins are membrane proteins. These are the proteins found within the membranes of all cells in the body and are responsible for a variety of functions such as cell signalling for immune responses.

There are currently several methods employed to study the structure of proteins, each with their advantages and disadvantages. The one that is most commonly employed is X-ray crystallography as this can provide very high resolution structural information. However, this technique requires proteins to be crystallised which has proved to be a major bottleneck in the structural determination of proteins, particularly membrane proteins. Other methods of studying protein structure include Nuclear Magnetic resonance (NMR), Circular dichroism (CD) and Fourier transform infrared spectroscopy (FTIR). These methods are useful in that they allow for the study of proteins in a variety of environments and are not limited to the study of crystalline proteins. These are most commonly applied as complementary techniques to X-ray crystallography and offer valuable insight into protein structure. However, efforts to improve the rate and ease of protein crystallisation experiments for X-ray crystallography are still considered to be important for structural biologists.

One of the major issues with membrane proteins is their tendency to non-specifically aggregate in solution which prevents the formation of protein crystals for X-ray analysis. This is overcome through the use of detergents but with over fifty different detergents available, obtaining the optimum conditions for crystallisation can be time consuming and expensive (Vergis et al., 2010). It is also difficult to obtain large quantities of membrane protein through standard protein expression methods meaning the ideal screening process for conditions should minimise the amount of protein used. In view of the development of biopharmaceuticals, a major problem in the development of this field is the tendency for the proteins to non-specifically aggregate at high concentrations (Cromwell et al., 2006). This can affect the drug potency and the immune response of the body. Given this, there is a demand to develop new ways in which to identify protein aggregation as early as possible during the drug discovery process as well as methods to screen extensive ranges of conditions that may reduce or prevent aggregation within samples.

In addition to the challenges detailed above, the interaction of proteins with surfaces is also an important area of research. During bioprocessing, understanding the role of surface interactions during isolation processes, for example, with the protein is also necessary to reduce the risk of the surface modifying the native protein conformation (Gerontas et al., 2013). This is equally true in other areas of research, such as for the development of biomaterials. Gradient surfaces have been shown to be an important tool in studying the effect of different surface properties in a high throughput manner although the current methods of characterising the protein adsorption onto the surface typically rely on the use of tags or dyes.

Attenuated total reflection (ATR) - Fourier Transform infrared (FTIR) spectroscopic imaging couples an infrared spectrometer and an FPA detector to provide both spatial and chemical information about the sample on the ATR crystal surface. This had been readily applied to the study of pharmaceuticals, biomedical samples and for art conservation, to give a few examples (Kazarian and Chan, 2013, Kazarian and Chan, 2010). It can be applied in a high-throughput manner, where several samples are measured simultaneously on the imaging surface of the ATR crystal. In this project, the high-throughput imaging capability of ATR-FTIR spectroscopic imaging has been further developed for the study of proteins.

The purpose of this literature review is to introduce the challenges faced within protein research, particularly within protein crystallisation studies, and consider how ATR-FTIR spectroscopic imaging may be used to help overcome some of them.

II. Proteins

i. Protein Structure

In simple terms, proteins are organic compounds composed of chains of amino acids folded into complex structures. They play an important role in every aspect of life from the processes within cells such as cell signalling and the immune response to the formation of muscle fibres. The field of proteomics is devoted to characterising the structure of every protein within the human genome in order to determine their functions, which has been shown to be dependent on the three dimensional structure of the protein. The rapidly growing field of bio-therapeutics, where recombinantly expressed proteins are used as drugs, also relies on accurate structural information in order to develop new targeted therapeutics.

The structure of a protein molecule can be divided into four main components, illustrated in Figure 1. The primary structure is the sequence of amino acids within the molecule. Twenty different amino acids can join in a particular order through peptide bonds to form a linear chain. This chain is then folded into local sub-structures formed by hydrogen bonding between peptide groups. These local 3D structures define the secondary structure of the protein, the most common being the α-helix and the β-sheet. Since the secondary structure is determined by the hydrogen bonding pattern between Amide and carbonyl groups of the polypeptide chain, it is possible to have several different types of secondary structural units within one protein molecule. The tertiary structure of the protein is formed from the packing of secondary structure subunits of one protein molecule into one globular unit and the quaternary structure is the interaction of several protein molecules into a single structure.

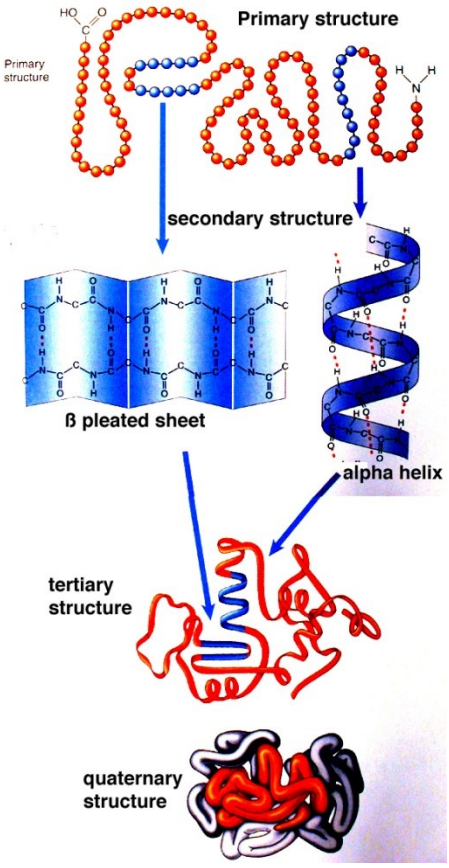

Figure 1 - Different types of protein structure.
(http://academic.brooklyn.cuny.edu/biology/bio4fv/page/3d_prot.htm)

Protein molecules have highly complex folding patterns which are dependent on the amino acid sequence and on several environmental influences. The folding of proteins is one of the most fundamental examples of self assembly in nature and the three dimensional structure along with amino acid sequence ultimately determines its molecular function (Dobson, 2003, Branden and Tooze, 1991).

ii. Protein structural studies

High resolution structural information of proteins provides unparalleled insight into protein function. This in turn can be used to understand the molecular basis of diseases and aid in the development of novel drugs. Vast amounts of resources are spent both obtaining protein structures and developing methods to rationalise and improve the structure determination process.

All structural analysis techniques require significant amounts of highly pure, stable and functional proteins. This can be challenging for many proteins but is particularly tricky for membrane proteins. Membrane proteins present within the lipid bilayer are classified as either peripheral or integral depending on how closely they are bound to the membrane (Hames and Hooper, 2005). Integral membrane proteins are amphiphilic and interact strongly with the hydrophobic core of the lipid bilayer. These proteins are involved in many biological processes such as respiration, uptake of nutrients and cell signalling (Alguel et al., 2010). Given the crucial role they play in cell function, integral membrane proteins are considered important drug targets. For example G-protein coupled receptors, which mediate cellular responses to a wide variety of biologically active molecules including hormones, neurotransmitters and a wide range of drugs (Bertheleme et al., 2013), represent a high percentage of all drug targets (Rask-Andersen et al., 2011). Aside from being drug targets, membrane proteins make up approximately 15 – 30 % of the proteome (the total complement of proteins present within a cell or cell type at a time) of organisms and hence in structural proteomics, they represent a large area of study within the field (Vergis et al., 2010).

The Protein Data Bank (PDB) is a database containing the results from structural proteomic projects worldwide. Despite constituting nearly half of a cell's proteome, the number of membrane protein structures present in the PDB is only about 1 % of the total number. As of September 2013,there were 93970 protein structures in the protein databank (http://www.pdb.org/pdb/home/home.do) of which 773 are membrane proteins (http://blanco.biomol.uci.edu/mpstruc/). Figure 2 is taken from the PDB and shows a snapshot of progress in structure determination as of April 2011; although this information is now out of date due to progress in the last two years, it does highlight the poor attrition rate within the structural proteomics pipeline for all classes of proteins.

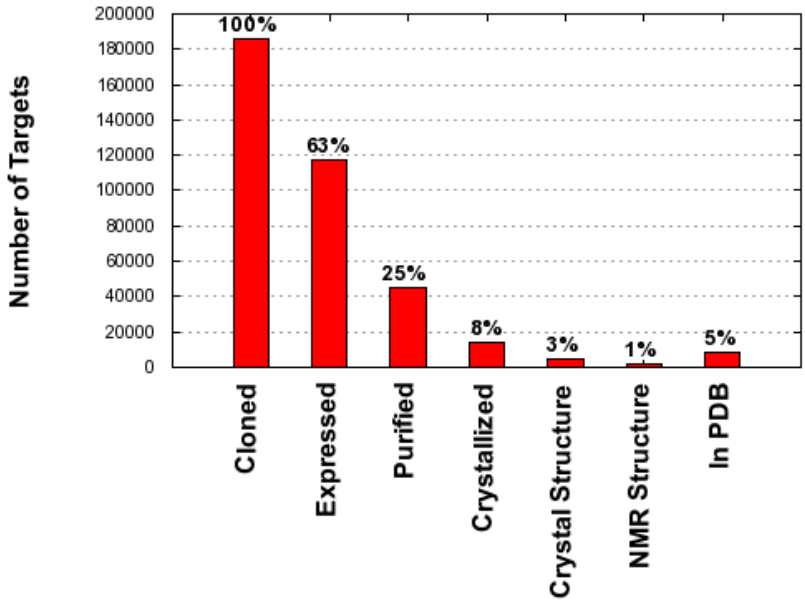

Figure 2 - Summary of all Major Structural Genomics projects worldwide on April 21, 2011 (http://targetdb.pdb.org). As of 21st April 2011, just over 186000 target proteins were successfully cloned, the initial stage in structural analysis. From these proteins only 9300 structures were deposited in the protein data bank.

There are technical challenges present at each stage of the structural characterisation process for proteins; from expression and purification through to structural determination (Bill et al., 2011, Carpenter et al., 2008). For the majority of target molecules, the first stage is recombinant expression of the protein which involves growing the protein often in a non-native source, for example bacteria or yeast cells. Although this has proved very successful for the production of large quantities of globular proteins, the same cannot be said for membrane proteins (Alguel et al., 2010). One hypothesis on this issue is that membrane proteins are toxic to host cells, particularly when bacteria are used (Wagner et al., 2008). This toxicity means that yields are often low. For every new target protein several different expression systems have to be trialled to optimise the amount of protein obtained or several homologues from different organisms are screened in order to identify the most tractable protein. Following expression, the target protein has to be purified with the aim of achieving a pure and stable protein, in a quantity suitable for structural studies.

X-ray crystallography is a key tool capable of providing high resolution structural images of proteins molecules and as such is the most powerful analytical technique for structural biologists (McPherson, 2004). X-ray radiation is directed at a protein crystal and is diffracted due to the arrangement of atoms within the crystal. The repetitive nature of structural units within a protein crystal produces a diffraction pattern, formed from the interference of the diffracted X-ray beams.

This diffraction pattern allows a three dimensional image of the electron density within the crystal to be generated and the position of atoms and chemical bonds within the structure to be determined. Hence, the three dimensional structure of a protein can be deduced from its X-ray diffraction pattern (Drenth, 1999). Obtaining well diffracting crystals is time consuming and expensive in terms of protein and laboratory consumables and is seen to be a major bottleneck in protein structural studies, especially for membrane proteins.

In order to crystallise a membrane protein, it must first be purified from the cells used to express the protein and solubilised. Detergents are used to extract and solubilise membrane proteins from the cell but also act to stabilise the protein in its native form in the absence of a membrane (Prive, 2007). The detergent molecules share the dual hydrophobic/hydrophilic characteristics of both the membrane lipids and membrane proteins. Detergents disrupt the interactions between the membrane proteins and the lipid bilayer and surround the hydrophobic regions of the membrane proteins effectively shielding the protein from the aqueous environment (Prive, 2007). The membrane proteins are then isolated using column chromatography techniques and if this is successful the protein is concentrated prior to use in crystallisation trials. However even when detergents are used the highly hydrophobic nature of the membrane proteins means they tend to non-specifically aggregate in solution (Alguel et al., 2010). Formation of these insoluble aggregates causes irreversible loss of protein during the solubilisation, purification and concentration processes. In addition, the presence of large detergent micelles around the hydrophobic regions of the membrane proteins significantly reduces the likelihood of forming crystals (Gutmann et al., 2007). Even when crystals can be obtained they are often small and diffract poorly.

Another technique which is being applied increasingly to protein structural studies is solution state nuclear magnetic resonance (NMR). This has the advantage that the protein does not need to be in crystalline form to be analysed. However, it is generally limited to the study of small proteins, (<40 kDa) and often requires high temperature data collection (up to 50°C). Membrane proteins require the presence of detergent to stay in solution and the resulting protein-detergent complexes are generally too large for study using solution state NMR for all but the smallest (Tamm et al., 2003) and most stable (Gautier et al., 2010) membrane proteins. Recent developments have also seen the use of the femtosecond X-ray free-electron laser technique to obtain protein structural information (Chapman et al., 2011). However, this still requires the growth of large numbers of perfectly formed protein nanocrystals, albeit the requirement for perfectly formed crystals of a certain size is reduced as it utilises nano-crystals. Furthermore, other spectroscopic methods such as Circular Dichroism (CD) (Whitmore and Wallace, 2008) and FTIR can offer valuable insight into protein structure and

behaviour; FTIR spectroscopy has many advantages for the study of proteins and will be discussed in more detail in Chapter 2.III.

However, as of September 2013 X-ray crystallography is still the main method of determining high resolution protein structures and accounts for 88.3 % of the 93970 structures deposited in the protein data bank (http://www.pdb.org/pdb/home/home.do). As a result, efforts to facilitate protein crystallisation for X-ray crystallography experiments are still considered to be very important. This represents a key aim of this research; to develop ATR-FTIR spectroscopic imaging to study protein crystallisation. It should also be noted that although the proteins used in this work are well characterised soluble proteins due to ease of availability, there is great potential for ATR-FTIR spectroscopic imaging to help address some of the challenges faced in the study of other more challenging proteins including membrane proteins in the future.

iii. Protein crystallisation

A major hurdle in the structure determination of proteins by X-ray crystallography is the production of well diffracting crystals. Protein crystallisation is often referred to as a "black art" since it is very difficult to predict the optimum crystallisation conditions for a particular protein (Chayen, 2004, Bolanos Garcia et al., 2009). Factors such as pH, temperature and precipitant, as well as the concentration of protein and of precipitant, all have to be optimised for every new protein being characterised in order to obtain diffraction quality crystals. The choice of crystallisation method is also important.

There are currently several crystallisation methods used in structural biology laboratories. The traditional approaches employing vapour diffusion methods such as hanging or sitting drop are the most widely used, however other methods including microbatch have been successfully used to crystallise a number of proteins. Other novel methods, including the use of porous surfaces and seeding technologies (Chayen et al., 2001, Bolanos Garcia et al., 2009)have been developed along with significant progress in nanocrystallography (Bodenstaff et al., 2002) as well as specialized techniques such as lipidic cubic phase (Cherezov, 2011) and bicelle crystallisation (Faham and Bowie, 2002) suitable for membrane proteins. Despite these exciting developments, hanging drop or sitting drop are still the most commonly employed methods.

Crystallisation is a phase transition phenomenon and each crystallisation method can be represented on a phase diagram (Figure 3). Protein crystals grow when the aqueous solution is brought into supersaturation which can be achieved by varying pH, temperature and precipitant, as well as the concentration of protein and of precipitant.

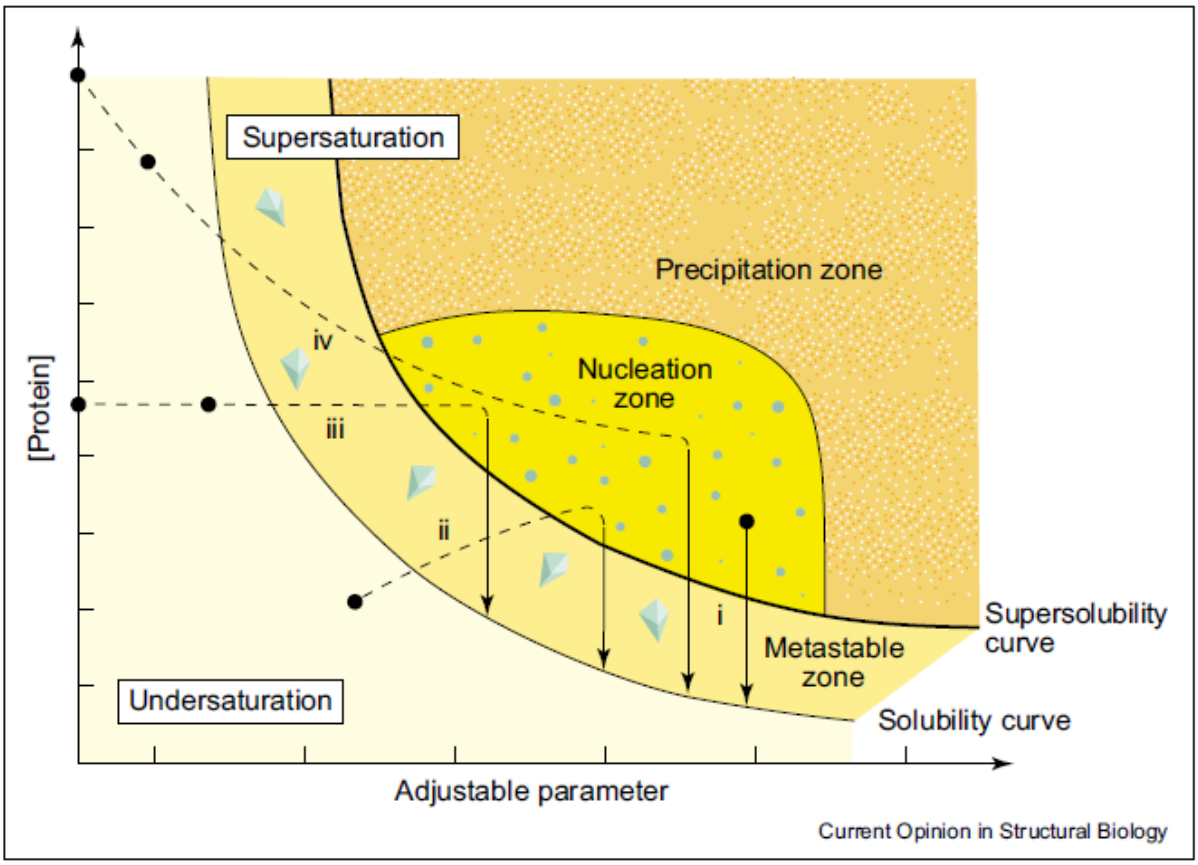

Figure 3 - Protein crystallisation phase diagram. The four major crystallisation methods are represented: (i) microbatch, (ii) vapor diffusion, (iii) dialysis and (iv) FID (Chayen, 2004).

There are four zones within the phase diagram, each representing different degrees of supersaturation of the protein solution. In the zone of supersaturation, the protein will precipitate out of solution without the formation of crystals. The zone of moderate supersaturation allows for spontaneous nucleation of protein crystals, called the nucleation zone. Below this is the metastable zone which will not allow for further nucleation but facilitates the growth of existing nuclei into well ordered crystals. Finally, the undersaturation zone is such that the protein will remain in solution and never form crystals.

Even within the nucleation zone, an energy barrier has to be overcome to create an interface between crystal nucleus and solution. When the probability of this occurring is identical at any position in the solution, this is termed homogenous nucleation. When some form of interface already exists within the system, for example a surface of some kind, the nucleation is termed heterogeneous. The likelihood of a nucleus forming on or around that surface is much higher than elsewhere in the solution as the energy required to form the initial interface is much lower (Garcia-

Ruiz, 2003). Homogenous nucleation is unlikely to occur under laboratory conditions as it will only occur within exceptionally pure solutions with the correct supersaturation (Garcia-Ruiz, 2003).

Each crystallisation method outlined on the phase diagram (Figure 3) aims to achieve the growth of crystals but through slightly different paths. The vapour diffusion approach is represented by path ii on the phase diagram and it involves equilibrating the protein solution against a reservoir solution containing crystallising reagents. A concentration gradient exists between the two causing the loss of water from the protein drop to the reservoir. This increases the concentration of protein in the drop, leading it into the nucleation zone and allowing the formation of protein crystals. The two main methods of vapour diffusion are sitting drop and hanging drop, shown in Figure 4.

Microbatch crystallisation is less popular compared to vapour diffusion methods, but is no less effective (Chayen, 2004). In this case, the formation of protein crystals takes place under oil. Unlike vapour diffusion methods, where the system is dynamic and conditions change throughout, in microbatch the protein and reagent concentration at start of experiment are such that upon mixing supersaturation occurs allowing the formation of crystals (Path i on phase diagram). Oil is used to prevent any evaporation from the system as illustrated in Figure 4.

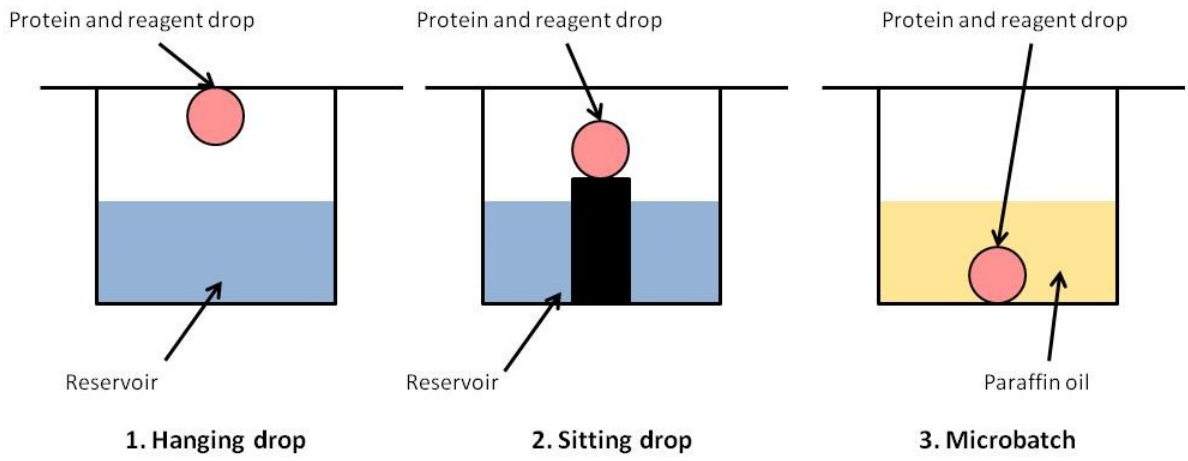

Figure 4 - Common methods of protein crystallisation.

There are other crystallisation techniques that can be used including dialysis and free interface diffusion but the most commonly applied are the vapour diffusion methods (Chayen and Saridakis, 2008). The main reason for this is that high throughput screening of crystallisation conditions can be carried out on commercially available plates designed for hanging or sitting drop experiments. However, despite this high throughput availability, the time to obtaining crystals has not been significantly reduced (Chayen, 2004). Screening using commercially available plates relies heavily on the use of optical microscopes to identify “hits”, that is to say conditions which have allowed the

formation of a crystal. The “hit” conditions are then further optimised until well-diffracting crystals of optimal size are obtained (Chayen and Saridakis, 2008)**.** It is important to note that throughout this optimisation process there is no effective way to distinguish between protein crystals and salt crystals. Current methods of identifying whether a crystal is proteinaceous involve the use of Coomassie Brilliant Blue dye or by means of a “crush test”(Chan et al., 2009). Both these methods are invasive and result in the damage or loss of a potentially viable protein crystal. This means that vast amounts of time could be spent optimising crystal conditions only to find at the very last stage via X-ray diffraction that the crystal is in fact that of the precipitant rather than protein.

Another issue within protein crystallisation studies is that of amorphous precipitation. These precipitates form when the protein crystallisation experiment is within the supersaturation zone of the phase diagram. In comparison to a protein crystal, amorphous precipitates are formed of protein molecules precipitated out of solution with a much less ordered structure; they cannot be used for diffraction experiments. However, amorphous precipitates tend to maintain the native secondary structure of the protein, in contrast to protein aggregates in which the protein is denatured through change in secondary structure. As shall be discussed in subsequent chapters, infrared spectroscopy can be used to obtain secondary structural information from protein systems. Therefore, one would expect there to be little difference in the secondary structural information obtained from the IR spectra of protein crystals and from protein amorphous precipitates. This does not negate the advantages of this technique for use in protein crystallisation and other protein studies though, which is discussed in more detail later.

Given the interest in facilitating the crystallisation process, there have been many developments in this area. The automation of screening trials through the use of robotics has dramatically reduced the drop volumes of protein solution (Ferrer et al., 2013, Santarsiero et al., 2002). Systems exist with potential to deposit picolitre volumes of protein solution (Cherezov and Caffrey, 2006). There have also been some exciting developments in the field of crystallisation using microfluidics (Li and Ismagilov, 2010, Yu et al., 2012, Perry et al., 2013). Although this miniaturisation offers some advantages for proteins that are hard to obtain in the quantities required for regular screening trials, the reduction in drop volume has some impact on the rate of nucleation and the degree of supersaturation often has to be higher (Bodenstaff et al., 2002). Also crystals grown under these conditions are often too small for X-ray analysis even if a synchrotron radiation source is used (Bodenstaff et al., 2002). Other areas, such as improving the rate and type of nucleation for growth of ordered crystals, have also been the focus of recent research. Such techniques include the use of seeding technologies and the use of porous Silicon surfaces, both of which act to control the

nucleation of crystals within a protein solution (Bolanos Garcia et al., 2009). Molecularly imprinted polymers (MIPs) are also increasingly being utilised to control the nucleation of protein crystals; the use of template molecules to create cavities specifically tuned to a target protein molecule can promote the formation of well ordered crystals for X-ray studies (Bergfors, 2003).

Even given these advances, challenges of protein crystallisation still remain and efforts to improve the protein crystallisation process are still important. A way in which to screen for conditions whilst distinguishing between different crystal types would be very advantageous to the facilitating of crystallisation trials. Also despite the number of crystallisation studies occurring worldwide, there is still a lack of understanding of the mechanisms of action of the precipitating agents with the protein and despite the phase diagram, it is very hard to predict the optimum conditions required for crystal growth because there is still a lack of understanding of the process kinetics (Chayen, 2004, Bolanos Garcia et al., 2009). One analytical technique that could be used to aid in both these matters is ATR-FTIR spectroscopic imaging. It can allow for the measurement of protein crystallisation in situ and is chemically specific without the need for additional dyes or labels. This shall be discussed in more detail in Chapter 2.III.

iv. Protein aggregation

As previously mentioned, protein molecules fold into complex structures in what can be viewed as the most fundamental example of biological self assembly. This assembly is dependent on the properties of the amino acid sequence and the protein's surrounding environment. A protein in its native environment is stable and able to fulfil the functions for which it was designed. The fundamental mechanism of protein folding can be described by the Energy Landscape theory (Stefani, 2008). A protein's energy landscape contains all possible conformations along with their corresponding free energy and entropy. In theory, a perfectly folded protein will occupy the conformation with the lowest free energy. In order to reach this state it will search stochastically through possible conformations meaning that at any stage in the folding process, misfolding could occur leading to the formation of protein aggregates (Dobson, 2003).

Protein aggregation is a major area of study because its consequences are very far reaching. In vivo, aggregation plays a role in many debilitating diseases for example Alzheimer's disease, Parkinson's disease and Prion disease. In these cases, aggregation of proteins leads to the formation of amyloid fibrils and inclusion bodies**.** In vitro, protein aggregation can be a hindrance to biological studies for example in protein structural studies. Within the bioprocessing field, aggregation can be a major issue for pharmaceutical companies where the manufacture and storage stability of therapeutic

proteins is very important. This is especially true since protein therapeutics represents the fastest growing sector within the pharmaceutical world (Jenkins et al., 2008).

This term, protein aggregation, refers to a wide range of folded states of the protein molecules that can be caused by a variety of different interactions. They can be classified into many types, mainly insoluble/soluble, covalent/non-covalent, ordered/disordered and native/denatured, depending on nature of the protein, the environment in which it is being studied and the stability of the aggregate (Cromwell et al., 2006). Covalent aggregates are the result of the formation of chemical bonds, for example disulfide bonds while non-covalent aggregates can be the result of hydrophobic interactions, hydrogen bonding or other electrostatic interactions. In vivo, amyloid fibrils are an example of highly ordered aggregates which have a characteristic cross β-sheet structure where as inclusion bodies are seen to be disordered (Fink, 1998).

The kinetics of aggregation are not fully understood and there are still key questions that need to be answered in order to consistently prevent their formation during the production of biotherapeutics or to aid in the development of treatments for protein deposition diseases (Dobson, 2003). These include the nature of the species responsible for aggregation, the underlying mechanisms and reaction kinetics as well as detailed structures of the aggregates, also why some folded intermediates form ordered aggregates whilst others form unordered species (Fink, 1998, Dobson, 2003).

The need to control the aggregation of proteins during the production of biotherapeutics is extremely important since aggregates are degradation products which affect the activity of the protein and may cause undesirable immunogenic reactions within patients (Cromwell et al., 2006, Rosenberg, 2006). They can occur at all stages of the manufacturing process from expression, purification, storage and transport, where each step represents a potential risk of degradation in the biological activity (Dengl et al., 2013, Arosio et al., 2011). This requires the use of accurate analytical methods to detect the formation of aggregates at different stages of the process, as a form of quality control. Without the use of such quality control measures, patients could be exposed to sub-quality and even dangerous products. The default method used for detection is Size exclusion high performance liquid chromatography (SE-HPLC) (Jenkins et al., 2008). However, results from this technique often have to be confirmed with orthogonal methods due to potential inaccuracies. These potential inaccuracies in the level of aggregation detected using SE-HPLC can arise from the adsorption of aggregates within the column itself meaning they do not elute from the column and from the formation or disassociation of aggregates during the sample run, for example (Carpenter et al., 2010). This highlights the need for accurate, high throughput analytical methods for the study of

aggregation in protein therapeutics as well as a need for greater understanding of protein behaviour during throughout the different stages of bioprocessing; ATR-FTIR imaging and Raman spectroscopy have good potential in this area.

v. The effect of surfaces on protein behaviour

Surfaces, both biological and synthetic can also have a major impact on the formation of aggregates. The physicochemical properties of a surface can be very different from that of a bulk solution. This may cause protein molecules to congregate on the surface and this increase in proximity or local concentration could cause the formation of aggregates. Also, hydrophobic surfaces may induce unfolding and aggregation; hydrophobic groups of a protein molecule which are normally hidden within the folded native state interact with exposed hydrophobic functional groups on the surface (Stefani, 2008). Understanding the effect of different surface properties on protein behaviour is an important area of research for the development of biomaterials for use in biomedical applications (Kim et al., 2008) and has far reaching implications within other areas as well, such as nanotechnology and bioprocessing (Gray, 2004). Also, as discussed in Chapter 2.II.iii, the role of surfaces in protein crystallisation experiments is also becoming increasingly important.

Given this importance, much time has been spent developing model systems and experiments employing surface engineering tools to allow for the controlled study of the mechanisms of these protein-surface interactions (Nath et al., 2004, Gray, 2004). The effect of wettability on protein adsorption (Cha et al., 2008, Krishnan et al., 2006) is a key area of interest as it is an important factor for biocompatibility and can greatly influence a protein's conformation (Kim et al., 2008). The role of surface properties on cell behaviour, such as proliferation and spreading is also of interest within the field of bioprocessing and for the development of biomaterials (Lee et al., 1994, Ruardy et al., 1997a, Ruardy et al., 1997b, Kennedy et al., 2006).

There are several methods of modifying a surface such as PEG grafting and the use of self assembled monolayers (SAMs) (Nath et al., 2004, Mrksich and Whitesides, 1996). SAMs can be applied to a range of surfaces and desired surface properties can be obtained through the selection of the "tail group" of the amphiphilic molecule. The ease and versatility of preparation as well as the extensive range of functional groups that could potentially be deposited for study in a controlled way, makes the use of SAMs well suited for fundamental studies on protein-surface behaviours (Mrksich and Whitesides, 1996, Prime and Whitesides, 1991). Alkanethiols deposited on gold coated surfaces and alkylsiloxanes on hydroxyl terminated Silicon surfaces are two of the most common SAMs systems.

In addition, the preparation of a gradient of surface properties, often using SAMs, has been shown to be useful for such studies. These gradient surfaces allow for the variation of one property, such as

wettability, along one direction of the surface and can be used to study the effect of the variable on protein behaviour, in one study (Kim et al., 2008, Elwing et al., 1987, Mei et al., 2005). This can save time and is more convenient than the preparation of separate surfaces with different properties (Kim et al., 2008). Gradient properties can be achieved using standard SAM preparation techniques such as vapour diffusion or solution deposition (Chaudhury and Whitesides, 1992, Ruardy et al., 1997b). Where a thicker layer of functionalised material is required, the use of polymer brushes has also been shown to allow for the formation of a gradient of surface properties, these can also allow for more variation in surface topography (Morgenthaler et al., 2008, Neuhaus et al., 2011).

Analytical methods such as contact angle measurements, AFM, ellipsometry and SEM are used extensively for the characterization of surface properties (Kim et al., 2008) but these provide limited insight into protein conformation and behaviour. Fluorescence microscopy can also be used to detect and quantify the presence of proteins, cells and other biological materials on the surface; however, this typically requires the addition of tags or dyes to the protein molecules (Kim et al., 2008). ATR-FTIR spectroscopy can offer insight into the behaviour of proteins on surfaces and has been used to great effect in this area. This shall be considered in more detail in Chapter 2.III.viii ATR-FTIR spectroscopic imaging has the potential to build on the advantages of traditional ATR-FTIR spectroscopy for use within this field as it could allow for chemical imaging of the effect of gradient surface properties on biological materials, such as proteins and cells to be studied simultaneously and *in situ*.

III. Fourier Transform Infrared Spectroscopy

This section aims to provide a brief introduction to FTIR spectroscopy and the underlying principles of the technique. The different sampling methods shall be discussed; its application to different protein studies examined as well as recent developments in the field, such as surface enhanced infrared spectroscopy (SEIRAS). Additionally, ATR-FTIR spectroscopic imaging shall be introduced and discussed in detail.

i. Introduction

Fourier Transform infrared spectroscopy is a powerful and versatile analytical technique that can be applied to a wide range of samples. It is based on the analysis of the interaction of infrared light with matter. When infrared radiation is directed at a sample, it is absorbed due to the vibrations of chemical bonds of the molecules. There is a correlation between the wavenumber at which samples absorb IR radiation and chemical structure. Thus, from an IR spectrum both the chemical components present in the sample and their molecular state can be determined.

In spectroscopic methods radiation is conventionally expressed as the reciprocal of wavelength, wavenumber with the units' cm^{-1} as shown in Equation 1. Infrared radiation is in the range of 33 – 12800 cm^{-1} and can be further divided into three types; near, mid and far infrared radiation, each with their own advantages for spectroscopic studies (Atkins and de Paula, 2002). Mid IR spectroscopy uses radiation from 400 – 4000 cm^{-1} (Smith, 1996).

$$\tilde{v} = \frac{1}{\lambda}\ cm^{-1} \qquad \textbf{Equation 1}$$

Fourier Transform infrared spectroscopy was first made possible by the invention of the Michelson interferometer by Albert A. Michelson in 1880. However, it wasn't until the development of computer processing power and the advent of the Fast Fourier algorithm by Cooley and Tukey in the 1960s that the technique became more widely used, as summarised by Griffiths (Griffiths and De Haseth, 1986). Further technological developments now mean that is possible to obtain high quality FTIR spectra from a sample in a matter of minutes or less. In addition, the wide variety of sampling techniques means the FTIR spectroscopy is one of the most versatile and useful chemical analysis methods available to scientists.

ii. FTIR Spectrometers

The fundamental principles of infrared spectrometers have remained unchanged for decades despite the improvements in data acquisition time. The typical arrangement consists of a source of infrared radiation, an interferometer, a sampling device, a detector and some form of analysis software.

Most common FTIR spectroscopy utilises the mid IR region, thus a spectrometer must have a source that emits IR radiation with a wavenumber range of 400-4000 cm^{-1}. Two of the most common sources are the Nernst filament and the Globar (Atkins and de Paula, 2002). A Nernst filament is a ceramic filament of lanthanide oxide which is heated to between 1200 and 2000 K enabling the emission of mid IR radiation. A Globar is a rod of Silicon carbide electrically heated to 1500 K.

At the heart of the infrared spectrometer is the Michelson interferometer. This optical device allows the absorption of IR radiation by the sample to be calculated and can be represented by the schematic in Figure 5**.** It typically consists of a source of IR radiation, a fixed mirror, a moveable mirror and a beam splitter. An interferometer works by splitting the incoming IR beam into two separate beams using the beam splitter which allows half of the radiation striking it to be transmitted to the fixed mirror and half of it to be reflected to the moveable mirror. The beam exiting the interferometer is a result of the two beams recombining with varying degrees of phase difference dependent on the position of the moveable mirror relative to the beam splitter.

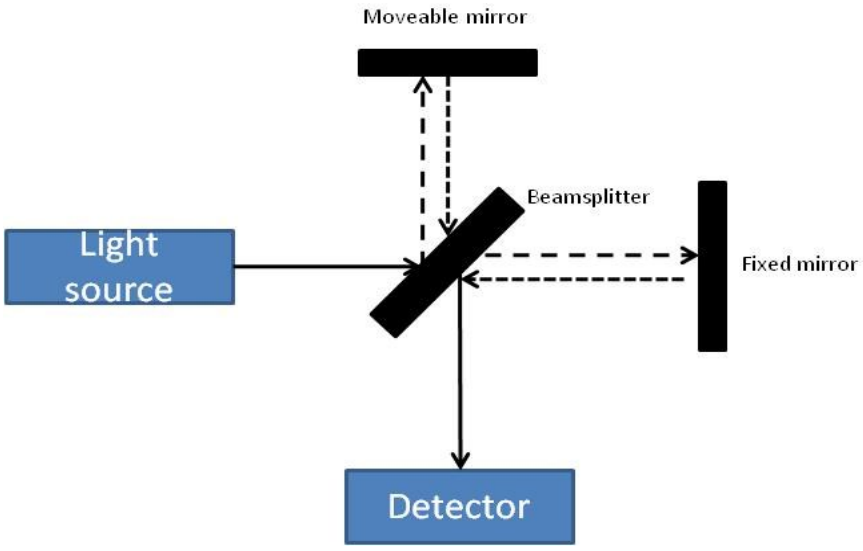

Figure 5 - Schematic of interferometer.

When the moveable mirror and fixed mirror are equidistant from the beam splitter, the distance travelled by each beam is the same. That is to say; there is zero optical path difference. The moveable mirror is translated away from the beam splitter to introduce an optical path difference, δ. The optical path difference is equal to twice the displacement of the mirror. The introduction of an optical path difference means that the two beams will interfere either constructively or destructively upon recombination because of the difference in phase between them. Constructive interference occurs when the optical pathlength is equal to a multiple of wavelength, $\delta = n\lambda$. Whereas destructive interference occurs when the beams are out of phase by half a wavelength, $\delta = (n+0.5)\lambda$.

The detector measures the variation of light intensity with optical path difference to produce an interferogram. This is a plot of light intensity against optical path difference and is generated by translating the moveable mirror back and forth once, in what is known as a scan. An interferometer works on the principle that light of different wavelengths will undergo constructive and destructive interference at different optical path differences producing their own unique interferogram. Therefore, the interferogram measured by the detector is actually the summation of all these individual interferograms, shown in Figure 6, and contains the intensity information for each wavelength. Fourier transform is then used to decode this intensity information to produce a spectrum based on the absorption of IR light by the sample being analysed.

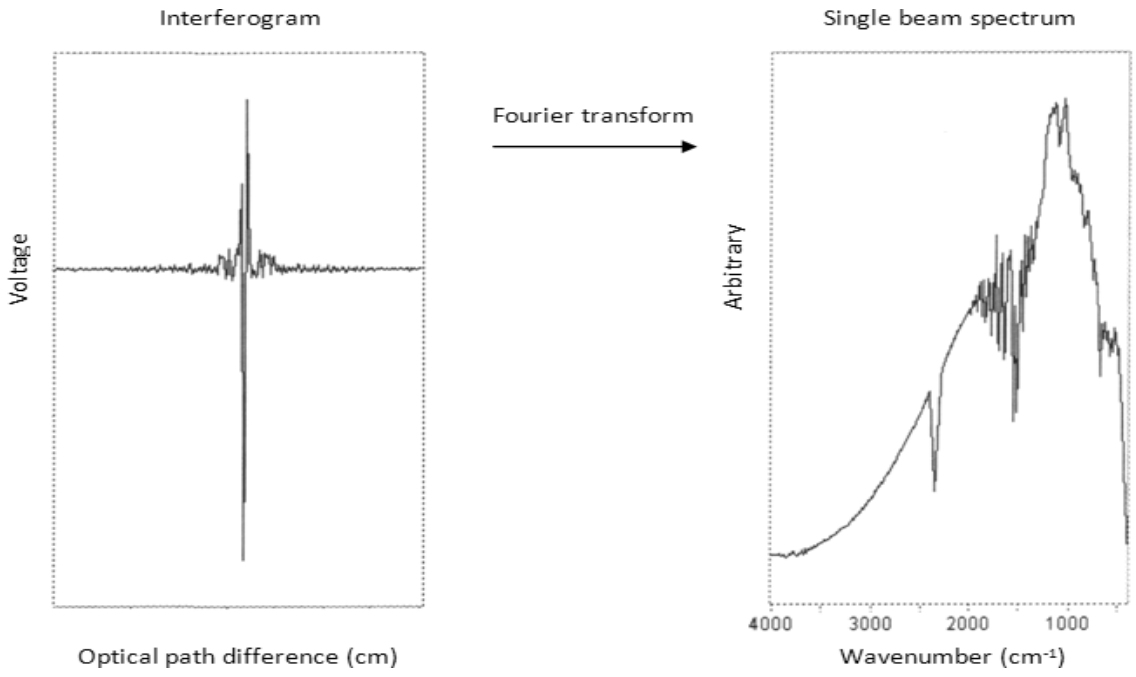

Figure 6 - Typical interferogram and transformation to spectrum (Smith, 1996).

iii. Quantitative analysis of FTIR spectra

FTIR spectrometers are typically single beam devices which means that in order to produce a spectrum of absorbance from a sample the measured spectrum has to be ratioed with a background spectrum (Smith, 1996). This background spectrum measures the distribution of infrared energy by IR source and the absorbance of IR by environment such as atmospheric water vapour or carbon dioxide. Thus, when a sample's spectrum is ratioed against the background, it should remove any influence of these environmental IR contributions from the sample's spectrum. A drawback of this is that during the course of a measurement the environmental conditions could change altering the background spectrum; this may produce artefacts in the sample's spectrum which could lead to the wrong assignment of peaks or masking of sample peaks.

Once ratioed against a background spectrum, a transmission spectrum for the sample is generated where the intensity of light transmitted through the sample (T) is calculated from:

$$T = \frac{I}{I_o}$$ **Equation 2**

Where I is the measured intensity when sample is present and I_o is the intensity measured when no sample is in the beam path (taken from the background spectrum). This can be converted into an absorbance spectrum using the equation:

$$A = \log_{10} T$$ **Equation 3**

Once a spectrum has been generated in absorbance units, it is possible to carry out quantitative analysis using the Beer-Lambert Law (Smith, 1996). This law states that the absorbance of infrared light by a component within a sample is proportional to the concentration of that component and the pathlength of light within the sample (Equation 4).

$$A = \varepsilon l c$$ **Equation 4**

Where: A = absorbance, ε = molar absorptivity, l= pathlength and c= concentration. The molar absorptivity is dependent on the particular vibrational mode associated with the absorbance. This relationship between concentration and absorbance adds to the versatility of FTIR spectroscopy by allowing quantitative analysis to be carried out on the components within a sample.

iv. Spectral Resolution

The performance of a spectrometer is defined by its spectral resolution and the signal to noise ratio achievable. The spectral resolution is the ability to distinguish between closely spaced spectral features. It is dependent on the maximum retardation of the moving mirror within the interferometer (Griffiths and De Haseth, 1986). As the optical pathlength increases, a spectrometer's ability to distinguish between features increases, that is to say its resolution is higher. There are several ways of defining spectral resolution. The Rayleigh criterion states that in order for two peaks of equal intensity to be just resolved, the valley between them must be 20 % lower than the tops of the peaks (Smith, 1996). Whereas the Full-width-half-height (FWHH) approach looks at the width of a band and states that for bands which are inherently narrow, the FWHH of the peak can be used to measure the spectral resolution. A spectral feature is not resolved until the space between peaks is greater than the FWHH of the peaks being studied (Griffiths and De Haseth, 1986).

Although the maximum spectral resolution is fundamentally dependent on the maximum optical path length of the spectrometer it is possible to adjust the resolution by determining the number of data points taken by the spectrometer to produce the spectrum, this is known as the instrumental resolution. For example a spectrum measured at a resolution of 8 cm^{-1} will contain a data point every 8 cm^{-1} which means for a spectrum of wavenumbers 400 – 4000 cm^{-1} there will be 450 data points on the spectrum. The retardation of the moving mirror is adjusted in order to achieve the resolution required.

Despite having the advantage of being able to resolve close peaks, using high resolution measurements will increase the noise of the spectrum. At lower resolutions, the optical path length of the infrared beam is shorter and therefore, measures less noise than that at higher resolutions. This has to be considered when selecting the resolution required for measuring the sample. High resolution spectrum will contain a lot more information but will be noisier meaning the lowest resolution possible should be chosen to enable spectral features to be resolved whilst keeping noise to a minimum (Smith, 1996).

Angular divergence of the infrared beam also limits the maximum resolution that can be achieved. The infrared beam passing through the interferometer is not perfectly collimated and as the pathlength increases, it can spread out further. Since light at the centre of the beam and at the edges will travel at different distances, destructive interference will occur as the beam travels to and from the moving mirror reducing the intensity of the beam returning to the beamsplitter. This increases the noise of the spectrum but is mainly applicable to resolutions above 4 cm^{-1} in which case an aperture can be used to overcome this problem (Griffiths and De Haseth, 1986).

v. Signal to Noise

FTIR spectrometers have several advantages over dispersive spectrometers and it is necessary to discuss these in order to understand signal to noise ratios. Dispersive instruments pass the IR beam through a monochromator which splits the light into different wavelengths using a diffraction grating or prism. The use of a slit decides which portion of these wavelengths passes through the sample to the detector and the position of this slit is adjusted so that over the course of a measurement each wavelength is detected. In this situation only a small portion of the IR beam is being measured by the detector at a moment in time. In comparison with an FTIR spectrometer which allows the entire IR beam to be incident on the detector at any one time; this is called the Jacquinot advantage. The higher optical throughput reduces the noise level compared to dispersive instruments. The second advantage is known as the multiplex or Fellgett advantage. The noise at a particular wavenumber is proportional to the time spent measuring that wavenumber. Therefore, since an FTIR spectrometer measure all wavenumbers simultaneously, more time can be spent observing them, reducing the noise compared to dispersive instrument measuring individual wavelengths within the same time frame.

The appearance of noise within a spectrum is the result of many variables such as the alignment of the spectrometer and the detector used. The signal to noise ratio (SNR) is a measure of the noise in a spectrum and is taken as the ratio between the heights of a component peak against a noise peak on the baseline nearby. In order to be considered as a real feature, a spectral peak must be three times the height of a noise peak. The SNR can be improved by several ways, one of which would be to measure at lower resolutions as discussed in Chapter 2.III. iv and another through the co-addition of scans which shall be considered below.

The multiplex advantage of FTIR spectrometers over dispersive instruments stated that noise was proportional to the square root of time spent measuring a particular wavelength (Griffiths and De Haseth, 1986). For a rapid scanning spectrometer with constant moving mirror velocity, this can be expressed as:

$$SNR \propto N^{\frac{1}{2}} \qquad \textbf{Equation 5}$$

Where: N is the number of scans. The co-addition of scans increases the possibility of random noise within the interferogram being cancelled out. Therefore, increasing the number of scans increases the signal to noise ratio. Although this suggests that increasing the number of scans will improve the SNR indefinitely, this is not the case. There is a limit in the improvement in SNR achieved with significantly larger number of scans due to the time it takes to obtain the measurement; over time

there is more likelihood of noise being introduced into the system from environmental fluctuations and from instrumental noise and vibrations which reduces the theoretical improvement in SNR.

vi. Sampling methods

The sampling method is the way in which the infrared beam is made to interact with the sample. There are several methods available, each with advantages and disadvantages but this versatility in sample analysis is one of Infrared spectroscopy's greatest advantages as it enables the technique to be applied to solids, liquids and gases. The multiple ways in which infrared light can be directed at samples and the range of detectors available allows for the analysis of a wide variety of samples in a range of conditions.

The most traditional method of FTIR spectroscopy uses transmission, where infrared light is passed through a sample; liquid and gaseous samples are sandwiched between two IR transparent windows, shown in Figure 7a. Although straightforward and applicable to all types of samples, it has some limitations. The sample thickness, for example is one. Since the beam is travelling through the absorbing sample, this method requires short pathlengths of typically no more than 6 – 10 μm between the IR transparent windows, particularly in the case of aqueous samples. This is important when aqueous samples are to be studied because water is a strong absorber of IR light; too long a pathlength would result in all the IR radiation being absorbed by the sample and none reaching the detector.

Reflectance infrared spectroscopy is where IR light is reflected off the external surface of a sample. Two types of reflection can occur; specular reflection, which occurs when the angle of reflection is the same as the angle of incidence of the IR beam and diffuse reflection, which results in the scattering of IR light in all angles. Both types of reflected IR radiation can be used to obtain chemical information from the sample although the method has several limitations. The use of reflectance mode can be useful especially if only the surface of a sample is of interest but it can be limited to the study of samples with polished surfaces. Diffuse reflectance FTIR has been found to be useful for the study of samples which strongly scatter as opposed to absorb IR light such as solid particulates. However, the sample often has to be ground into a non-absorbing medium such as KBr and since the intensity of diffusely reflected IR light tends to be weak, long acquisition times are required to obtain a good SNR.

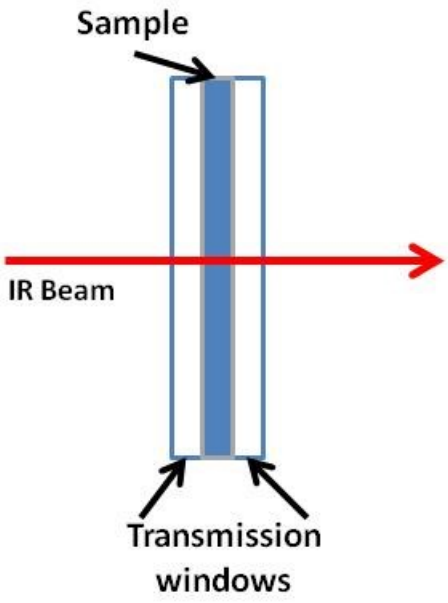

Figure 7 - Schematic showing the transmission sampling mode.

Attenuated Total Reflection offers an alternative sampling method that overcomes the pathlength limitations of transmission. In this method the IR beam is directed at a prism made of IR transparent material with a high refractive index known as an internal reflection element (IRE), such as Zinc Selenide, Germanium or Diamond, Figure 8. The angle of incidence of the beam is greater than the critical angle of the material and as such total internal reflection occurs. The critical angle (θ_{crit}) is dependent on the refractive indices of the internal reflection element (n_1) and the sample (n_2), according to Snell's law (Equation 6).

$$sin\theta_{crit} = \frac{n_2}{n_1}$$ **Equation 6**

At the reflecting surface, a standing wave of radiation is established normal to the surface. This is known as an evanescent wave and it decays exponentially with distance from the surface. This evanescent wave interacts with the sample on the top surface of the ATR crystal as shown in Figure 8. The sample absorbs infrared radiation, attenuating the evanescent wave and its IR spectrum is measured.

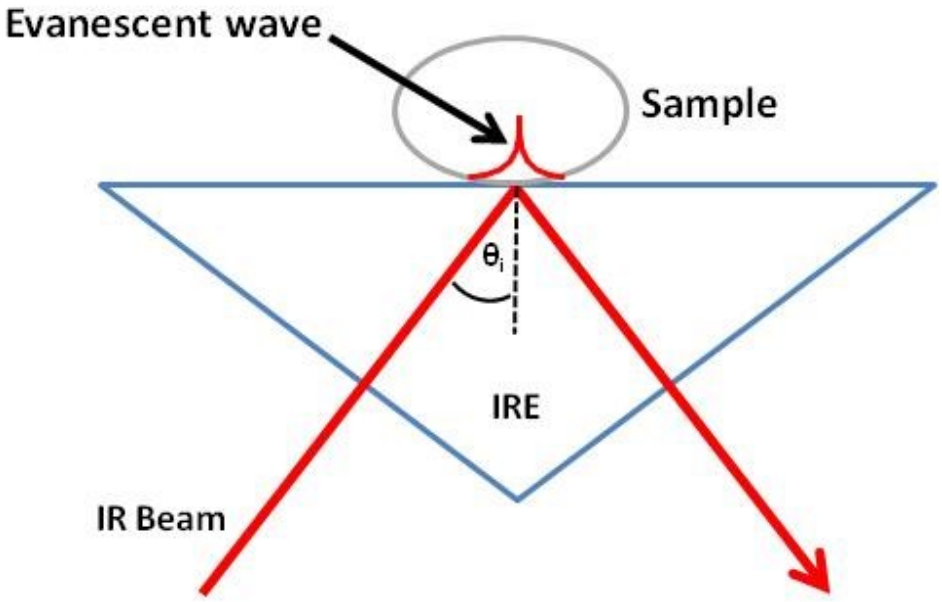

Figure 8 - Schematic of infrared path through ATR prism where the angle of incidence of the IR beam (θ_i) is greater than the critical angle (θ_{crit}).

The depth of penetration of the evanescent wave is the depth at which its electric field is decreased to 1/e of its maximum value and is dependent on the wavenumber, refractive indices of both the crystal and the sample and the angle of incidence of the IR beam, as shown in Figure 9 and Equation 7. It is typically in the range of 0.5 -2 µm although it should be noted that absorbance information is obtained from the sample beyond this range, as the evanescent wave probes deeper than the depth of penetration. Therefore, ATR measurements contain chemical information from approximately three times the penetration depth (Kazarian and Chan, 2010). Table 1 shows the properties of some ATR crystals and their typical depths of penetration.

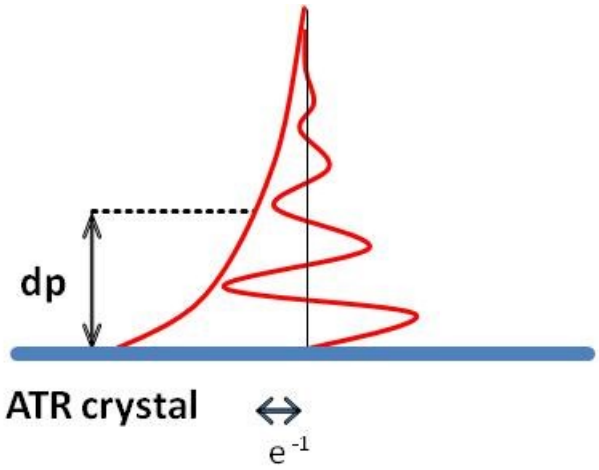

Figure 9 - Electric field of IR beam at ATR surface.

$$d_p = \frac{\lambda}{2\pi(n_1^2 sin^2\theta - n_2^2)^{1/2}}$$ **Equation 7**

Since ATR-FTIR is inherently a surface layer technique in that the evanescent wave only interacts with the several micrometer thick surface layer of the sample, it has advantages for protein studies in particular. In comparison with transmission, it is much more amenable to the study of aqueous samples and the sample preparation is generally much simpler. Additionally, it is a non destructive technique in that samples can be deposited directly onto the ATR crystal with very little sample preparation and removed again easily. This makes it applicable for a wide variety of samples and is particularly useful where samples need to be measured using more than one technique. For the study of proteins in solutions, particularly their behaviour at surfaces, ATR-FTIR spectroscopy is commonly used, this is considered in Chapter 2.III.viii.

Table 1 - Properties of ATR crystals (Pike Technologies).

ATR crystal	n1	LWL, cm-1	dp	Water Solubility, g/100g	pH Range	Hardness, Kg/mm2
Diamond	2.4	525	1.66	Insoluble	1-14	5,700
Germanium	4	780	0.65	Insoluble	1-14	550
KRS-5	2.37	250	1.73	0.05	5-8	40
Silicon	3.4	1500	0.84	Insoluble	1-12	1150
ZnS	2.2	850	2.35	Insoluble	5-9	240
ZnSe	2.4	525	1.66	Insoluble	5-9	120

n1 = refractive index of ATR crystal

LWL = long wave length cut-off

dp = depth of penetration in micrometers @ 1000 cm-1

(http://www.piketech.com/technical/crystal-selection-ATR.html)

One aspect that has to be considered during the analysis of FTIR spectra is the comparison between spectra measured using different sampling techniques. For example, when comparing between ATR and transmission spectra, the thickness of the sample measured in transmission does not equal the depth of penetration of the evanescent wave in ATR mode. In order to determine the transmission pathlength required to produce the same absorption as ATR, the effective pathlength of the evanescent wave should be considered (Averett et al., 2008). However, when measuring in ATR mode, the electric fields for parallel and perpendicular light in the sample medium are different, meaning their effective pathlengths are different. Therefore, the effective pathlengths for both polarizations of light must be calculated. This can be done from equations derived by Harrick, Equation 8 and Equation 9 (Harrick, 1967). From these equations, the effective pathlength for an unpolarized beam can be calculated as the average of the effective pathlengths.

Equation 8 - Effective pathlength for s-polarized IR light.

$$d_{e,s} = \frac{\lambda\left(n_2/n_1\right)\cos\theta}{\pi\left[1-\left(n_2/n_1\right)^2\right]\left[\sin^2\theta-\left(n_2/n_1\right)^2\right]^{0.5}}$$

Equation 9 - Effective pathlength for p-polarized IR light.

$$d_{e,p} = \frac{\lambda\left(n_2/n_1\right)\cos\theta\left[2\sin^2\theta - \left(n_2/n_1\right)^2\right]}{\pi\left[1-\left(n_2/n_1\right)^2\right]\left\{\left[1+\left(n_2/n_1\right)^2\right]\sin^2\theta - \left(n_2/n_1\right)^2\right\}\left[\sin^2\theta - \left(n_2/n_1\right)^2\right]^{0.5}}$$

In addition to this, when comparing between spectra measured in different sampling modes or arrangements, anomalous dispersion (AD) should also be taken into consideration. Anomalous dispersion results in a Z-shaped variation in the refractive index of a material with wavelength compared to normal dispersion which shows a monotonic decrease in refractive index with wavelength. It is much more apparent at angles of incidence closer to the critical angle for a system (Harrick, 1967). As seen from Equation 8 and Equation 9, the effective pathlength for polarized light is highly dependent on the refractive indices of the sample, the angle of incidence and the IRE. At the higher energy side of an absorbance band, the sample's refractive index is smallest meaning the effective pathlength is smaller whereas at the other end of the band, the refractive index is largest making the effective pathlength larger. As a result, an absorption band will shift towards lower energy wavenumbers compared to transmission (Hancer et al., 2000, Harrick, 1967). This can be particularly problematic if the ATR spectrum is to be used for qualitative and quantitative analysis through comparison with transmission spectra and also when comparing with measurements taken at different angles of incidence of IR radiation. A more detailed discussion of anomalous dispersion and ways in which to overcome it shall be discussed in Chapter 4.

vii. FTIR Spectroscopy of Proteins

The use of IR spectroscopy to gain insight into protein structure and behaviour has been continually developed since the first work on characterising the spectral features of different polypeptide secondary structures and amino acids (Krimm, 1962, Byler and Susi, 1986, Miyazawa and Blout, 1961). The infrared spectra of proteins exhibit 5 characteristic bands, three of which are known as Amide bands. The Amide bands are most commonly used in infrared protein studies. The Amide I band, which has the strongest absorption of infrared light, is found between 1600-1700 cm^{-1}. It is primarily caused by stretching vibrations of C=O coupled weakly with C-N stretch and N-H bending. The exact band position is determined by the backbone conformation and the hydrogen bonding pattern within the protein molecule (Haris and Severcan, 1999). The Amide II band occurs at 1500-1600 cm^{-1} and is mainly derived from the C-N stretch along with N-H in-plane bending. Lastly, the Amide III band is found at 1200-1300 cm^{-1}. The vibrations responsible for this band are a complex mix of N-H bending and C-N stretching along with deformation vibrations of C-H and N-H (Haris and Severcan, 1999, Barth and Zscherp, 2002, Sarver Jr and Krueger, 1991).

Although all three bands can be useful to elucidate the secondary structure of a protein, the Amide I band is the most sensitive to structural changes and is the most commonly used in secondary structure analysis. Factors responsible for the conformational sensitivity of the Amide I band include hydrogen bonding and coupling between transition dipoles, both inter and intra molecular, which will impact the way in which a protein molecule interacts with IR light (Surewicz et al., 1993). From the study of simple homopolypeptides of known single structure, the relationship between Amide I band position and structure has been proposed allowing predictions about the secondary structure of proteins to be made from IR spectra (Miyazawa and Blout, 1961, Barth and Zscherp, 2002). Further analysis of the Amide Iband is required in order to obtain the types and amounts of secondary structure present; this is achieved through Fourier deconvolution and second derivative, curve fitting and spectral subtraction, for example and shall be discussed below. Multivariate analysis and other statistical methods are also increasingly being applied to the analysis of protein spectra because of their usefulness in interpreting the wealth and complexity of information contained within the spectra (Shashilov and Lednev, 2010, Goormaghtigh et al., 2006, Trevisan et al., 2012).

There are many examples in the literature of the assignment of protein secondary structure based on the analysis of the Amide I band (Byler and Susi, 1986, Miyazawa and Blout, 1961, Haris and Severcan, 1999, Surewicz et al., 1993, Dong et al., 1990). In general, α-helical structures have a band peak at wavenumbers 1650-1658 cm^{-1}; β-sheet structures tend to have bands between 1620-1640 cm^{-1} and between 1670 – 1695 cm^{-1}; random coil structures occur at around 1644 cm^{-1} (Surewicz et

al., 1993). It is even possible to assign more complex structures such as an α-helix overlapped with random coil which can absorbs IR radiation at 1654-1656cm^{-1} (Haris and Severcan, 1999). Figure 10 shows an example of a protein spectrum, the inset shows curve fitting of the Amide I band for different structural components (Sarver Jr and Krueger, 1991).

The study of aqueous protein samples is challenging because of the overlap of the water bending mode with the Amide 1 band at 1600 cm^{-1}. This could be overcome through the use of D_2O; however this can affect the native secondary structure of the protein. Current FTIR spectrometers allow for accurate subtraction of the water band, although care should be taken to avoid over subtraction. There are several papers with guidelines for this procedure but it is widely accepted that the integrity of protein spectral data can be maintained by meeting two subtraction criteria; accurate subtraction of water vapour bands between 1800 – 1500 cm^{-1} and ensuring a straight baseline between 2000 – 1750 cm^{-1} upon water subtraction (Dong et al., 1990, Kong and Yu, 2007).

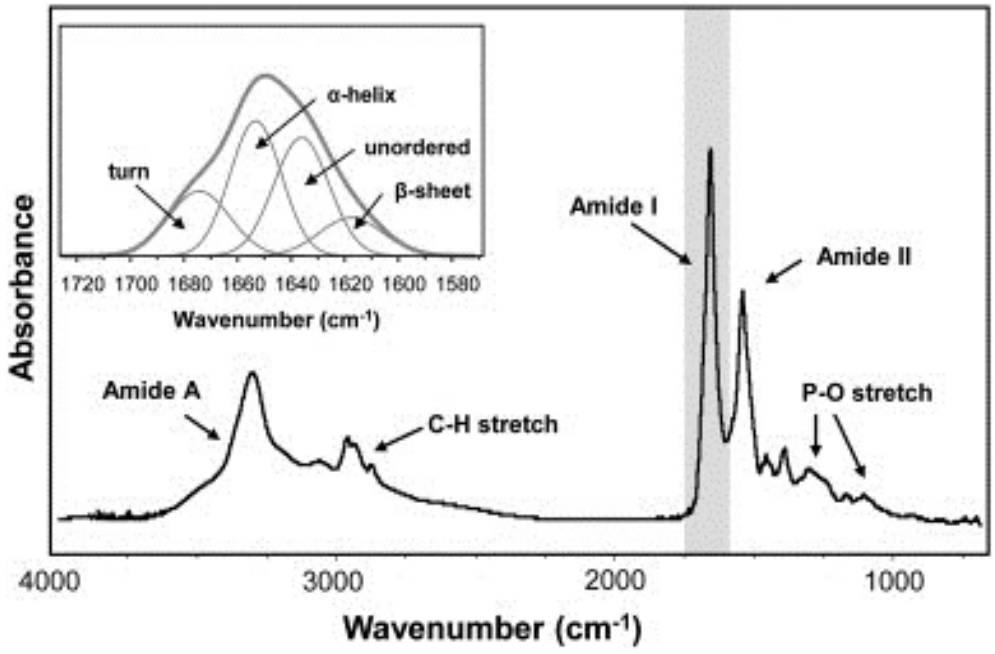

Figure 10 - FTIR spectrum of a typical protein illustrating the Amide I and Amide II bands at ~1650 cm^{-1} and ~1540 cm^{-1}, respectively. (Inset) Expanded view of the Amide I band, which can be deconvolved into its secondary structure components (Sarver Jr and Krueger, 1991).

As discussed previously, proteins are complex structures consisting of many polypeptide segments folded into different types of secondary structure. One single protein can contain segments with α-helix, β-sheet and random coil structures. Therefore, the observed Amide I band can consist of many overlapping bands representing each of the structural elements present within the protein sample. From direct observation of the Amide I band the individual components cannot be easily identified because the widths of component bands are greater than the separation between maxima of adjacent peaks (Surewicz et al., 1993).Therefore, in order to carry out secondary structure analysis on protein spectra, some form of spectral manipulation is required.

There have been several different types of spectral manipulation and analysis applied to the study of protein secondary structure analysis in literature, mainly by taking the second derivative, band narrowing through Fourier deconvolution, as well as pattern recognition and difference spectroscopy. There is also potential to carry out quantitative analysis through the use of curve fitting which allows the determination of the percent contribution from each type of secondary structure present within the sample.

One of the most common methods of ascertaining the individual component peaks of the Amide I band is by taking the second derivative of the spectrum. Second derivative analysis is a mathematical means of enhancing the spectral resolution, by reducing the effect of gradual curvature in broad peaks and increasing the contribution from sharp absorption features (Whitbeck, 1981). An example of the second derivative spectrum of the Amide I band of Cytrochrome c can be seen in Figure 11. The number and position of downward pointing peaks indicates how many overlapping peaks there are in a broad absorption band. Therefore, this allows for different structural elements of the protein's secondary structure to be identified from the second derivative spectra. It should be noted however, that in taking the second derivative of the spectrum the SNR can be reduced by approximately one order of magnitude (Griffiths and De Haseth, 1986) which will increase the likelihood of misidentification of structural peaks. Therefore in order to carry out this analysis, or indeed any secondary structure analysis, high quality spectra with good signal to noise are required. Figure 11 also demonstrates the effect that inaccurate water subtraction can have on the second derivative spectra (Figure 11a, which meets both water subtraction criteria showed the most accurate secondary structure bands for Cytochrome C compared with Figure 11b and Figure 11c), highlighting why it is important to follow the subtraction criteria described above.

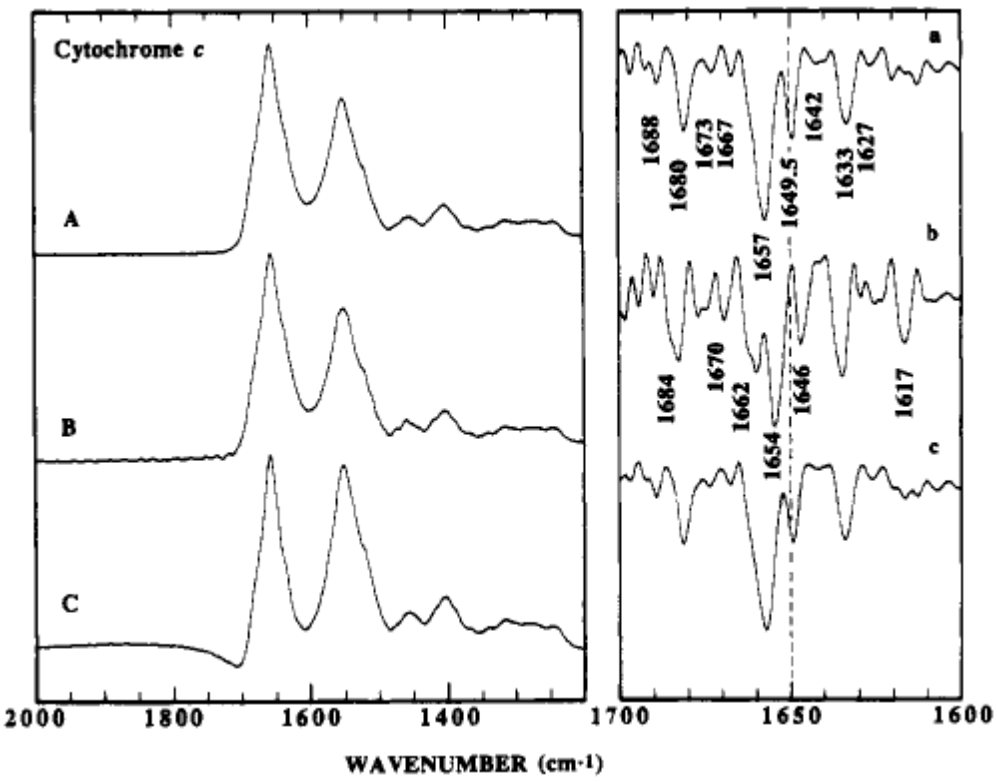

Figure 11 - Spectra showing effect of different water subtraction criteria and corresponding second derivative spectra. a) both subtraction criteria fulfilled, b) inaccurate subtraction of water vapour but with straight baseline between 2000 – 1750 cm^{-1}, c) accurate subtraction of water vapour but over subtraction of water, highlighted by non straight baseline between 2000 – 1750 cm^{-1} (Dong et al., 1990).

Fourier deconvolution is another form of mathematical resolution enhancement by decreasing the band width of each component band and increasing the separation between them. This can then allow each deconvolved band to be assigned a particular secondary structure based on theoretical calculations or by spectra-structure correlations from proteins of known structure (Yang et al., 1985). The application of this technique is fundamentally limited by the resolution of the instrument used to measure the spectrum meaning there is a limit to the amount of deconvolution that can be applied (Smith, 1996). Despite this, one still has to be careful not to over deconvolute as this may create imaginary peaks and distort any conclusions made from the analysis (Surewicz et al., 1993). Comparison with the sample's second derivative spectra can aid in the prevention of over deconvolution.

The deconvolution process involves carrying out reverse Fourier transform on a section of interest of the spectrum. This generates what is known as a Cepstrum which is mathematically enhanced by a factor of $e^{\alpha x}$, where α is the degree of resolution enhancement and x is the optical retardation. The enhanced cepstrum is then Fourier transformed to produce the deconvolved spectrum (Smith,

1996). Most spectrometer's software packages allow the user to choose the degree of resolution enhancement applied to a spectrum**.** Figure 12 shows an example of deconvolved Amide bands for a predominantly α-helical membrane protein.

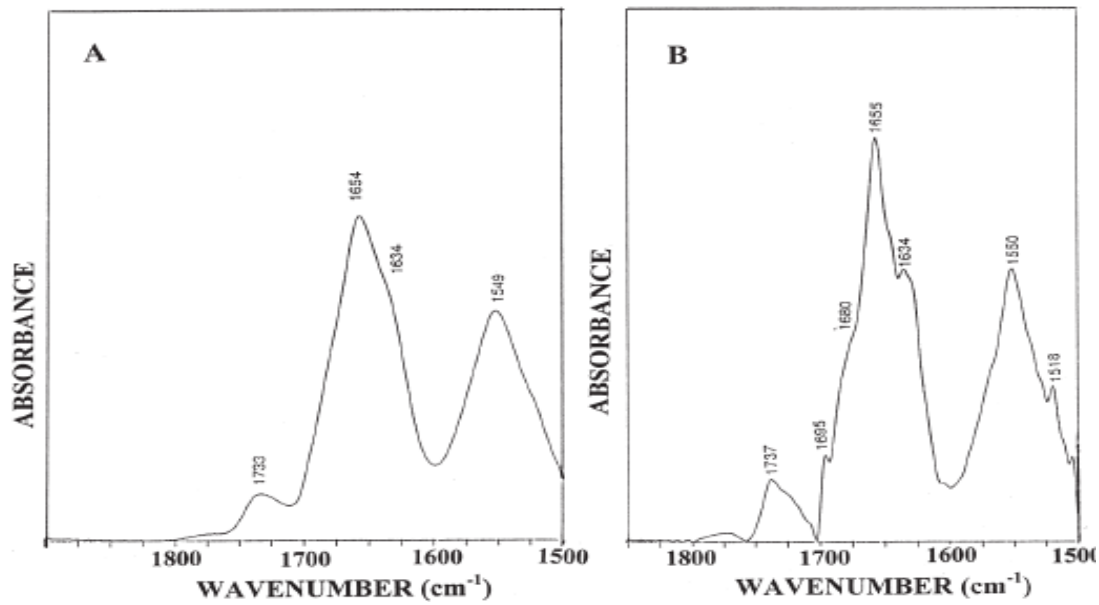

Figure 12 - Absorbance (A), deconvolved (B) spectra of a predominantly α-helical membrane protein, the reaction centre from R. sphaeroides, in H_2O phosphate buffer (Haris and Severcan, 1999).

Pattern Recognition can be compared to methods used for determining protein secondary structure in Circular Dichroism. This method involves a series of mathematical manipulations based on a calibration matrix of IR spectra of proteins with known structure. Any conclusions based on this method are drawn from mathematical correlations and thus eliminate the subjectivity associated with Fourier deconvolution. The most common approach uses a statistical method called Partial Least Squares regression (Surewicz et al., 1993).

Another method for analysing protein behaviour is Difference Spectroscopy. As the name suggests, this method is more useful for determining any changes that may have occurred within a sample rather than direct structure information (Surewicz et al., 1993). The subtraction of spectra from two different states of the sample will leave a spectrum displaying only the difference between the two states. This can allow for small transitions such as changes in functional groups and hydrogen bonding to be followed (Pinkerneil et al., 2012). As well as allowing the detection of small differences between spectra, it can also eliminate water from the spectrum. This is particularly useful for secondary structural analysis of proteins in solution.

Potential exists to quantify the percent of each structure present within a protein through curve fitting. The curve fitting procedure iteratively determines the fraction of the Amide I band associated with each structure and this is assumed to represent the percentage of each (Byler and Susi, 1986). This is most often applied to spectra that have already been mathematically enhanced, such as to deconvolved spectra or second derivative spectra (Byler and Susi, 1986).

viii. ATR-FTIR spectroscopy of surfaces and proteins

FTIR spectroscopy is a powerful tool for the study of proteins in any environment. The fact that measurements can be taken in situ, particularly when using ATR approaches and that secondary structural information can be obtained from IR spectra means that FTIR spectroscopy is well suited to the study of protein structural changes such as crystallisation and aggregation.

Studies of heat induced aggregation of Lysozyme carried out by van de Weert *et al.* showed the appearance of a new band at 1625 cm^{-1} when second derivative manipulation was carried out on the spectra. This is taken to be the characteristic band of non-covalent aggregates (van der Weert et al., 2000). Whereas Clark et al followed the formation of a well defined Amide band at 1620 cm^{-1} in five different globular proteins at temperatures greater that 60 °C, without having to carry out spectral manipulations. This was assigned to the anti parallel β-sheet structure associated with protein aggregates (Clark et al., 1981).

The environment of a protein at an interface is very different from its environment in bulk solution and is very dependent on the properties of the interface such as its charge or hydrophobicity. At hydrophobic surfaces, proteins can unfold into non-native conformations without the energy penalty of exposing their inner hydrophobic sections to water (Sethuraman and Belfort, 2005) . This effect is known as surface denaturation and aggregation. ATR-FTIR is well situated to study this phenomenon as it measures the IR absorption of a protein at the ATR surface which can then be analysed to look at differences in secondary structure at the interface compared to the bulk solution. The use of ATR-FTIR to study the effect of surface properties on aggregation offers several advantages in that it can offer insight into the adsorbed structure of the protein, something that is very difficult to obtain using X-ray diffraction or Circular Dichroism.

The study of the interaction of proteins with different surfaces is important for the design of biomaterials, biomedical devices and for the production of biopharmaceuticals (Nakanishi et al., 2001, Cha et al., 2008, Sethuraman and Belfort, 2005, Green et al., 1999, Sethuraman et al., 2004). Both the surface chemistry and topography can play a major role in the behaviour of biological

materials (Reynolds et al., 2013) . As described above, ATR-FTIR spectroscopy is a surface layer technique where the absorbance is measured only from the portion of a sample in direct contact with the ATR surface rather than from the bulk. The surface of an IRE (or ATR crystal) can be easily modified making it well placed to study the effect of different surfaces on proteins without the need for additional labelling (Chittur, 1998). It can also easily be coupled with other experimental methods designed to induce changes within proteins such as photochemistry, heat and electrochemistry (Rich and Iwaki, 2007). Together with the variety of ATR crystals made from different materials available, this provides many opportunities to study the effect of surfaces on the sample. The sensitivity of measurements could potentially be increased by making use of multiple reflection objectives; this increases the pathlength of the measurement (Pinkerneil et al., 2012, Rigler et al., 2003). However, multiple reflection objectives cannot be used in FTIR imaging because absorbances are measured at several different locations. This would create overlap in the images which are based on absorbance values meaning for FTIR imaging single reflection objectives are required (Kazarian and Chan, 2010).

There have been several investigations carried out using ATR-FTIR spectroscopy to study the effect of polyelectrolyte multilayers on protein adsorption and on proteins within the layers (Salloum and Schlenoff, 2004, P. Schwinté, 2001, Steiner et al., 2007). Figure 13 demonstrates the usefulness of ATR penetration depth for examining the multilayer. BSA is adsorbed only into the positively charged layer and as such will absorb infrared. Heat can be applied to the multilayer and the stabilising effect on the protein against heat induced structural changes can be followed by examining the secondary structure from the Amide I band (Salloum and Schlenoff, 2004).

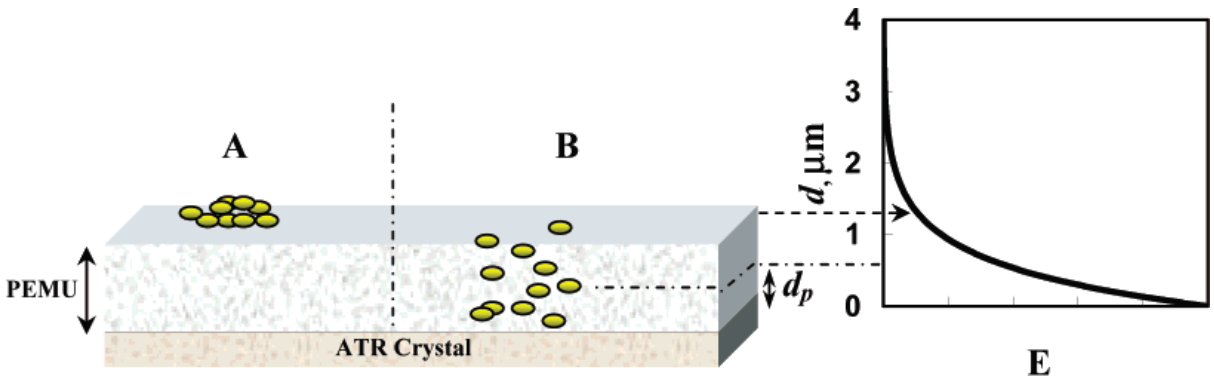

Figure 13 - Evanescent wave electric field amplitude (E) falls off exponentially away from the surface of the crystal. (A) BSA adsorption on the negatively charged surface. (B) BSA adsorption on the positively charged surface. d_p represents the penetration depth of the evanescent wave normal to the surface of the crystal, using Ge (n = 4.0) in contact with the medium of n = 1.42 (Salloum and Schlenoff, 2004).

Difference spectroscopy is a key tool in the analysis of proteins using ATR-FTIR spectroscopy. Whereas absorption spectra can provide global information about the sample such as secondary structure, difference spectroscopy can allow small changes in functional groups, hydrogen bonding changes and chemical reactions to be followed in situ using ATR-FTIR spectroscopy (Pinkerneil et al., 2012, Rigler et al., 2003). This allows for sensitive measurements to be made following subtle changes in protein conformation and can be used to provide details of mechanisms of molecular reactions. One method, demonstrated by Pinkerneil *et al.* shows the advantages of immobilizing polyhistidine tagged proteins onto the surface of a multiple reflection ATR crystal by first preparing a modified lipid bilayer containing nitrilotriacetic acid (NTA) groups on the surface (Pinkerneil et al., 2012). Such immobilization is based on established immobilized metal ion affinity chromatography where the selective binding of proteins is activated by the formation of transition metal ion complexes (Rigler et al., 2003). Once proteins are immobilized on the surface, reactions induced by changes in heat, pH for example, can be followed in situ by difference spectroscopy. This could be potentially applied to any polyhistidine tagged protein of interest.

A study by Onodera *et al.* demonstrated the ability of ATR-FTIR spectroscopy to explore protein-protein interactions by immobilizing antigens on a functionalised GaAS ATR element (Onodera et al., 2007). The selective binding of a specific antibody can then be followed in comparison with a non-specific antibody by comparing the secondary structures of the adsorbed proteins from the second derivative spectra of the Amide I band. It was shown that the selective binding of IgG to the antigen sensing layer resulted in spectra high in β-sheet content, consistent with known IgG structure (Onodera et al., 2007). However, the spectra of the non specific protein showed no significant Amide peaks allowing the differences in specific and non specific binding to be distinguished.

Opportunities also exist to examine protein reactions and behaviour by functionalizing Germanium or Silicon ATR elements (Schartner et al., 2013, Aamouche and Goormaghtigh, 2008). Schartner *et al.* have shown that in combination with difference spectroscopy and by using multiple reflection IREs, the functionalized Ge surface ensures sufficient binding of protein and SNR to probe protein reactions at an atomic level and can be applied to both soluble and transmembrane proteins (Schartner et al., 2013). This work is particularly exciting because it does not require the use of SEIRAS, which shall be discussed below, to achieve spectra of monolayer levels of proteins.

A recent review by Rich and Iwaki highlights some of the key ATR-FTIR methods available to analyse protein transitions. The authors describe the experimental set ups required and advantages of combining ATR-FTIR with photochemistry, electrochemistry and perfusion to explore redox reactions, ligand binding and conversions between catalytic intermediates (Rich and Iwaki, 2007).

The useful combination of photochemistry and ATR-FTIR spectroscopy was also recently demonstrated by Bouhekka & Bürgi (Bouhekka and Burgi, 2012). In this study, the effect of visible light on BSA adsorbed onto TiO_2 particles was examined *in situ* using multiple reflections ATR-FTIR spectroscopy. TiO_2 is of interest because it is regularly used as biomedical implant material (Dolamic and Burgi, 2011). In situ measurements over time allowed structural transitions to be followed through the curve fitting of the second derivative spectra, as shown in Figure 14. It was shown that under visible light illumination the Amide I band of adsorbed BSA shifted from 1653 cm^{-1} to 1648 cm^{-1} over an one hour time interval, indicating that the unordered structure within the protein had increased; this is highlighted by the red dashed line labelled Time in Figure 14 (Bouhekka and Burgi, 2012).

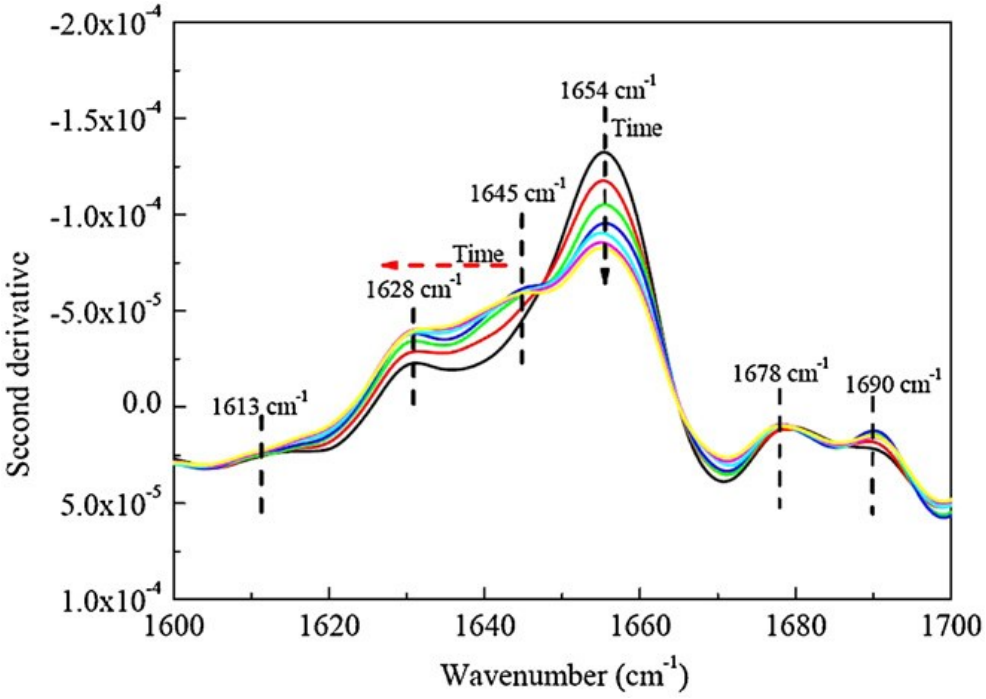

Figure 14 - Second derivative of Amide I region for corrected equilibrium adsorption spectrum of BSA on TiO_2 under rinsing by water and irradiation with visible light (VL) for around 1 h. Intervals between spectra are around 10 min (Bouhekka and Burgi, 2012).

The study of protein behaviour using ATR-FTIR spectroscopy is fundamentally limited by the signal to noise ratio that is achievable using current instruments. As such it is mostly limited to providing information on a macromolecular scale (Wang and Jiang, 2012). This does not negate the advantages such as the ease of sample preparation and the possibility for *in situ* analysis, making it a highly valuable technique for protein conformational studies. It should be noted, however, that when combined with difference spectroscopy, it does allow for an increase in sensitivity comparable with SEIRAS, allowing molecular reactions to be followed (Pinkerneil et al., 2012, Rigler et al., 2003), particularly when combined with chemically functionalized IREs (Schartner et al., 2013).

ix. Surface Enhanced Infrared Absorption Spectroscopy

Recent developments in the area of Surface enhanced infrared absorption spectroscopy (SEIRAS) overcome some of the limitations of sensitivity of detection presented by using traditional ATR-FTIR spectroscopy to study proteins. Complimentary to surface enhanced Raman spectroscopy, this technique utilises the surface plasmon effect from the interaction of light with metallic nanoparticles (Aroca et al., 2004, Ataka et al., 2010, Osawa et al., 1986, Osawa and Ikeda, 1991). These nanoparticles, mainly silver or gold, are deposited onto the surface forming metal island films which provide localised enhancement of IR absorption. It is important to note that unlike SERS, the effect of enhancement in SEIRAS is not limited to gold or silver but has also been shown for other metals (Heaps and Griffiths, 2006, Hartstein et al., 1980). It is thought that the main contributing factor to the SEIRAS effect is the polarization of the metal island films by the incident IR radiation. This induced dipole generates a local electromagnetic field and the coupling of the local electromagnetic field with that of the incident IR radiation produces one that is stronger than the incident photon field, in the vicinity of the metal islands (Nishikawa et al., 1993, Osawa et al., 1993). The dipolar moment of molecules absorbed onto the metal islands is enlarged because of this, enhancing the infrared absorption of the molecules. In addition the optical near field effect limits the enhancement to the vicinity of the metal island films, thus there is little contribution from the bulk sample to the measurement (Wang and Jiang, 2012, Osawa et al., 1993, Ataka and Heberle, 2007). Chemical interactions also contribute to the SEIRAS effect (Merklin and Griffiths, 1997b). The enhancement factor of the metal island films is highly dependent on the metal and on the morphology of the film (Nishikawa et al., 1993, Merklin and Griffiths, 1997a); those islands with greatest enhancement factors have been shown to be smaller in size than the incident radiation wavelength (Nishikawa et al., 1993, Wang and Jiang, 2012). It should be noted, that one of the major drawbacks of SEIRAS can be the loss of spectral intensity due to the metal film deposited on the IRE surface if, for example, the film is too thick. Therefore, preparation of the metal island film is very important.

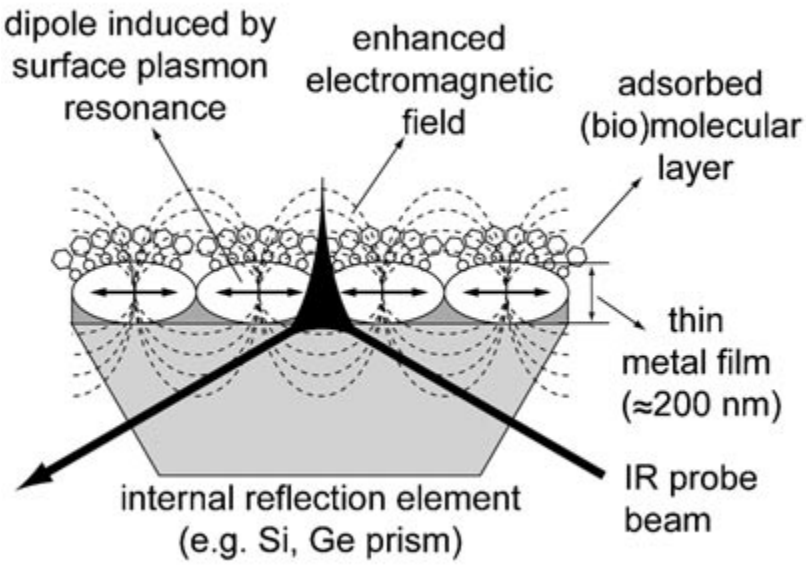

Figure 15 - Experimental set up for SEIRAS (Ataka et al., 2010).

The signal enhancement of adsorbed protein achievable from SEIRAS is in the range of 2 orders of magnitude greater than without enhancement (Ataka and Heberle, 2007). This technique was first applied to proteins by Ataka et al in 2003 (Ataka and Heberle, 2003) and further developments since have expanded its application to other protein studies (Ataka and Heberle, 2007, Ataka et al., 2010, Jiang et al., 2008, Wang and Jiang, 2012). The high sensitivity of the technique provides information from monolayer level and this is useful for examining the structure, function and assembly of molecules at the ATR interface. As with traditional ATR-FTIR spectroscopy, measurements are carried out *in situ* meaning that dynamic processes on a molecular level can be studied using SEIRAS (Hirano-Iwata et al., 2009). Figure 15 shows the set-up for a typical SEIRAS experiment (Ataka et al., 2010). It is worth mentioning that the signal enhancement drops off rapidly within 10 nm from the surface and as such it is necessary to ensure that the biological material being studied is attached to the metal island film, often achieved through chemical modification of the film itself (Ataka et al., 2010). Polarization modulation infrared reflection absorption spectroscopy (PMIRRAS) is also often used to study biological monolayers, particularly lipid monolayers (Cornut et al., 1996, Damalio et al., 2013). Whilst this method can provide information on orientation and structure of protein monolayers, the technique lacks the sensitivity to detect minute structural changes that could occur during functional studies, which is one of the main advantages of SEIRAS (Ataka et al., 2010).

Ataka's group is leading the field in applications of SEIRAS to proteins having pioneered its use to the study of membrane proteins in 2003 (Ataka and Heberle, 2003). They have shown the potential of

this method to study the catalytic action of membrane proteins driven by redox potential, in combination with electrochemistry (Ataka and Heberle, 2008). The use of difference spectroscopy allows the changes in protein spectra to be observed following an induced perturbation. The SEIRAS arrangement can be easily adjusted to allow an electric current to be applied directly to the monolayer. The analysis of SEIRAS spectra is powerful in revealing the electron transfer mechanism of redox proteins

SEIRAS has been applied increasingly to the study of membrane proteins because it has the potential to provide molecular level information on the structure, function and orientation of the membrane protein, often within the membrane itself (Ataka and Heberle, 2006, Jiang et al., 2008, Ataka et al., 2010). Again by utilising difference spectroscopy, structural changes occurring in a self assembled monolayer can be monitored and it can also be used to study hydrogen bonding interactions in nucleic acids. Ataka et al were able to follow each step of the exchange of an oriented, immobilised monolayer of detergent solubilised membrane protein into a lipid bilayer via detergent substitution and then examine the protein funtionality, using SEIRAS (Ataka et al., 2004). This could potentially be applied to the study of the reaction mechanism of any membrane protein, particularly those which are medically and pharmaceutically important.

The development of biofunctional surfaces is a growing area because of their potential for use in medical devices where ensuring the proper orientation and functionality of the protein is critical. However, one of the major challenges within the design of the surfaces is the ability to assess the functionality of the surface (Ataka and Heberle, 2007, Wang and Jiang, 2012). SEIRAS has the ability to provide molecular information on proteins in monolayers and can be performed *in situ* preserving the integrity of the monolayers. The orientation of proteins within the monolayer can be also determined from the infrared spectra (Jiang et al., 2008).

One of the major advances in the use of SEIRAS is within the field of biosensing and immunoassays to provide information on the binding mechanisms underlying biological function (Brown et al., 1998, Xu et al., 2012, Wang and Jiang, 2012). The use of gold nanoparticles can allow for the competitive adsorption of different molecules to be examined (Tsai et al., 2011). Following the formation of the gold film, a monolayer of selected antibody or antigen is deposited to form a biosensing layer. Xu *et al.* used anti rabbit antibodies (anti rIgG) from goat to study the binding mechanism of the corresponding antigen (Xu et al., 2012). A background measurement is taken after the formation of the biosensing layer meaning only molecules that specifically bind to the substrate can be detected in future measurements. SEIRAS successfully allowed the target rIgG bound onto the surface to be observed by molecular recognition (Figure 16), allowing *in situ* monitoring of the

immunoreactions (Xu et al., 2012). From the absorption data gathered it is possible to determine the reaction kinetics of the antigen-antibody binding. All of which can be achieved *in situ* without the need for additional dyes or labels and as such this method shows considerable promise for real time sensing of biomolecular bonding (Xu et al., 2012).

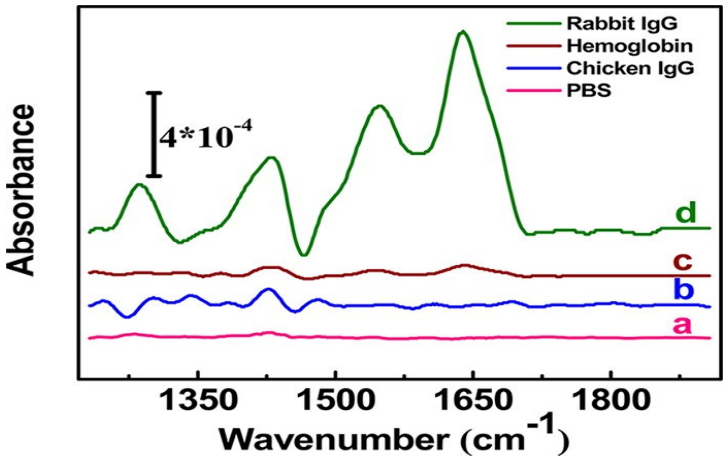

Figure 16 - (a) Background spectrum of the goat anti-rIgG modified substrate in PBS. (b) SEIRA spectrum of chicken IgG (0.3 µg/mL). (c) Hemoglobin (3 mg/mL), and (d) rIgG (0.3 µg/mL) after 35 min immunobinding to goat anti-rIgG surface. Before each injection of protein solution, the chamber was rinsed with pure PBS buffer (Xu et al., 2012).

Gold nanoparticles have a number of uses within biomedical applications and in combination with ATR-FTIR spectroscopy. In some cases, nanoparticles are used to introduce drugs into specific sites because they have a particularly good uptake within cells (Lane and Seo, 2012). Another exciting application presented by Lane and Seo demonstrated that ATR-FTIR spectroscopy can be used to distinguish between cancerous and benign cells containing gold nanoparticles (Lane and Seo, 2012). The presence of the nanoparticles within the cells allows an enhanced IR absorbance, similar to the effect seen when the surface is modified as described above. This development further emphasises the potential of ATR-FTIR spectroscopy for medical diagnostics and is not limited by the reproducibility issues still present within SEIRAS studies. This approach does not depend on the formation of metal island films, like in the SEIRAS approach, as the gold nanoparticles are present within the cells themselves but the level of signal enhancement is dependent on the concentration of nanoparticles (Lane and Seo, 2012). It is also possible to study cells using ATR-FTIR without the use of gold nanoparticles, as shall be discussed below. However, the demonstration of the enhanced IR absorbance achieved when the nanoparticles are present could have some interesting applications, particularly to study the delivery of drugs within cells.

Despite these exciting advances and the growing use of SEIRAS in protein studies, there is still potential for further development. This mainly concerns the development of a reproducible method for surface preparation and in turn, a greater understanding of the mechanism of SEIRAS (Wang and Jiang, 2012). Once this has been achieved, SEIRAS could have a much greater impact within proteomics studies and could be used more reliably within medical diagnostics. At present there is still too much uncertainty for it to be used routinely in these areas (Xu et al., 2012, Tsai et al., 2011).

IV. ATR-FTIR Spectroscopic Imaging

Detectors normally used for FTIR spectroscopy are single element detectors and when used to measure the absorbance of a sample they present a spectrum based on the average absorbance across the whole sample, unless an aperture is used. Traditionally, if one wanted to analyse the difference in absorbance throughout the sample a technique known as mapping was used. This time consuming method involves point by point analysis of the sample using an aperture and a computerised stage.

Spectroscopic imaging couples an FTIR spectrometer with an infrared array detector to allow for the simultaneous collection of the infrared spectra of a sample from multiple locations within the sample. This allows the generation of chemical images indicating locations of high absorbance at a particular wavenumber for different components within a sample. Whereas, previously these chemical images were generated by time consuming point by point mapping of a sample, the development of infrared array detectors has rapidly improved the ability to obtain infrared images. In particular, the advent of the Focal Plane Array detector enables spatially resolved chemical information to be obtained from the sample by measuring thousands of spectra from different locations within the sample simultaneously. Originally developed for military purposes, this type of detector consists of a 64 x 64 up to a 128 x 128 grid of pixels meaning at least 4096 spectra can be obtained in one single measurement. From these spectra an image of the sample can be build up based on the distribution of the absorbance of particular spectral band of the sample, showing the locations of high absorbance and hence high concentration of a particular substance (Figure 17).

Linear array detectors allow for an image to be obtained through rastering of rows of a sample in comparison with focal plane array detectors that collect the infrared absorbance from all locations within a sample simultaneously. Both approaches have advantages and disadvantages which are discussed at length elsewhere (Steiner and Koch, 2009, Kazarian and Chan, 2010, Kazarian and Chan, 2013). The main advantage of using an FPA detector is that since all the data are acquired simultaneously it is particularly suitable for the study of dynamic systems and multiple samples; this

is not the case with the linear array detector (Kazarian and Chan, 2013, Joseph et al., 2010). It should be noted, however, that linear array detectors have better signal to noise ratios and as such may be more suitable for sensitive analysis (Kazarian and Chan, 2013). In both instances, it is possible to obtain detailed chemical and spatial information from samples and the variety of sampling arrangements available means that this chemical imaging approach has opened up some exciting opportunities for protein studies.

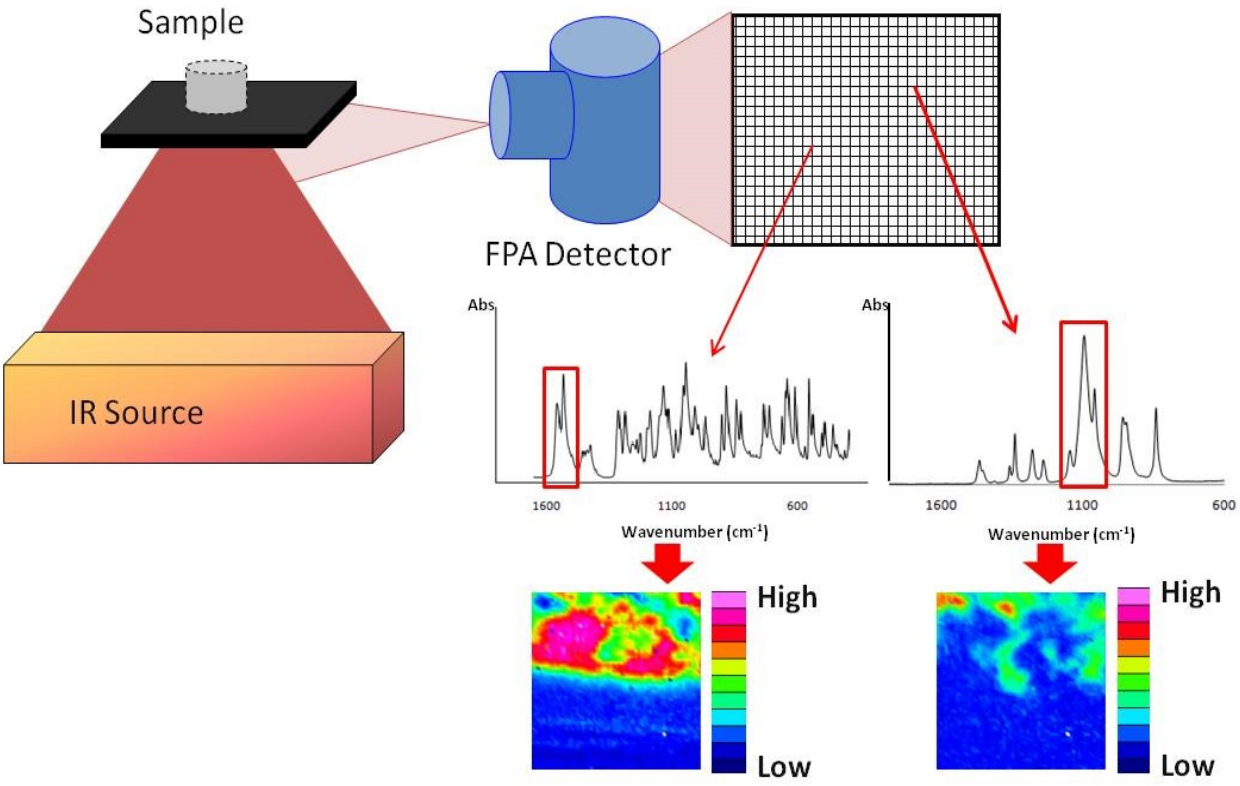

Figure 17 - Schematic demonstrating how ATR-FTIR images are obtained using an FPA detector. Figure adapted from Kazarian & Ewing 2013 (Kazarian, 2013).

An FTIR spectrometer coupled with an FPA detector can be used with several different ATR approaches to obtain chemical and spatial information from samples to varying degrees of spatial resolution. These approaches are known as Micro and Macro ATR-FTIR spectroscopic imaging and both are widely applicable to a range of sample types.

i. Micro ATR-FTIR Spectroscopic imaging

Micro ATR-FTIR combines a cassegrain type objective and an infrared microscope operating in reflection mode, shown in Figure 18. The angle of incidence of the cassegrain objective is typically 30° meaning a Germanium ATR element (n = 4) is used to ensure total internal reflection of the IR beam occurs. The high refractive index of the Germanium element combined with the IR microscope means that spatial resolution of approximately 4 µm can be achieved (Kazarian and Chan, 2010).

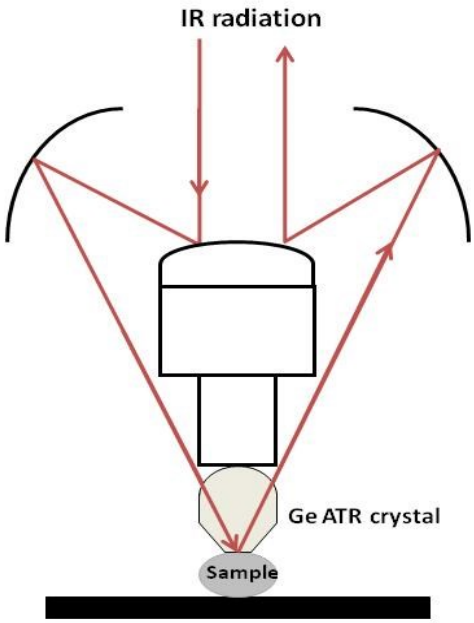

Figure 18 - Schematic of Micro ATR optics.

The spatial resolution of an imaging system using a microscope objective is diffraction limited and can be described by the Rayleigh criterion (Chan and Kazarian, 2003) (Equation 10). This defines the distance required between two points for them to be just resolved.

$$r = \frac{0.61\lambda}{NA}$$ **Equation 10**

NA is the numerical aperture of the system and λ is the wavelength of light. The minimum distance for which two objects are fully resolved is 2r. The numerical aperture of the system can be described by Equation 11:

$$NA = n \sin \theta$$ **Equation 11**

Where n is the refractive index of the objective and θ is equal to half the angular aperture. Therefore, from the above equations, it can be seen that the theoretical spatial resolution of a system is dependent on the wavelength of infrared light, angle θ and the refractive index of the IRE material, since this is a factor of numerical aperture. However, in practice, the actual spatial resolution achieved may be two to four times lower that the theoretical value because of optical aberrations (Kazarian and Chan, 2010).

The field of view with this approach is limited and the size of the imaging area has been measured at approximately 64 µm x 64 µm. Despite this small imaging area, Micro ATR-FTIR spectroscopic imaging has great potential for the study of biomedical materials where it has been employed to analyse cross sections of hair (Chan et al., 2005), aorta and arteries (Palombo et al., 2009) as well as chemically image live cancer cells (Kuimova et al., 2009). It has also successfully been used to analyse cross sections of paint for art conservation (Spring et al., 2008).

A recent review by Miller et al discussed the application of FTIR Microspectroscopic imaging to the study of protein aggregation within cells (Miller et al., 2013). The method discussed in the review mostly concentrates on operation in transmission mode and using a synchrotron source. Whilst the use of synchrotron source can allow higher SNR to be achieved and can allow sub-cellular information to be obtained from a sample (Nasse et al., 2011), it is still currently limited to use with transmission mode, which, as previously discussed, requires a very short path length for aqueous samples. Chan *et al.* showed that Micro ATR imaging can provide high spatial resolution without the need for a synchrotron source by measuring a cross section of human hair (Figure 19) (Chan et al., 2005). The spatial resolution achievable with Micro ATR-FTIR imaging is dependent on the numerical aperture of the system and wavelength of light which, when combined with a Germanium ATR crystal of high refractive index means that high spatial resolutions can be reached, in comparison with transmission that uses objectives with lower numerical apertures (e.g. four times lower) (Chan et al., 2005, Kazarian and Chan, 2010). Micro ATR-FTIR imaging has previously been demonstrated allowing the measurement of live and fixed cells without the need for synchrotron source (Kazarian and Chan, 2013, Wrobel et al., 2012).

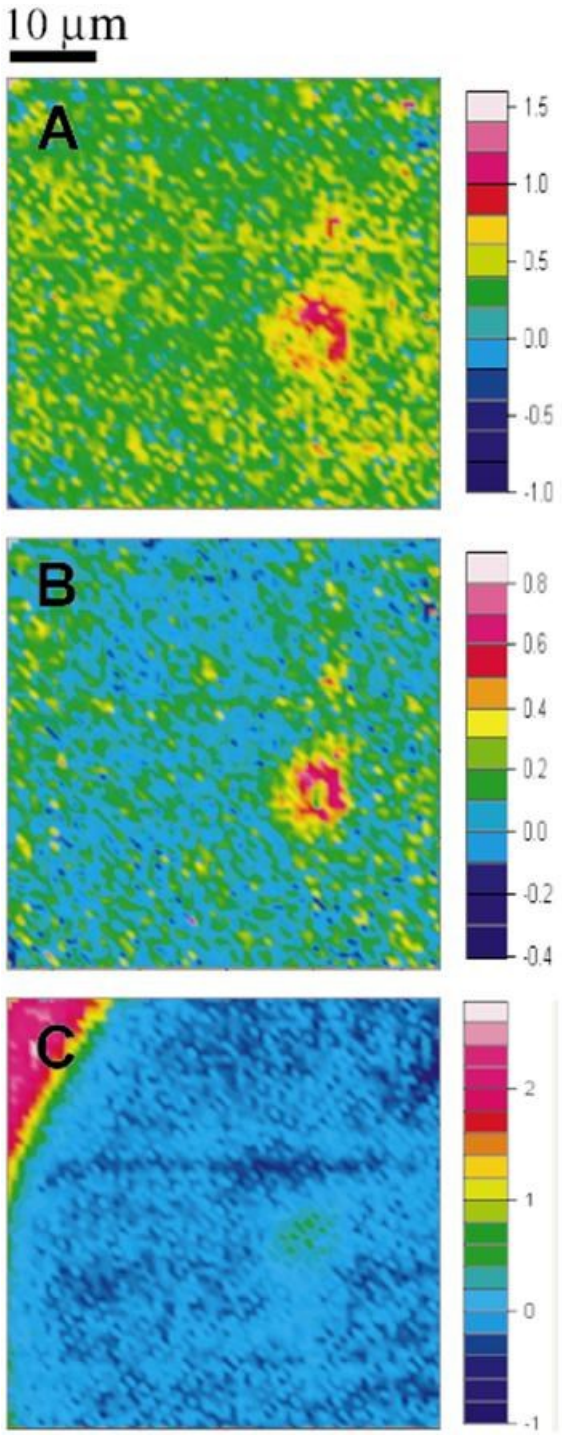

Figure 19 - ATR-FTIR images of cross section of human hair, generated by plotting absorbance at (A) 2925 cm^{-1}, (B) 2855 cm^{-1} and (C) 1734 cm^{-1}; the colour scale bar shows the value of the integrated absorbance for each band. Image size is 50 x 50 μm^2 (Chan et al., 2005).

ii. Macro ATR-FTIR Spectroscopic Imaging

Macro ATR-FTIR spectroscopic imaging is performed without use of a microscope and instead it couples an FTIR spectrometer, equipped with an inverted prism ATR accessory, with a focal plane array detector. The detector size can be varied between 64 x 64 pixels up to 128 x 128 pixels allowing between 4096 to 16384 spectra to be obtained from the sample in one measurement. This imaging approach can be used with different ATR accessories which allows for a range of different imaging areas and spatial resolutions. These ATR accessories are single reflection inverted prisms which make them suitable for imaging and for easy sample handling; samples can be deposited directly on the top surface of the inverted prism as required. Opportunities exist to combine accessories with heated ATR crystals, allowing for in situ studies of the effect of temperature or for more accurate control of temperature during experiments. The range of fields of view and spatial resolution which can be achieved using different ATR-FTIR spectroscopic imaging accessories combined with a 64 x 64 pixel FPA detector are summarised in Table 2.

The simplest Macro ATR imaging accessory (Figure 20) can be combined with a Zinc Selenide, Germanium or Silicon IRE, depending on the sample being analysed. The optical design of this commercially available Macro imaging sample compartment has a magnification of 1:1 meaning the imaging field of view is the same size as the detector with an image distortion in Y-direction due to geometry of the inverted prism IRE crystal. This image distortion occurs because the reflected light is collected at an angle to the image plane but can be accounted for by multiplying the length of the y-axis by a correction factor. For a collection angle of 45°, the y-axis should be multiplied by a correction factor of 1.4 (Chan and Kazarian, 2003). Therefore, a 64 x 64 pixel FPA detector with a pixel size of 40 µm will have an imaging field of view of approximately 2.56 mm x 3.58 mm.

Table 2 - Summary of fields of view and spatial resolutions possible with different ATR-FTIR accessories (when using a 64 x 64 pixel FPA detector).

Accessory	Field of view (mm x mm)	Estimated spatial resolution (µm)
Macro ATR (Figure 20)	2.6 x 3.6	40
Diamond Golden Gate (Figure 21)	0.64 x 0.64	15 - 20
Variable Angle accessory (VeeMax II accessory)	3.9 x 5.5	150
Expanded field of view (Figure 22)	15.4 x 21.5	500
Micro ATR with Ge crystal (Figure 18)	0.06 x 0.06	4 - 10

Diamond offers some major advantages over other infrared transparent materials in that it is much stronger and hence less easily damaged. However, until recently it was not used for Macro ATR imaging because the cost of a large diamond prism compatible with the large sample compartment would be excessive. Now, diamond ATR accessories, such as The Golden Gate, are commercially available for imaging purposes. The Diamond Golden Gate accessory uses lenses to focus and collect the IR light, shown in Figure 21, giving an imaging field of view of 640 µm x 640 µm and spatial resolution in the range of 15 – 20 µm (Kazarian and Chan, 2010).

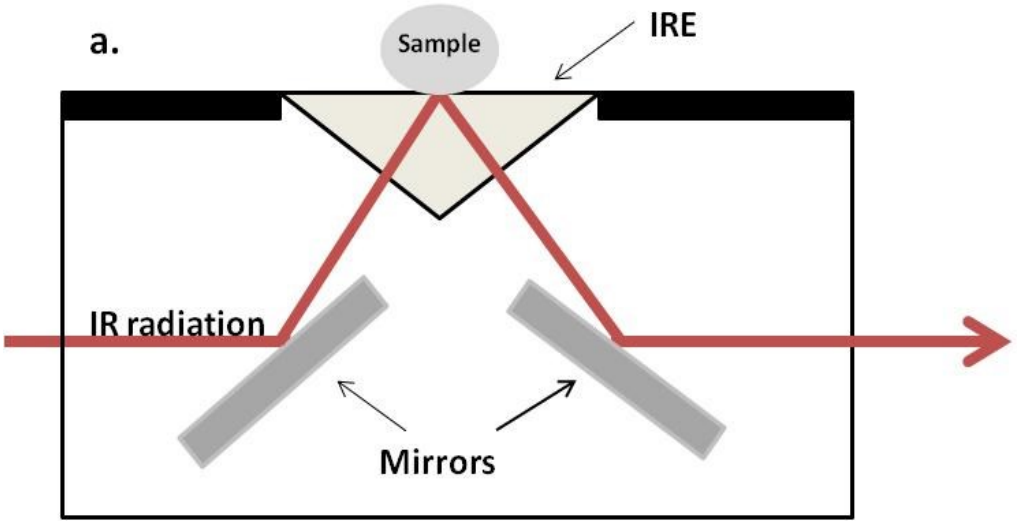

Figure 20 - Macro ATR-FTIR imaging accessory showing IR light directed into IRE using mirrors.

Macro imaging with a diamond accessory has been used extensively in pharmaceutical studies where good contact is required for the analysis of tablet compaction and dissolution (Kazarian, 2013). It also offers the opportunity to carry out depth profiling of samples by varying the angle of incidence and hence the depth of penetration (Chan and Kazarian, 2007, Frosch, 2010). This is achieved by fitting an aperture to the lens, effectively blocking portions of the IR beam and restricting the IR beam to a certain angle of incidence.

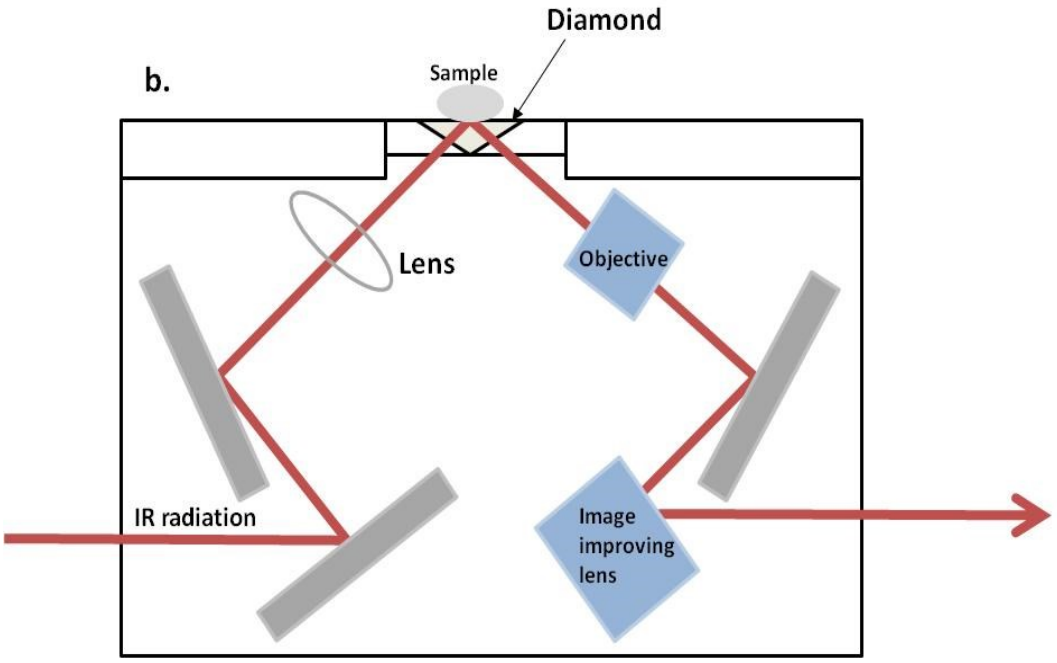

Figure 21 - Diamond Imaging Golden Gate ATR accessory showing IR beam directed and focused into Diamond IRE using mirrors and lenses.

The variable angle imaging accessory can also be combined with a Germanium, Silicon or Zinc Selenide but consists of additional lenses allowing the angle of incidence of the IR beam to be selected. This accessory is known as the VeeMax II Pike accessory and due to the optics has a slightly larger imaging field of view than with the standard Macro imaging accessory. The spatial resolution achievable is also much lower at approximately 150 µm. One can observe, from Table 2 that as the imaging field of view increases there is a sacrifice in spatial resolution. For example, the expanded field of view accessory, shown in Figure 22, has concave lenses to increase the area of illumination of the IR beam hence increasing the field of view. In this set up the maximum achievable spatial resolution is approximately 500 µm. When spatial resolution is not a high priority, the accessories with a large field of view can be very advantageous for high throughput studies, where a large number of samples can be deposited on the surface for simultaneous analysis. However, opportunities exist for high throughput analysis through the combination of Macro imaging and mapping (Chan and Kazarian, 2008). This allows for an increase in the number of samples studied but without the reduction in spatial resolution associated with larger accessories.

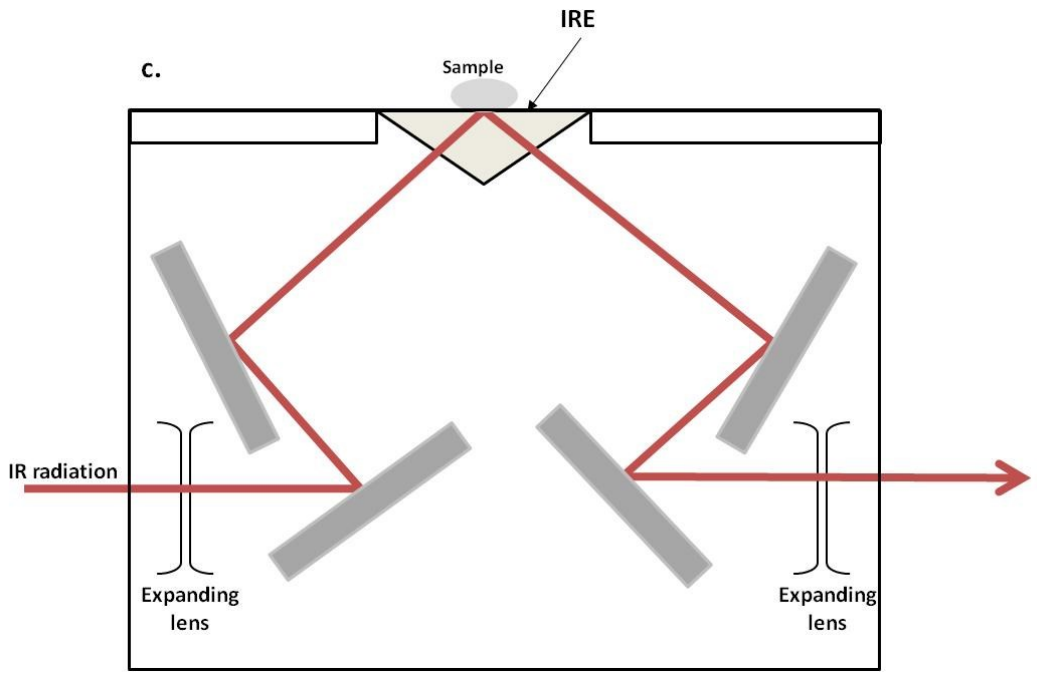

Figure 22 - Expanded field of view Macro ATR imaging accessory showing IR beam expanded by lenses and directed at IRE by mirrors.

iii. High Throughput applications of ATR-FTIR spectroscopic imaging

ATR-FTIR spectroscopic imaging in its Macro and Micro modes has been applied across many different areas of research, from pharmaceutical tablet analysis (Wray et al., 2008, Kimber et al., 2011, Kazarian, 2013), art conservation (Joseph et al., 2010) through to understanding the fouling in heat exchangers (Tay and Kazarian, 2009). It has also been applied in several biomedical studies such as to the study of arthrosclerosis plaques in arteries (Palombo et al., 2009) and drug permeation through skin (Andanson et al., 2009). The most relevant applications, which shall be highlighted here, focus on the inherent capacity of this approach for high throughput (HTP) studies (Chan and Kazarian, 2005, Chan et al., 2007). High throughput studies allow for the analysis of multiple samples simultaneously. This can save both time and money by reducing the amount of sample required and also the time spent on analysis, especially in optimisation trials. In the case of Macro ATR-FTIR spectroscopic imaging, high throughput studies have been carried using either a PDMS or wax grids defining multiple areas for sample deposition on the surface of an IRE used. The wax grid can be printed directly onto the measuring surface of an IRE using a microdroplet system (Autodrop, Microdrop, Germany). This system can also be used for the deposition of nanolitre volumes of samples onto the surface. Chan *et al* successfully applied this method to study pharmaceutical formulations without using a grid (Chan and Kazarian, 2005) and with a wax grid to study protein crystallisation (Chan et al., 2009).

This approach was applied to the crystallisation of proteins as a potential means of optimising crystallisation conditions (Chan et al., 2009). Protein crystallisation is seen as an important step in structural proteomics studies (McPherson, 2004) and the use of various high throughput approaches to optimise this step have had major impact on the field (Saridakis, 2012). A common method of protein crystallisation is microbatch crystallisation where the crystallisation occurs in aqueous medium placed under oil. This method can be used directly on the surface of an inverted prism where PDMS wells are used to contain the oil. A protein and precipitant sample can be deposited prior to or after the oil is in place, since the protein/precipitant solution is less dense than the oil, the drop of the solution will then displace oil on the surface of the ATR prism allowing it and not the oil to be measured by ATR-FTIR imaging. For HTP studies, a wax grid was printed on the surface allowing up to six different crystallisation conditions to be studied simultaneously. For multiple samples, the protein solutions were deposited after the oil was in place to prevent evaporation from the solution drops whilst the deposition takes place, although it does reduce the degree of control one has for positioning the samples (Chan et al., 2009).

Figure 23a shows the crystallisation of Lysozyme within one drop of protein and precipitant solution on a ZnSe ATR crystal where the location of crystals is determined from the plot of the distribution of the integrated Amide II band. When the optical image in Figure 23b is overlaid with the infrared image, as in Figure 23c, it can be seen that the locations of the crystals in the ATR image correspond almost entirely with those in the optical image, confirming that this technique is successfully identifying protein crystals. The use of Macro ATR-FTIR imaging to optimise for protein crystallisation conditions is advantageous as it allows one to determine if crystals formed are indeed protein rather than salt crystals without moving or destroying the crystals, a common problem in crystallisation studies (Chan et al., 2009). Possibilities exist to expand this to study to studies of many more samples simultaneously and to proteins that are more challenging to crystallise and study, as shall be discussed in Chapter 5.

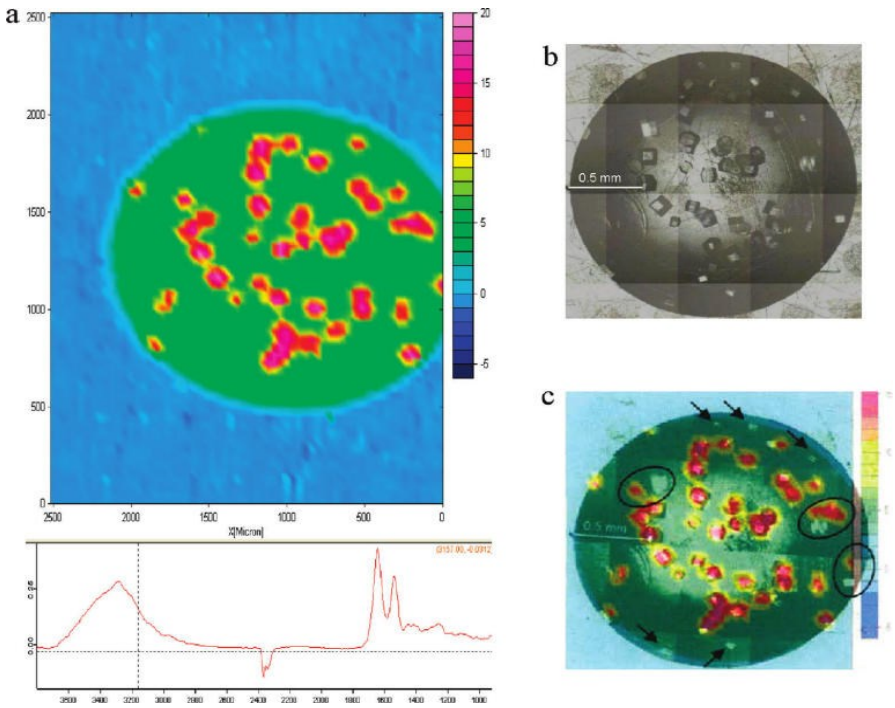

Figure 23 - (a) ATR-FTIR image (imaged area is approximately 2.5 × 3.6 mm^2) of the protein crystal formed on the measuring surface 20 h after the introduction of the crystallizing agent. Red represents high protein concentration. The visible image (b) shows the protein crystals formed coincide well with the location of the red spots on the ATR-FTIR image. (c) Result of overlaying images (a) and (b). Five out of 50 crystals (highlighted with arrows) were not captured in the ATR-FTIR image and 3 crystals (circled) were mislocated (Chan et al., 2009).

Recent advances in the area have also seen the combination of Macro imaging and microfluidics (Chan et al., 2010, Chan and Kazarian, 2012). Using a computerised wax printing device, microfluidic channels can be printed either directly onto the surface of an ATR element or onto transmission slides. This has been applied to the study of reactions (Figure 24) (Chan and Kazarian, 2012) and cells (Chan and Kazarian, 2013). However as interest in protein crystallisation using novel methods such as microfluidics continues to be explored (Yu et al., 2012, Li and Ismagilov, 2010), this method could easily be adapted for this and given the advantages of allowing proteinaceous crystals to be identified in situ without additional labels, this presents a future application for the field. Using transmission FTIR, work has been carried out to study protein conformational changes due to pH in microfluidic flows (Prim et al., 2011), there is potential for this to also be applied using FTIR imaging. It should also be noted that studies of live cells in microfluidic devices in situ using FTIR spectroscopic imaging in transmission mode has also became possible very recently due to new developments in methodology (Chan 2013).

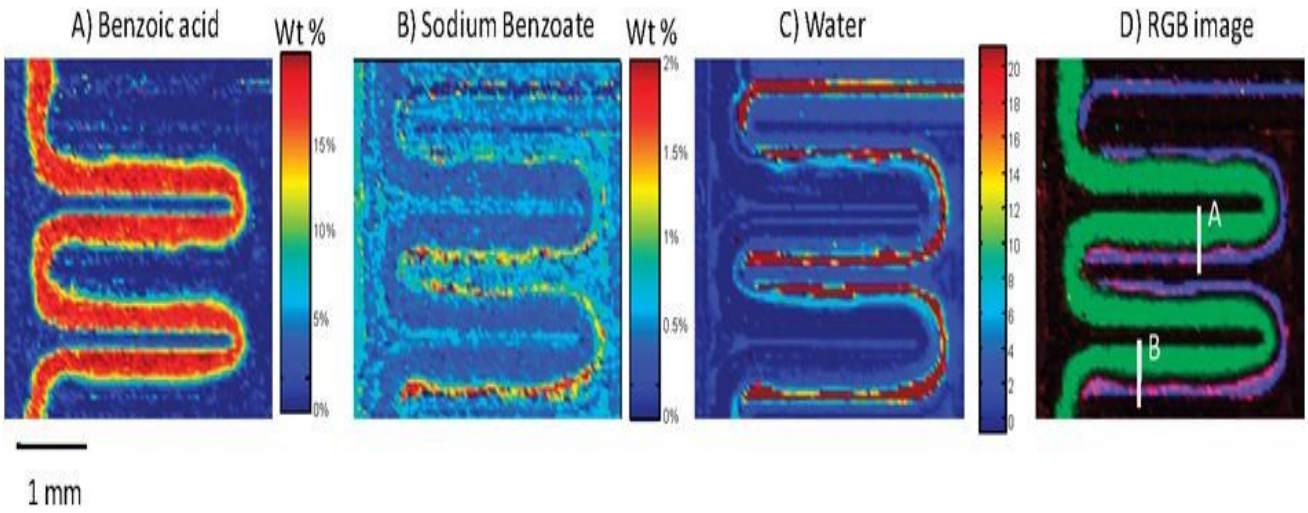

Figure 24 - ATR-FTIR imaging results from a microfluidic device with a wide plain T-junction. (A) FTIR image showing the concentration (wt %) distribution of benzoic acid in the channel. (B) FTIR image showing the concentration (wt %) distribution of sodium benzoate in the channel. (C) FTIR image showing the distribution of water in the channel. Colour represents local concentrations according to the scale shown on right of the images except water which has an arbitrary colour scale. (D) An RGB image showing the overlapped images of panels A – C. Benzoic acid is presented in green, sodium benzoate is presented in red and water is presented in blue (Chan and Kazarian, 2012).

Chapter 3 - Experimental instrumentation

I. FTIR imaging system

The work presented in this thesis made use of FTIR spectrometers coupled with a Large Sample Compartment. The majority of the work was carried out on a Varian 670-IR (Agilent) spectrometer with a Large Sample Compartment for housing ATR imaging accessories and an FPA detector (Figure 25). Some experiments were carried out on similar Bruker instruments where such compartment is called a Macro Chamber. The instrument used and the settings applied are specified in each chapter to avoid confusion. All the spectrometers used were purged with dry air. This acts to reduce the presence of water vapour and carbon dioxide within the instrument and is necessary to maintain constant background levels which helps to preserve the quality of the spectra measured. The purge dry air supply also powers the air bearings of the interferometer.

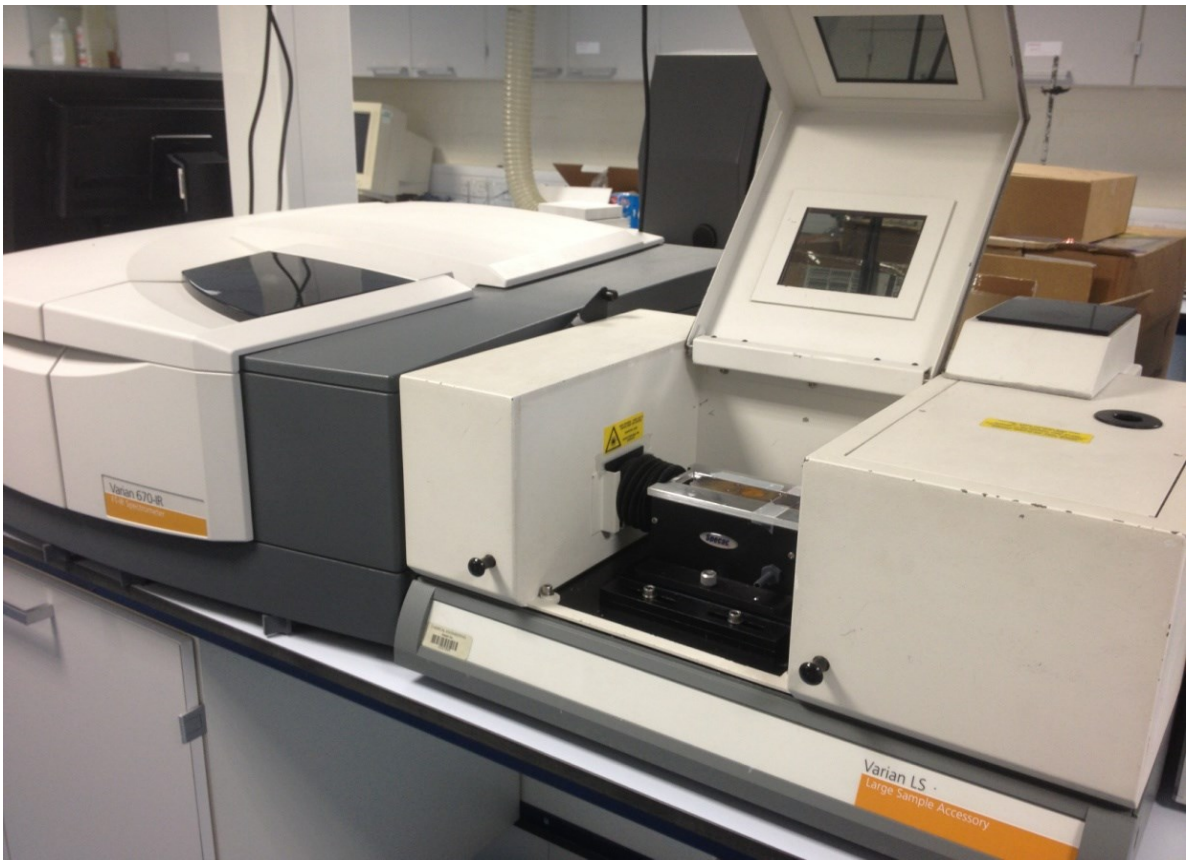

Figure 25 - Varian 670-IR with Large Sample Compartment. A Macro ATR imaging accessory with a ZnSe crystal is shown in the Large Sample Compartment.

FPA detectors were originally developed for military purposes but have been available for use in civilian research for over 15 years (Figure 26). The maximum size of the FPA detector is 128 x 128 pixels but this can be changed to either 64 x 64 pixels or 96 x 96 pixels depending on the requirements of the experiment and the imaged size used in the different areas of work presented in this thesis is specified in each chapter. The detector is liquid nitrogen cooled and the ATR element in the Large Sample Compartment is aligned to ensure optimum illumination of IR light on the detector. The spectral range of the FPA detector is 4000 - 900 cm^{-1}.

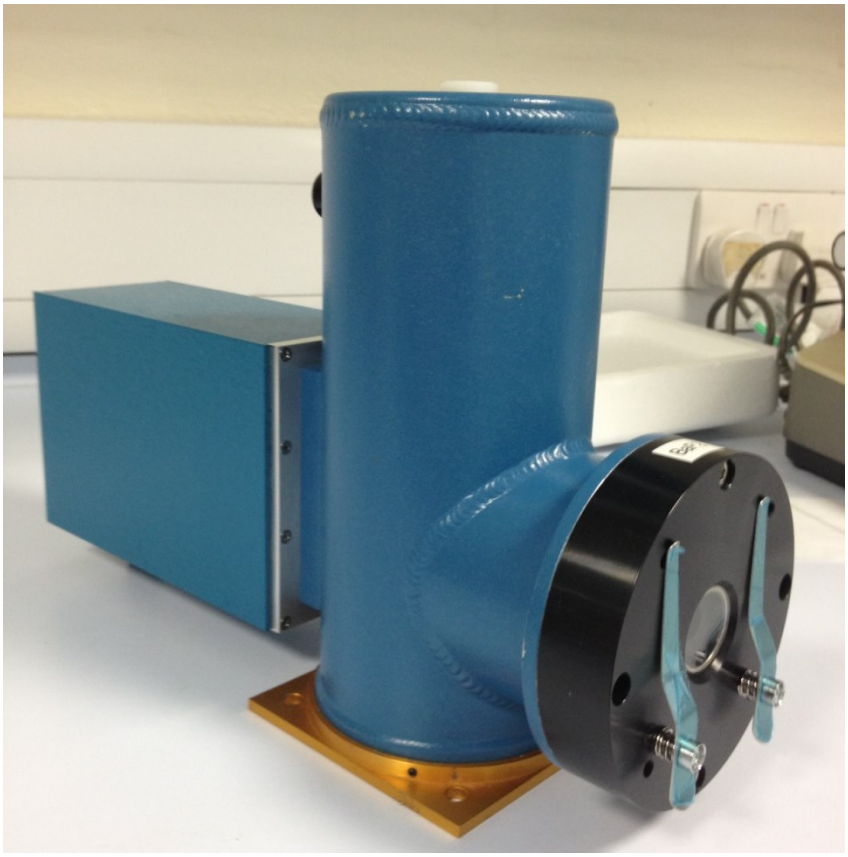

Figure 26 - Focal Plane Array (FPA) detector.

The alignment of the ATR imaging accessory in the Macro chamber is very important, care must be taken to ensure the optics are focused and the illumination of the FPA detector is at a maximum. Poor alignment will negatively impact the spatial resolution and quality of images as well as the S/N ratio of spectra obtained. Alignment is achieved through the use of the live imaging window of Agilent Resolution Pro software (or OPUS for Bruker systems) and by finely adjusting the optics of the accessory being used. This program gives a live feed of the light reaching the detector and allows for adjustments to be easily made regarding signal, illumination area and focus as well as to aid in the deposition of samples. Figure 27 shows the live imaging window for 128 x 128 pixels FPA with ZnSe in a Macro imaging accessory with a finger pressed onto the ZnSe surface to check the focus of the system.

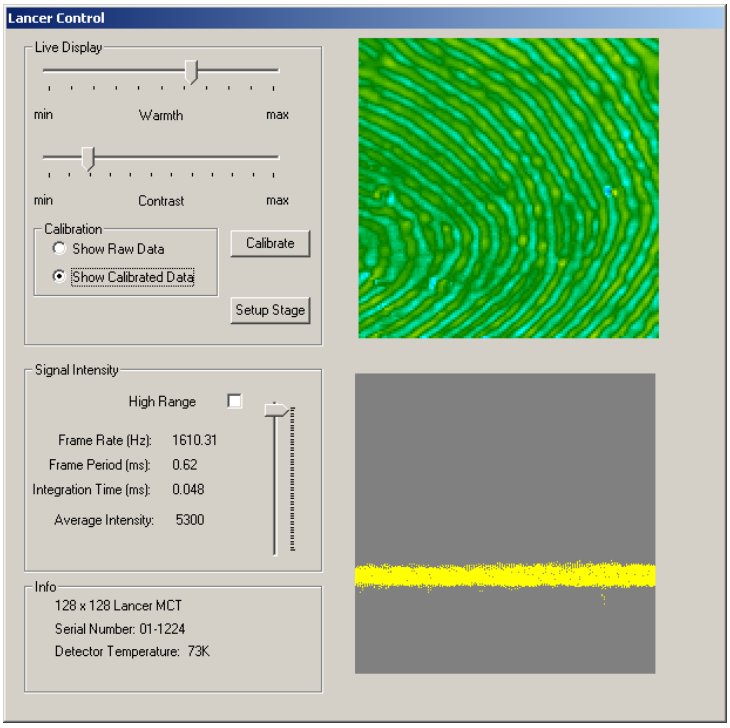

Figure 27 - Live imaging display window of Agilent Resolution Pro software with finger pressed onto ZnSe crystal to check focus.

i. Micro ATR-FTIR imaging system

The Micro ATR-FTIR imaging system consists of an infrared microscope attached to a standard FTIR spectrometer (Figure 28a). The IR microscope consists of a cassegrain objective, a removable Germanium ATR crystal mount (Figure 28b) and houses an FPA detector. The option also exists to carry out singe spectrum measurements using the single element MCT detector, also present in the IR microscope, as well as to carry out imaging measurements in transmission mode, although this was not used in the work of this thesis. As discussed in section IV.i. of Chapter 2, the field of view in this arrangement is 64 x 64 μm^2 with a maximum spatial resolution of 3 – 4 µm. In normal operation, the area of interest within a sample is first located without the Ge crystal in place and the microscope operating in visible light mode. Following this the Ge crystal slides into the ATR objective and the stage is raised until good contact between the sample and the Ge crystal is obtained; contact determined by observing the live imaging display window of Resolution Pro software.

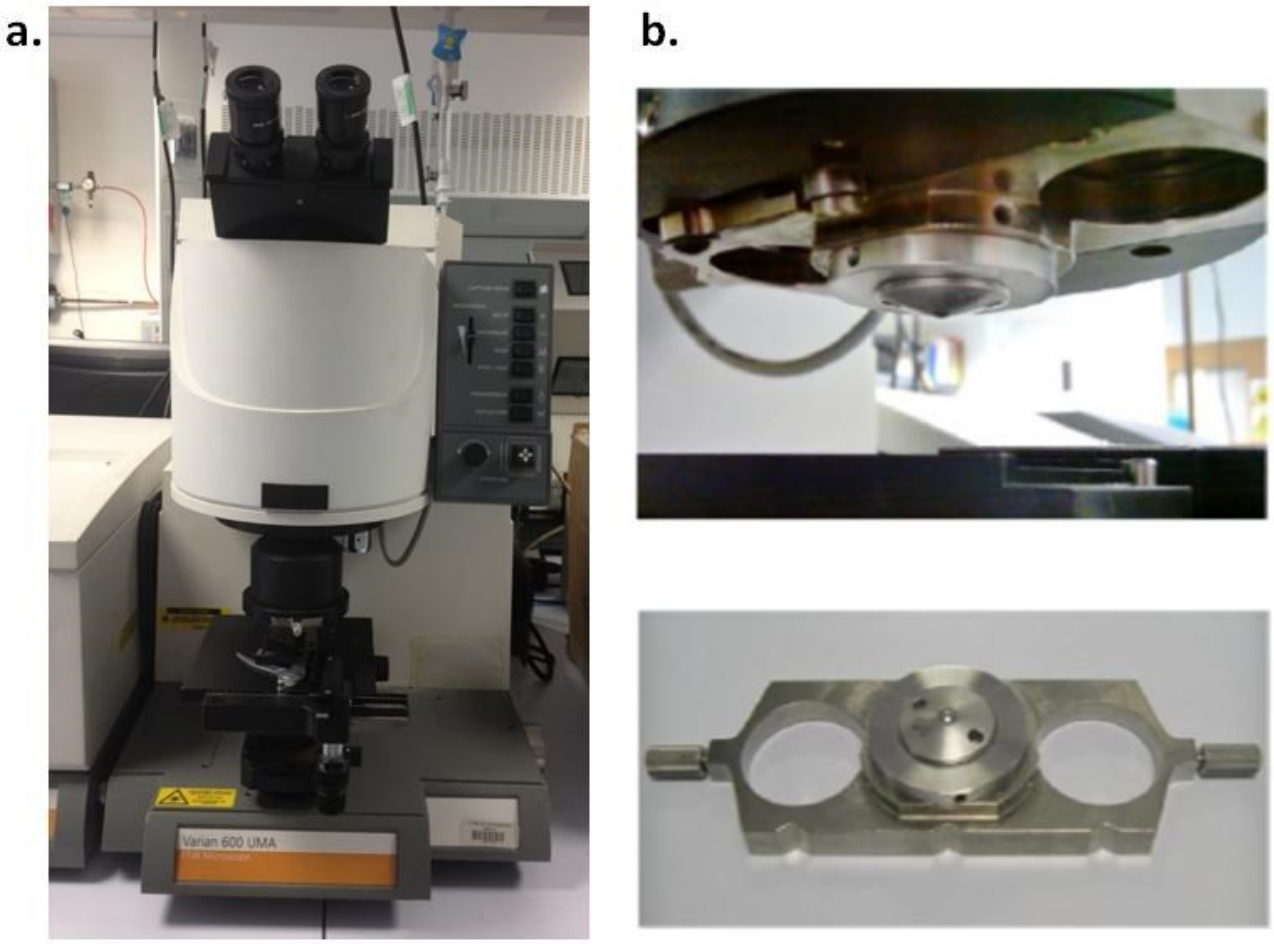

Figure 28 - a) Varian 600 UMA IR microscope with b) removable Germanium objective.

ii. ATR imaging accessories

The range of accessories along with the field of view and spatial resolution achievable with each one was described in Chapter 2 section IV.ii. However a brief summary of the particular accessories used within the work of this thesis shall be presented here.

The diamond imaging Golden Gate ATR accessory (Figure 29a) features only in the initial investigation into the use of variable angle apertures to reduce the effects of anomalous dispersion. An imaging field of view of this accessory ca. 640 x 640 μm^2 and spatial resolution of ca. 15 µm is achieved through the use of mirrors and ZnSe/Ge lenses that focus the light onto the diamond ATR crystal. The size of the diamond crystal on the Golden Gate accessory limits its use to a FPA detector size of 64 x 64 pixels.

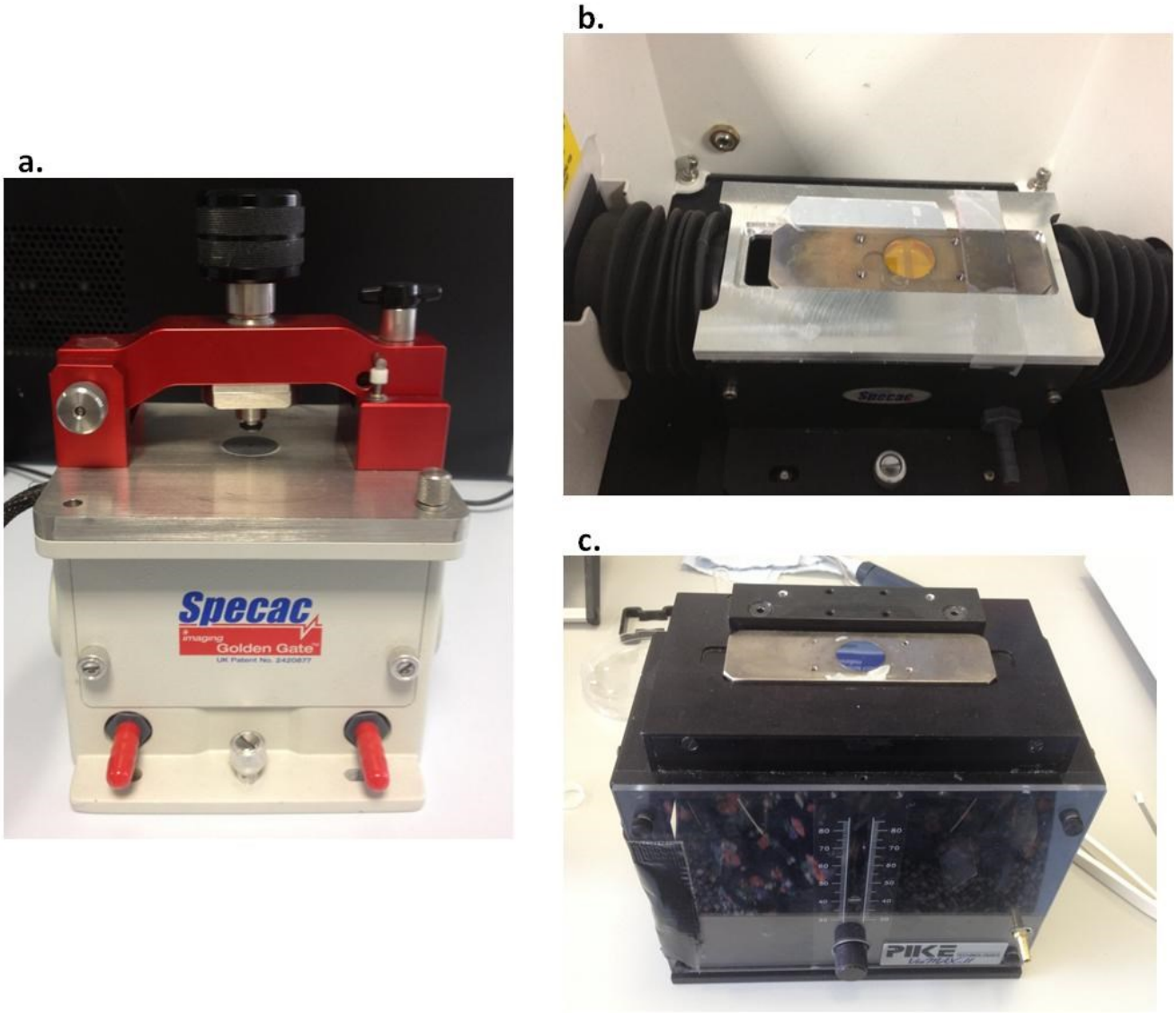

Figure 29 - Macro ATR-FTIR imaging accessories used in this work, a) Diamond imaging Golden Gate, b) Macro ATR-FTIR imaging accessory with ZnSe ATR crystal, c) Veemax II variable angle accessory with Si ATR crystal.

The Macro ATR-FTIR imaging accessory is shown in Figure 29b, this set up can be combined with various large IRE's such as ZnSe (shown in picture), Silicon and Germanium. Silicon and ZnSe were employed in this work. The field of view with this accessory is determined by the size of the FPA detector and the spatial resolution is limited by the pixel size, 40 µm, because there are no focusing optics involved. The Veemax II variable angle accessory (Pike) is shown in Figure 29c. This accessory allows the angle of incidence to be changed by turning the dial present on the front, which in turn alters the position of the mirrors enclosed within. The field of view is slightly expanded because of the expanding optics but again is also dependent on the number of pixels of the FPA detector and the spatial resolution is lower at 150 µm. The expanding optics results in the projected area for each pixel being increased and also reduces the numerical aperture of the system, thus reducing the spatial resolution achieved by this accessory.

II. Microdrop printing system

The Autodrop system (Microdrop, Germany) was used for experiments to print wax grids onto the surface of ATR crystals, thus dividing the measuring area into well defined separate sample areas and allowing for multiple samples to be studied simultaneously. The Autodrop system is an automated dispensing machine (Figure 30a); it consists of a platform with capacity for four dispensing heads (Figure 30b) and cameras which are used for positioning and drop size calibration purposes. The dispensing heads (Figure 30c) consist of a sample chamber and nozzle, both of which can be heated. The size of the drop deposited by the head is controlled by setting the voltage and pulse width within the Microdrop computer settings. The voltage controls the speed at which a droplet is forced through the nozzle and the pulse width controls the time over which this occurs, thus the size of drop dispensed can be varied according to the application. The frequency at which the drops are dispensed can also be selected. The nozzle head is 100 µm in diameter and typical drop volume is in the range of approximately 90 – 380 pl. The pattern of dispensing can be controlled by programming the computer with a macro instructing it on the x, y, z – direction and distances to travel.

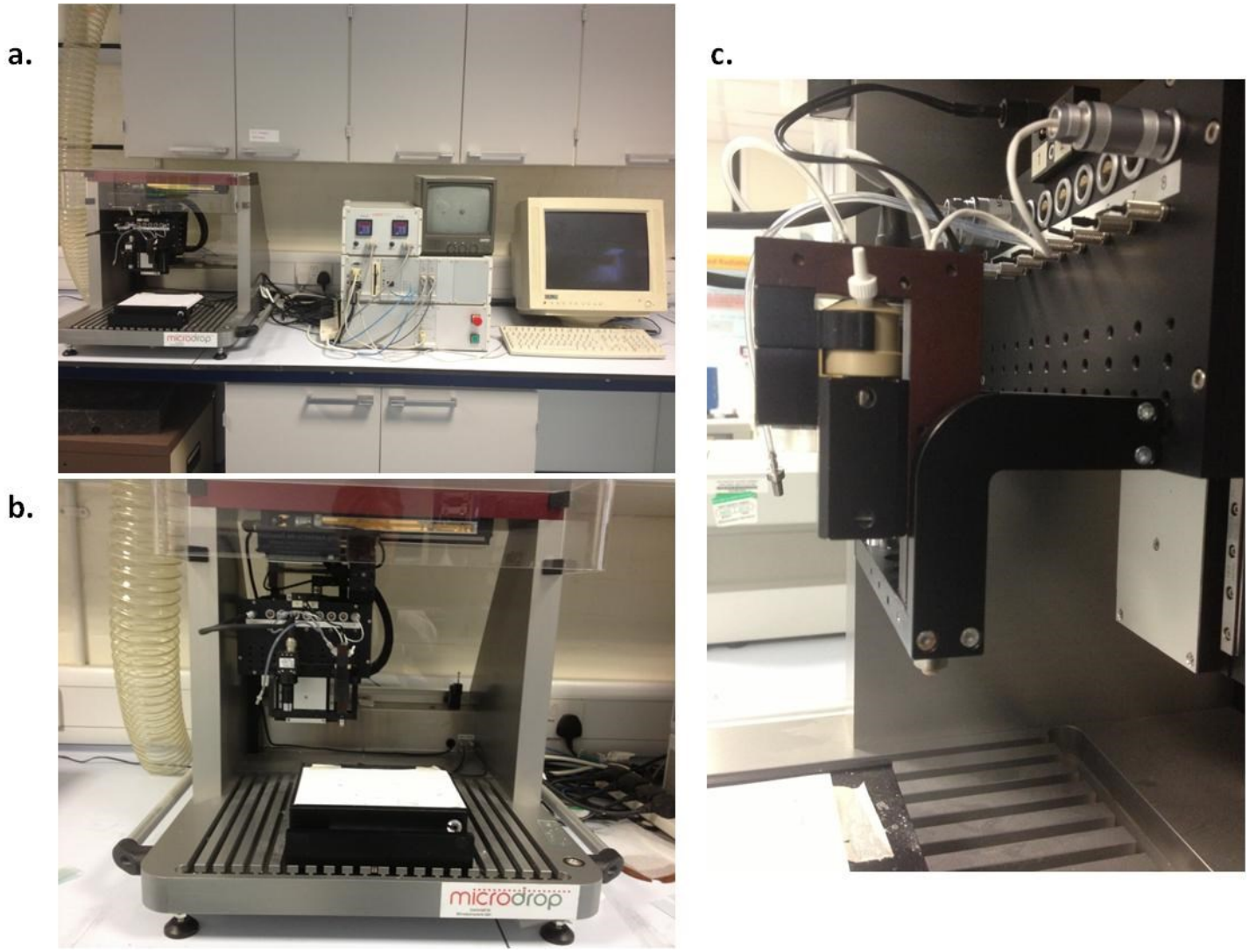

Figure 30 - Autodrop dispensing system (Microdrop, Germany): a) The complete setup of the Autodrop system consisting of dispensing platform, computer and heating system with screen for camera view, b) close up of dispensing platform, c) close up view of dispensing head showing sample chamber and nozzle.

In addition to printing wax grids for high throughput studies, this system is increasingly being applied in microfluidic research, primarily in Kazarian's research group where wax microfluidic channels can be printed directly onto the ATR crystals and transmission slides (Chan et al., 2010). It can also be used for the direct deposition of samples, where the use of multiple nozzles containing different formulations allows for additional high throughput applications (Chan and Kazarian, 2005).

Chapter 4 - Application of variable angle Diamond ATR-FTIR imaging to reduce the effects of anomalous dispersion in protein studies

I. Introduction

The diamond Golden Gate imaging ATR accessory has been extensively used across a range of applications. It was considered for use within work in this thesis for applications to protein studies. However, due to anomalous dispersion (AD), spectral band shifts can occur when using diamond as an ATR element compared with the use of Germanium or measurements in transmission (Figure 31). This section examines the use of movable apertures to increase the angle of incidence of IR light in order to determine their effectiveness at reducing the effect of anomalous dispersion.

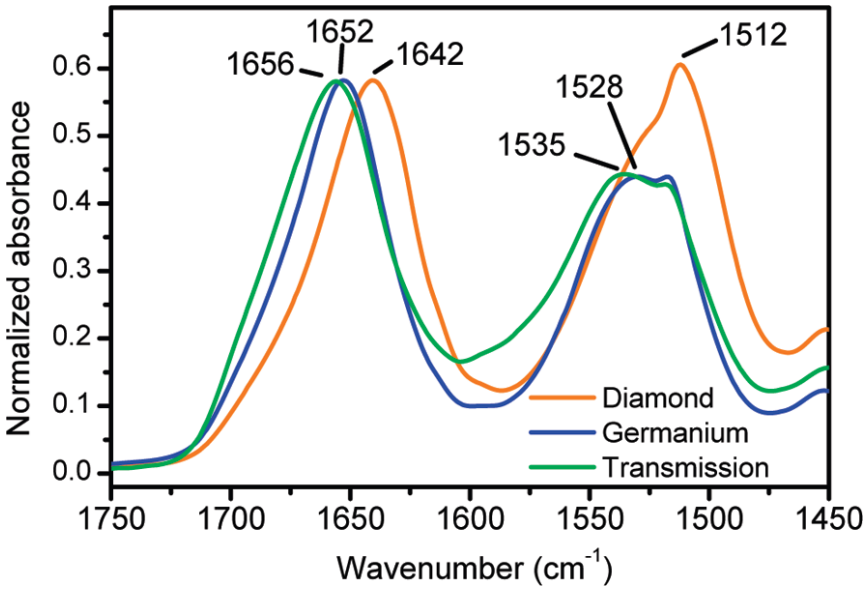

Figure 31 - Transmittance spectrum and s-polarized diamond and Germanium ATR spectra of a *B. mori* silk fibroin film. The spectra were normalized so that the peak heights of the Amide I bands were equal. The Germanium ATR spectrum has been multiplied by 5.98 with respect to diamond ATR (Boulet-Audet et al., 2010).

As discussed in Chapter 2, the nature of ATR spectroscopy is such that the measured spectra can be strongly affected by the anomalous dispersion of refractive indices (AD), causing a shift of spectral bands. Anomalous dispersion results in a Z-shaped variation in the refractive index of a material as a function of wavelength, this is shown in Figure 32 for poly(pheny methyl siloxane), compared to normal dispersion which displays a monotonic decrease in refractive index as a function of wavelength. The phenomenon of AD is much more apparent at angles of incidence closer to the critical angle for a system (Harrick, 1967).

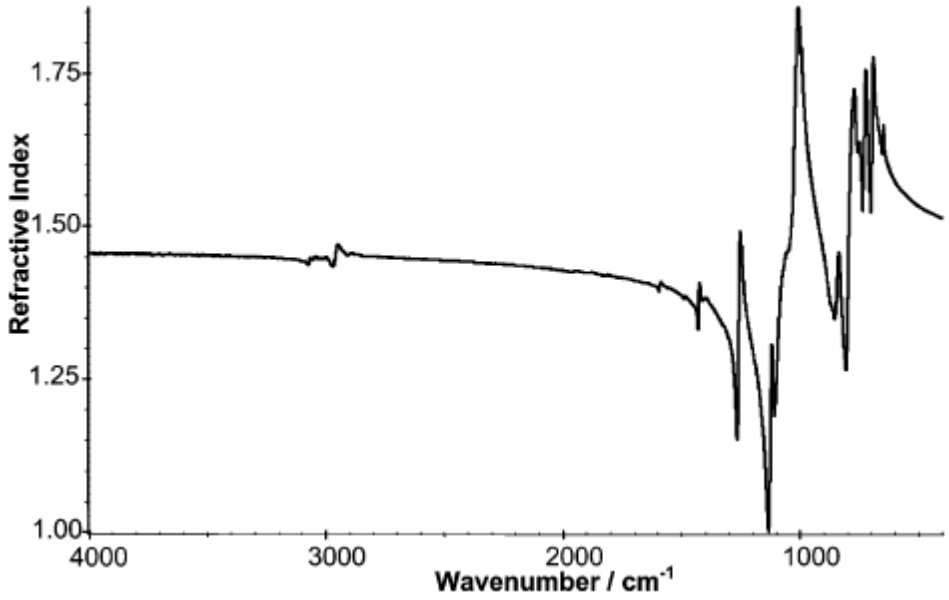

Figure 32 - Variation in refractive index (n_2) with wavenumber for poly(pheny methyl siloxane) (Averett et al., 2008).

As seen from Equation and Equation , derived by Harrick, the effective pathlength for polarized light is highly dependent on the refractive indices of the sample and the IRE, the angle of incidence and wavelength of light (Harrick, 1967). At the higher energy side of an absorbance band, the refractive index of the sample is at its smallest value meaning the effective pathlength is shorter whereas at the other end of the band, the refractive index is largest making the effective pathlength longer. As a result, an absorption band will shift towards lower energy wavenumbers compared to transmission (Hancer et al., 2000, Harrick, 1967). This effect is most noticeable for strong absorption bands.

Equation 8 – Effective pathlength for s-polarized IR light.

$$d_{e,s} = \frac{\lambda\left(n_2/n_1\right)\cos\theta}{\pi\left[1-\left(n_2/n_1\right)^2\right]\left[\sin^2\theta-\left(n_2/n_1\right)^2\right]^{0.5}}$$

Equation 9 – Effective pathlength for p-polarized light.

$$d_{e,p} = \frac{\lambda\left(n_2/n_1\right)\cos\theta\left[2\sin^2\theta - \left(n_2/n_1\right)^2\right]}{\pi\left[1-\left(n_2/n_1\right)^2\right]\left\{\left[1+\left(n_2/n_1\right)^2\right]\sin^2\theta - \left(n_2/n_1\right)^2\right\}\left[\sin^2\theta - \left(n_2/n_1\right)^2\right]^{0.5}}$$

The band shifts associated with AD have significant implications for quantitative and qualitative analysis using the ATR spectrum. For example, for secondary structure analysis of the strong Amide I band in a protein spectrum, because the shift in band position due to AD could lead to errors in secondary structure assignment and possible misinterpretation of protein structure.

Diamond is an excellent material for use in ATR measurements but due to its relatively low refractive index, its use may result in spectral distortions because of anomalous dispersion, particularly at incident angles close to the critical angle. Boulet-Audet *et al.* demonstrated that under certain conditions the Amide I band of measured protein shifts significantly compared to the actual position of the band as a result of AD. The authors correct for these distortions by quantifying the distortion through the mathematical determination of optical constants for silk worm fibroin protein (Boulet-Audet et al., 2010).

However, since ATR spectra are much more affected by the effects of anomalous dispersion if the angle of incidence is close to the critical angle, especially for strong absorbance bands (Harrick, 1967); theoretically, one could minimise spectral distortions caused by anomalous dispersion by adjusting the angle of incidence of IR radiation to be further from the critical angle.

There are different ways to change the angle of incidence in ATR spectroscopy. The use of apertures to change the angle of incidence for ATR measurements with a diamond Golden Gate accessory has already been successfully applied in the Kazarian group for FTIR imaging with depth profiling of samples (Chan et al., 2008a, Frosch, 2010). A moveable aperture can be fitted to the imaging optics of the diamond Golden Gate accessory to restrict the angle of incidence to certain values, as illustrated in Figure 33. Increasing the angle of incidence could, therefore, be an effective way of removing distortion in protein spectra caused by AD. Therefore, the aim in this part of the thesis was to determine if the increase of angle of incidence could be used to reduce the spectral shift of the Amide I and Amide II bands of Lysozyme when compared with its transmission spectrum.

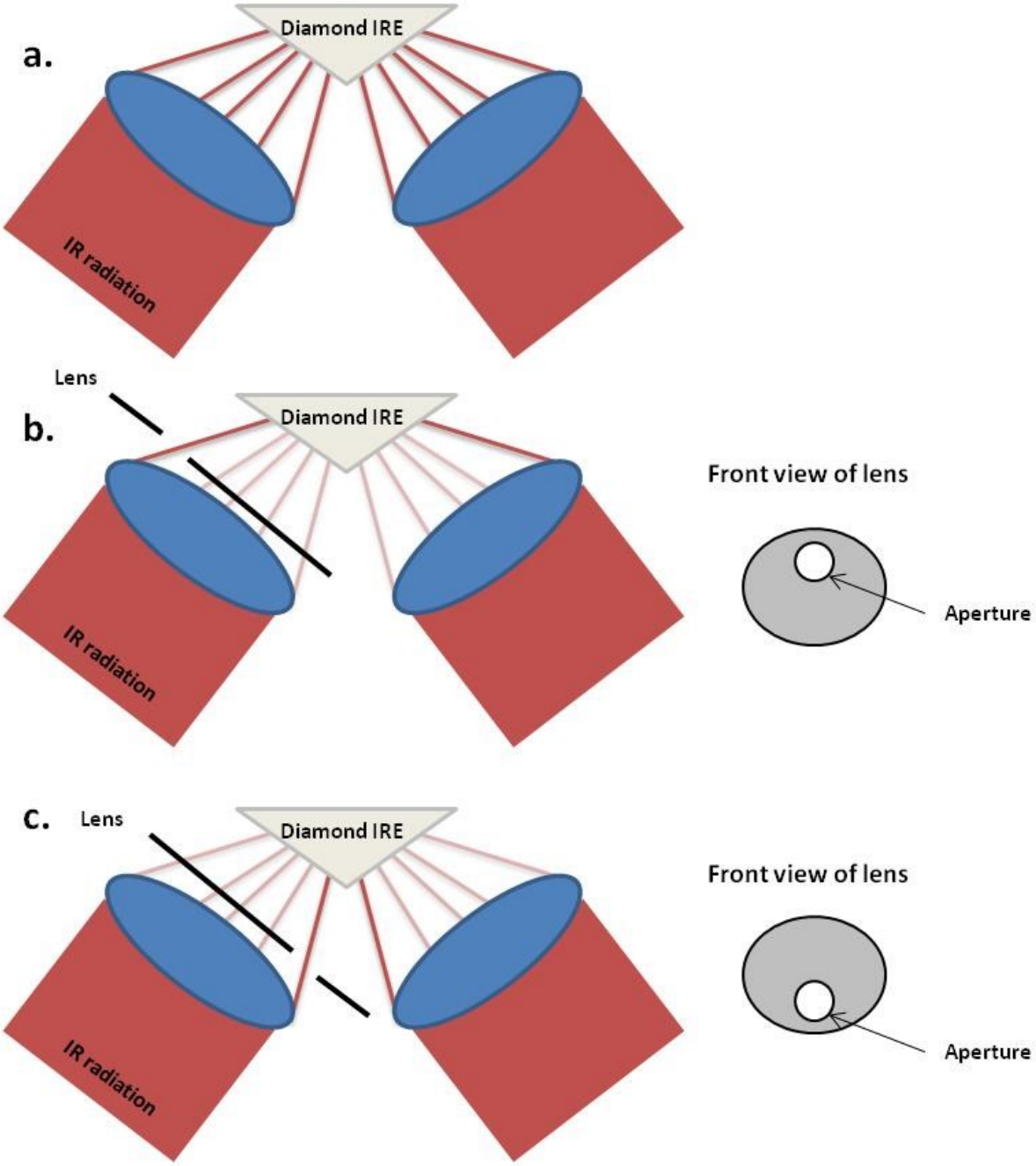

Figure 33 - The use of lenses with apertures to vary the angle of incidence in a diamond Golden Gate ATR accessory; a. normal operation of diamond Golden Gate ATR accessory, b. large angle of incidence set up, c. small angle of incidence set up.

The angle of incidence at each aperture position can be calculated by determining the effective pathlength experimentally by measuring a model sample and then using Equations 12 and 13 to find the angle at which the known effective pathlength was equal to $d_e = 0.5\ (d_{e,s} + d_{e,p})$, the average of effective pathlength for s- and p- polarized light. The effective pathlength is defined as the pathlength in transmission that produces the same absorbance as that in ATR mode. Therefore, by measuring the increased absorbance with increasing pathlength in transmission mode, a calibration curve of absorbance versus pathlength (and therefore effective pathlength in ATR mode) could be generated allowing the effective pathlengths of ATR measurements on the diamond Golden Gate accessory to be determined.

II. Experimental

i. Materials

Hexadecane and Lysozyme were used as purchased from Sigma Aldrich. To form Lysozyme films, a concentrated solution of 60 mg/ml Lysozyme in distilled water was deposited onto either the transmission windows or ATR crystals and left to dry overnight to ensure all water had evaporated from the film.

ii. Transmission FTIR spectroscopy

Transmission FTIR spectroscopic measurements were carried out on a Bruker Equinox spectrometer combined with a transmission window and a single element MCT detector. Barium fluoride windows were used with various spacers (6, 12 and 25 µm) to vary the pathlength. 100 scans were co-added at 4 cm^{-1} resolution and each measurement was ratioed against an air background with the same number of scans and spectral resolution.

iii. ATR-FTIR imaging measurements

ATR-FTIR spectroscopic imaging measurements were taken using a Bruker Equinox spectrometer coupled with a Macro chamber for the diamond Golden Gate ATR accessory and a 64 x 64 pixel FPA detector. Measurements were taken at 4 cm^{-1} resolution and 100 scans were co-added for comparison with the transmission spectra. An air background at 100 co-added scans and 4 cm^{-1} resolution was taken prior to the hexadecane and Lysozyme film measurements at each different aperture position. Apertures were used to vary the angle of incidence of the Diamond Golden Gate accessory as described above.

III. Results and Discussion

i. Calibration of angles of incidence

There were three apertures available that could be fitted to the condenser lens of the diamond imaging optics meaning there were 5 different angles of incidence depending on the position of the aperture. The schematic in Figure 34 shows the positions of the three apertures mounted on the lens. The angle of incidence with no lens was also recorded making the total number of different angles 6. In order to determine the angle of incidence associated with each aperture and for the accessory without any apertures, it was first necessary to calibrate them using hexadecane as reference. It is important to use a model substance that has low volatility with distinct absorbance bands; in addition the absorbance of these bands should be within the absorbance scale at longer pathlengths in transmission.

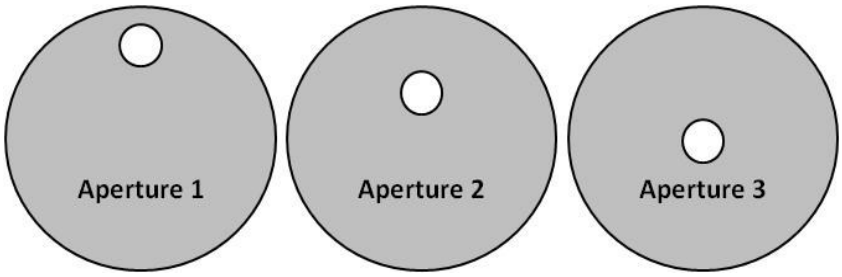

Figure 34 - Schematic of the three lenses used to give 5 different aperture positions and hence 5 varied angles of incidence.

The absorbance of hexadecane in transmission at different pathlengths was measured to allow a comparison with ATR measurements at different angles of incidence. The transmission spectra for hexadecane at 6 µm, 12 µm and 25 µm are shown in Figure 35. Measurements at each pathlength were taken three times and the average integrated absorbance of the CH_3 bending band at 1300-1400 cm^{-1} was used to determine the relationship between pathlength and absorbance. This band was selected because it was the smallest absorbance band and would allow more accurate comparison of effective pathlength when measured using ATR mode. Also, as a weak absorbance band, it is less affected by anomalous dispersion. The average integrated absorbance of hexadecane against pathlength was plotted and is shown in Figure 36. As expected, from the Beer-Lambert Law, as the pathlength increases, the integrated absorbance increases linearly.

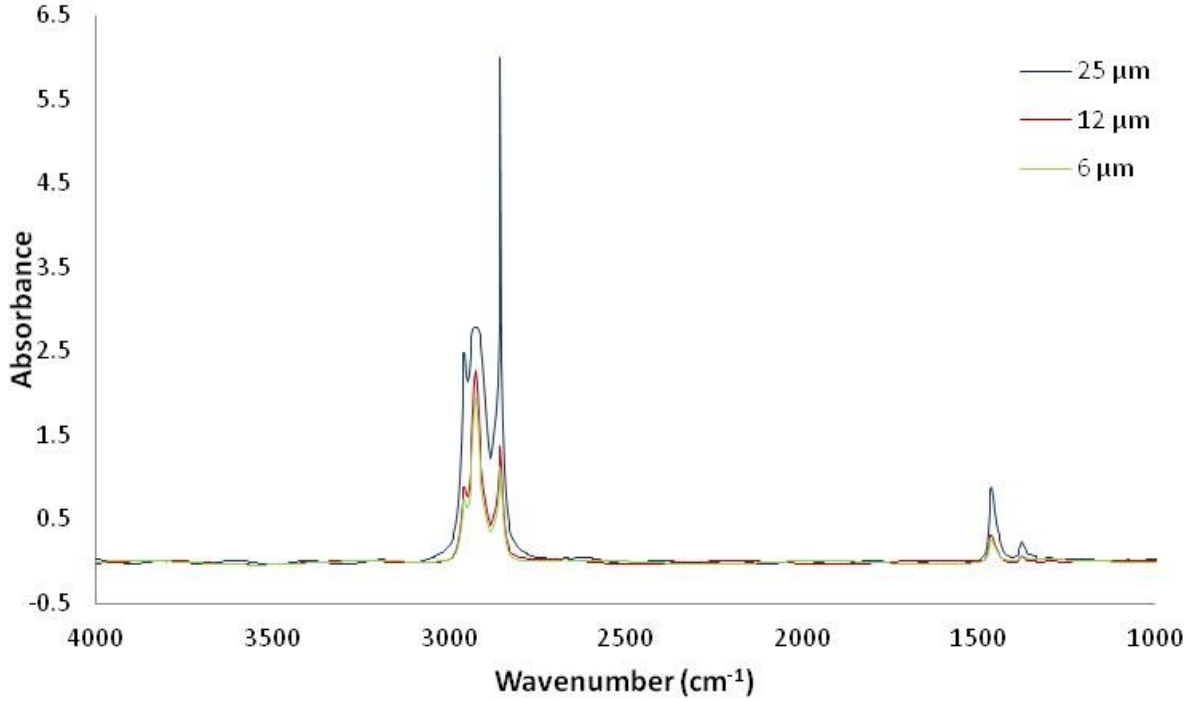

Figure 35 - Transmission FTIR spectra of Hexadecane at different pathlengths.

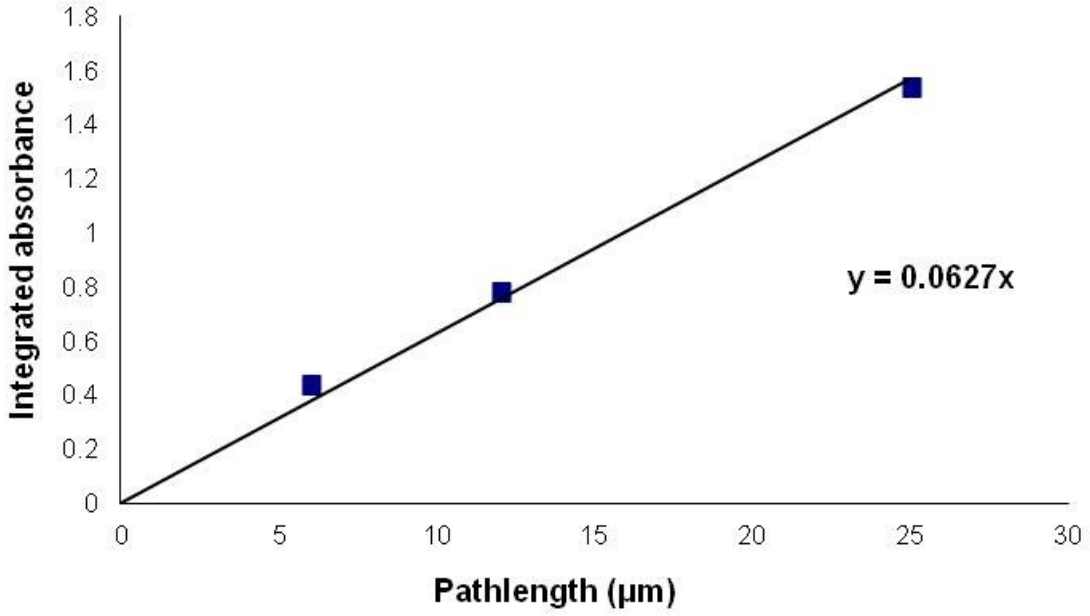

Figure 36 - Plot of integrated absorbance of the CH_3 bending band at 1300-1400 cm^{-1} of Hexadecane versus pathlength.

This plot could then be used for comparison with the integrated absorbance of the same hexadecane band measured using the ATR diamond Golden Gate accessory at different angles of incidence, from which the effective pathlength for each aperture position could be calculated. The angle of incidence at each aperture position could then be determined from Equations 8 and 9, also knowing the refractive index of diamond (n = 2.4) and of hexadecane (n = 1.4).

ATR-FTIR imaging measurements of hexadecane on the diamond Golden Gate accessory were taken at each aperture position and images were generated by plotting the integrated absorbance of the CH_3 bending mode band at 1300 – 1400 cm^{-1}. Spectra were then extracted and averaged from the entire region, in order for the absorbance at each angle to be compared with that of a single element MCT detector. The integrated absorbance from this averaged spectrum allowed for the effective pathlength to be determined from Figure 36. The effective pathlength and angle of incidence at each aperture position are summarised in Table 3 and were shown to range from 37° to 45°.

Table 3 - Summary of integrated absorbance, effective pathlengths and calculated angles of incidence at different aperture positions.

	Integrated absorbance (1300-1400 cm^{-1})	Effective Pathlength (µm)	Angle of incidence θ_i (°)
No aperture	0.2482	3.96	41
Aperture 1 top	0.15592	2.49	45
Aperture 1 bottom	0.62239	9.93	37
Aperture 2 top	0.17362	2.77	44
Aperture 2 bottom	0.44513	7.09	38
Aperture 3	0.20576	3.28	42

ii. Comparison of Lysozyme spectrum in transmission with diamond ATR at different angles of incidence

One of the major effects of anomalous dispersion is the band shift to lower wavenumbers at angles close to the critical angle. This could be problematic for the analysis of the Amide I band which is known to contain a vast amount of structural information based on the position of this band. The objective of the study described here was to determine if the angle of incidence could be adjusted to minimise the band distortion in ATR spectra of Lysozyme when compared with transmission spectra. A reference spectrum of pure Lysozyme in transmission was measured at a pathlength of 25 µm and is shown in Figure 37. The locations of the Amide I and Amide II peaks were recorded to be 1655 cm^{-1} and 1542 cm^{-1}, respectively from this spectrum.

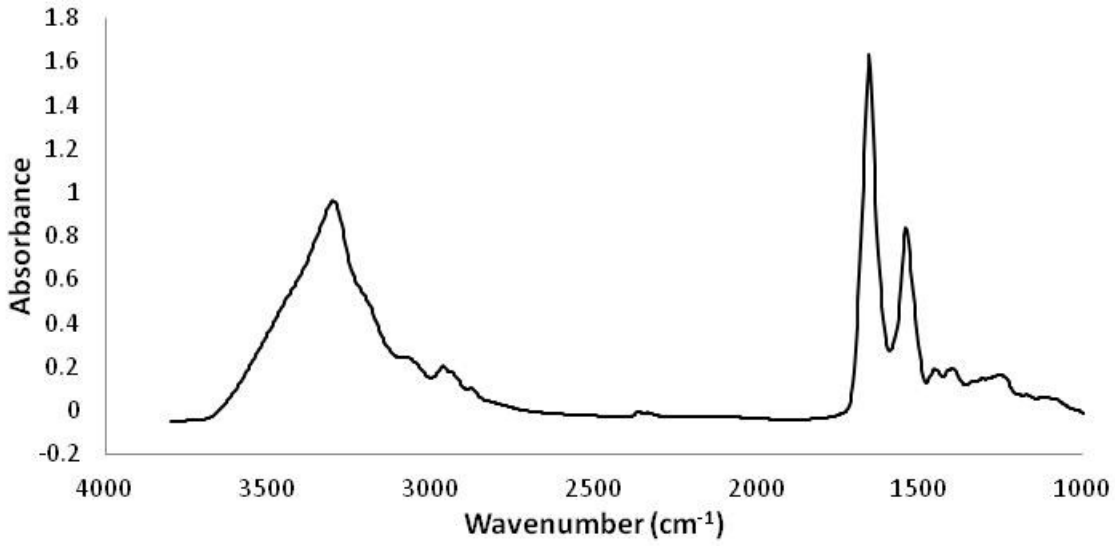

Figure 37 - FTIR spectrum of thick film of Lysozyme measured in transmission with 25 µm pathlength.

A film of Lysozyme was formed on the surface of the diamond ATR crystal before measurements were recorded at each of the different aperture positions using the same procedure described for the hexadecane measurements. ATR-FTIR images were generated by plotting distribution of the integrated absorbance of the Amide I band (1700 – 1600 cm^{-1}) shown in Figure 38. These indicated that the film had not formed homogeneously on the surface, therefore spectra were extracted from the area of highest protein concentration (the region marked by the black box in Figure 38), averaged and are presented in Figure 39 for each angle of incidence. There are two points to note about both the spectra and images obtained at different angles of incidence; the effect on the ATR image itself and the position of the Amide bands.

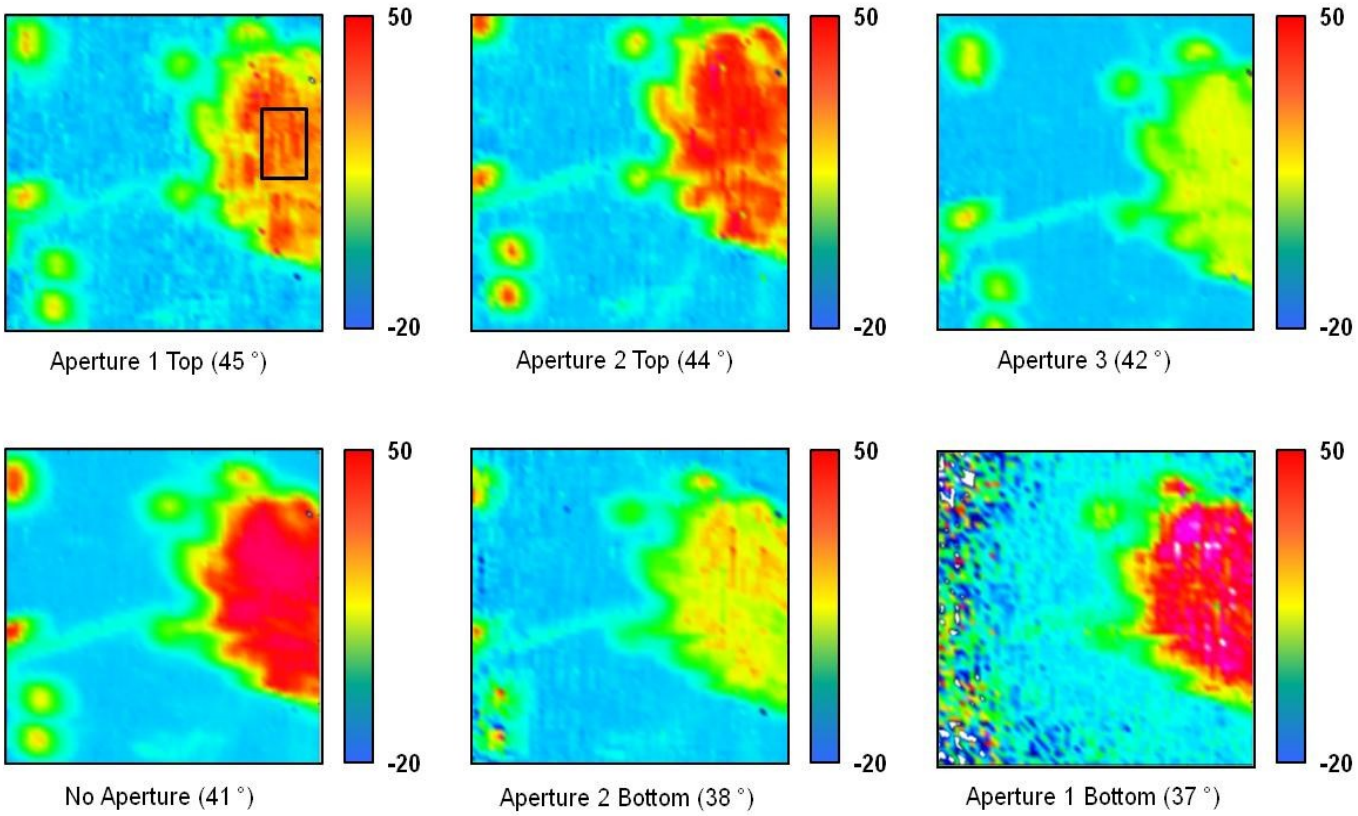

Figure 38 - ATR-FTIR spectroscopic images of Lysozyme film on the surface of the diamond at different angles of incidence. Images generated by plotting the integrated absorbance of the Amide I band (1600 – 1700 cm^{-1}), spectra extracted and averaged from region marked by black box in top image (as for each other image).

From the spectra in Figure 39, it can be seen that the Amide I band shifts towards higher wavenumber as the angle of incidence is increased. This is summarised in Table 4. It is also noticeable from Figure 38 and Figure 39 that the absorbance of the Amide bands decreases as the angle of incidence increases; this is due to the decreased effective pathlength at higher incident angles.

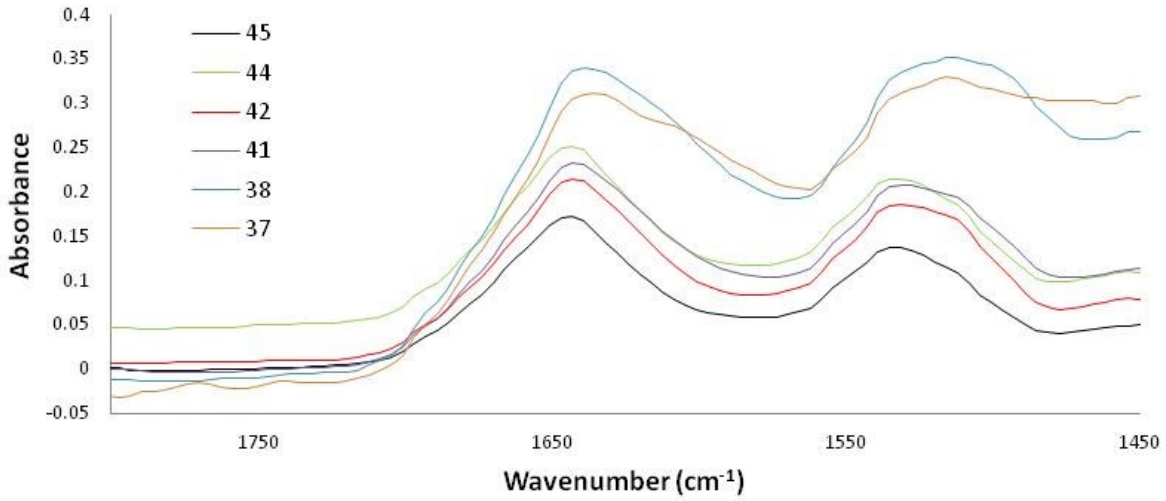

Figure 39 - ATR-FTIR spectra of Lysozyme film at various angles of incidence.

Table 4 - Peak positions of the Amide I bands at different angles of incidence.

Aperture	θ_i (°)	Amide I peak (cm^{-1})	Amide II peak (cm^{-1})
Aperture 1 bottom	37.7	1636	1515
Aperture 2 bottom	38	1637	1511
No Aperture	41	1641	1529
Aperture 3	42	1644	1532
Aperture 2 top	44	1645	1535
Aperture 1 top	45	1645	1535

From Table 4, it can be seen that there is a shift in the Amide band position to higher wavenumbers as the angle of incidence is increased. The critical angle for protein solution (approximately n = 1.33) and diamond (n = 2.4) is 33.7 °, therefore according to the theory of anomalous dispersion, at angles of incidence closer to this critical angle there will be a greater band shift to lower wavenumbers for strong absorbance bands when compared to transmission spectra. This can indeed be seen in Table 4, where at the lowest angle of incidence the shift in Amide I band is 19 cm^{-1} lower compared to the Amide I band in transmission, which was observed at 1655 cm^{-1} as discussed above. This significant difference is reduced almost linearly as the angle of incidence is increased but there is still a difference of 10 cm^{-1} in Amide I peak position at the highest angle of incidence. Therefore, although the spectral shift at greater angles of incidence was smaller, the effect of anomalous dispersion has not been removed fully.

IV. **Conclusions**

Analysis of protein secondary structure uses the assignment and interpretation of the corresponding peaks of the Amide I band. Misinterpretation of the data is possible if peak assignments are made solely based on the position of the corresponding peaks in transmission spectra because as demonstrated here the position of the Amide I peak varies greatly with angle of incidence when the ATR mode of measurement is used. It was hoped, that the application of a variable angle of incidence for imaging of protein samples could remove these shifts in protein spectral bands associated with anomalous dispersion by increasing the angle of incidence so that it was further from the critical angle.

ATR spectra were measured at different angles of incidence and the resulting Amide band positions were compared with their position in transmission mode. Investigating this confirmed that increasing the angle of incidence reduced the effect of anomalous dispersion in the ATR spectra. However, within the current arrangement it is not possible to achieve an angle of incidence great enough to completely negate the spectral distortion present in ATR measurements. In addition, the reduced absorbance of spectral bands, as a result of decreased effective pathlength at greater angles, may also be a limitation. The diamond Golden Gate ATR accessory could be re-aligned to increase the possible range of angles but in doing so the fraction of the diamond imaging surface area illuminated by the IR light is affected. This, in turn can influence the quality of measurements obtained. The intensity of infrared radiation directed at the surface is restricted by the aperture and this reduces the SNR of the spectra obtained. Realignment to a greater range of angles of incidence reduces the SNR further as the area illuminated on the surface was also reduced. In addition, the spatial information could also be degraded as the focus of the image is changed with realignment. This could affect the ability to carry out protein studies, especially secondary structure analysis based on Amide bands which requires very high quality data. Therefore, it was decided not to carry out realignment of the diamond Golden Gate accessory to increase the angle of incidence further because of the degradation in spectral quality and spatial resolution.

Although some correction of the Amide band positions was observed using the variable angle of incidence method, it is recommended that in order to reduce the possible misinterpretation of protein spectra, the higher refractive index internal reflection elements such as Germanium or Silicon should be used. Like diamond, ZnSe is also a material with a relatively low refractive index. It is conventionally used in a Macro imaging accessory with a flat mirror fixed at 45° and as such the degree of band distortion (particularly for less strong absorbance bands) will be less significant compared with the diamond Golden Gate ATR accessory which uses lenses to focus the IR light and

thus some distribution of angles of incidence. Therefore, ZnSe could potentially also be used for protein studies.

Additionally, the assignment of the peaks in the Amide I band corresponding to secondary structures of protein, measured by ATR-FTIR spectroscopy should not be based solely on the position of these peaks in FTIR spectra measured in transmission, to avoid possible misinterpretation. One could also consider quantifying the effect of AD on the Amide band positions using methods discussed in literature, for each ATR accessory to be used, prior to secondary structure analysis. As this was not carried out during these experiments, a quantified effect of AD has not been discussed but this may be of more interest when the diamond Golden Gate ATR accessory is used for protein analysis.

Chapter 5 - ATR-FTIR spectroscopic imaging of protein crystallisation

I. Overview

The crystallisation of proteins in order to determine their 3D structure has become an increasingly challenging area of research, especially with the continuing development of structural proteomics projects. A lot of time and effort is spent generating the target protein in sufficiently large amounts (mg) and with suitable stability. The protein is then submitted to a large number of both preliminary and optimisation crystallisation trials with the aim of gaining a 3D structure from X-ray crystallography, the best available method for obtaining high resolution structural information (McPherson, 2004). However, despite many efforts focussing on rationalisation, the crystallisation of proteins is still largely an empirical process and involves a significant amount of trial and error (Chayen, 2004). Even when protein crystals are formed, it is still very difficult to obtain ones that are useful for X-ray diffraction (Chayen, 2004). Often protein crystals can be too small or slightly imperfect, producing weak or poor quality diffraction patterns which can be difficult to interpret. In addition to this, there is currently no easy way to distinguish between a protein and salt crystal within the crystallisation drop meaning that time and resources are often wasted optimising conditions, only to discover during final stages that the crystal is in fact not proteinaceous (Chan et al., 2009).

Infrared spectroscopy has already been extensively used for the study of protein behaviours such as surface adsorption (Sethuraman and Belfort, 2005) and in solution (Oberg and Fink, 1998). Characteristic absorption bands for proteins are sensitive to protein conformation and there are many examples in the literature for the assignment of protein secondary structure based on the analysis of the Amide I band (Surewicz et al., 1993, Haris and Severcan, 1999, Barth and Zscherp, 2002). The recently developed techniques of ATR-FTIR spectroscopic imaging is an extremely versatile analytical technique that allows for the measurement of chemically specific images of a sample, without the need for additional dyes or labels. This means chemical imaging offers exciting opportunities for the study of protein crystallisation in situ.

The work in this chapter shows the progress in the application of ATR-FTIR imaging to the study of protein crystallisation. The first section concentrates on the further development of high throughput ATR-FTIR imaging for microbatch protein crystallisation as a means of screening for crystallisation conditions. The second section demonstrates the use of Micro ATR-FTIR imaging to study in situ hanging drop protein crystallisation which could potentially be used for in situ studies of microscopic protein crystals that do not form crystals large enough for X-ray crystallography.

II. ATR-FTIR spectroscopic imaging for high throughput protein crystallisation

i. Introduction

As mentioned above, the optimum crystallisation conditions for each protein are identified by extensive screening. The development of new analytical techniques to screen for successful crystallisation conditions and to explore crystallisation kinetics by measuring growth in situ would greatly facilitate the development of rational crystallisation approaches. The chemical specificity of infrared spectroscopy means that crystals can easily be identified as protein and the range of imaging areas available with ATR-FTIR spectroscopic imaging have capacity for high throughput experiments. The technique could also provide some insight into structural kinetics of crystallisation through the use of secondary structure analysis of the protein spectra obtained from the crystals.

As outlined in section IV of Chapter 2, the application of Macro ATR-FTIR spectroscopic imaging to the study of protein crystallisation in a high throughput manner was shown by Chan *et al.* (Chan et al., 2009). This work demonstrated that ATR-FTIR spectroscopic imaging could be used to distinguish between 6 different crystallisation conditions simultaneously using a Macro approach, where the spatial resolution is limited to 40 µm using a Zinc Selenide ATR accessory or 15 – 20 µm with a diamond accessory (Chan et al., 2009). A wax grid can be printed onto the surface of the ATR element to create wells allowing for different samples to be deposited without cross contamination.

Microbatch crystallisation is less popular compared to vapour diffusion methods, but has been used to great effect (Chayen, 2004). In this type of crystallisation, the formation of protein crystals takes place in aqueous solutions covered by paraffin oil. Unlike vapour diffusion methods, where the system is dynamic and conditions change throughout, in microbatch the protein and reagent concentration at the start of the experiment should be such that upon mixing supersaturation occurs, allowing the formation of crystals (Figure 3). Paraffin oil is used to prevent any evaporation from the system. It is however, most suited for the combination with Macro ATR imaging as the crystals can be grown directly on the ATR surface.

This section builds on the preliminary study of 6 samples of lysozyme by Chan et al (Chan et al., 2009), expanding the use of ATR-FTIR spectroscopic imaging to up to 20 protein samples simultaneously and applied to another model protein, Trypsin. It shows the use of this method to determination of the minimum Trypsin concentration required to achieve crystallisation as well as the effect of different concentrations of a precipitant, polyethylene glycol, within these experimental conditions.

ii. Experimental

ATR-FTIR spectroscopy measurements

All measurements were carried out using an Agilent 670 IR spectrometer equipped with a Large Sample Compartment and a 128 x 128 pixel FPA detector. A single reflection ZnSe ATR crystal was used and 64 scans were co-added at 8 cm^{-1} resolution for each measurement. A background measurement was taken each time prior to deposition of protein solutions, either before or after the wax grid was printed. In this arrangement the imaging area is approximately 5 x 7 mm^2 and a spatial resolution of 40 µm. This is determined by the size and number of pixels on the FPA detector. The measurement time to obtain one image was approximately 3 minutes.

Spectral analysis of the protein crystals was carried out by averaging the spectra within the specific region and then subtracting water from the spectrum. This was achieved using a combination of Agilent Resolution Pro software and Cytospec. The Cytospec software was used to average and extract spectra from specific regions.

Visible images were obtained using an optical microscope (Varian FTS-7000 coupled with IR microscope operated in visible light mode) with various magnifications depending on area being examined.

Crystallisation conditions

Trypsin (T1426) and all the chemicals used in the reservoir solutions were obtained from Sigma-Aldrich and used without any further processing. Various concentrations of Trypsin (mg/ml) were prepared in 0.1 M Sodium Cacodylate pH 6.5 buffer with 0.2 M Ammonium Sulphate. The reservoir solutions contained 15 – 32 % w/v PEG 8000 in the same buffer. A commercially available screening solution was also used throughout the experiments containing 30% PEG 8000 w/v in 0.2 M Ammonium Sulphate, 0.1 M Sodium Cacodylate pH 6.5 purchased from Hampton Research. These solutions are used to determine the minimum protein concentration for screening experiments. The screen conditions used are known to produce protein crystals at high protein concentrations based on work by Jancarik & Kim (Jancarik and Kim, 1991). Protein concentration is a significant variable, so being able to determine an appropriate initial concentration quickly is important. The use of the screening solution is denoted by the term “screen” when describing the results of crystallisation trials below. For all measurements the Trypsin solution was mixed in 1:1 ratio with reservoir solution. The drop volume varied from 3 µL for 9 and 12 well trials, 2 µL for 15 wells and 1.5 µL for 20 well trials.

Wax grid printing and crystallisation solution deposition strategy

A paraffin wax grid was printed onto the measuring surface of the ZnSe ATR crystals using the microdroplet system (Autodrop Compact, microdrop Technologies). This was used to create square wells of various sizes depending on the number of protein samples to be deposited. The measurement of up to 20 samples is demonstrated in this section.

Microbatch crystallisation occurs under paraffin oil. To facilitate this, a PDMS well is placed onto the ZnSe surface surrounding the wax grid. The PDMS forms a seal on contact with the surface, preventing the leakage of oil. Once the PDMS well was filled with oil, protein solution and precipitant solution were deposited into the individual wells outlined by the wax grid, as shown in Figure 40. Filling the PDMS well with oil prior to depositing the protein samples ensures that no evaporation occurs from the sample drops during the experimental set up of multiple samples.

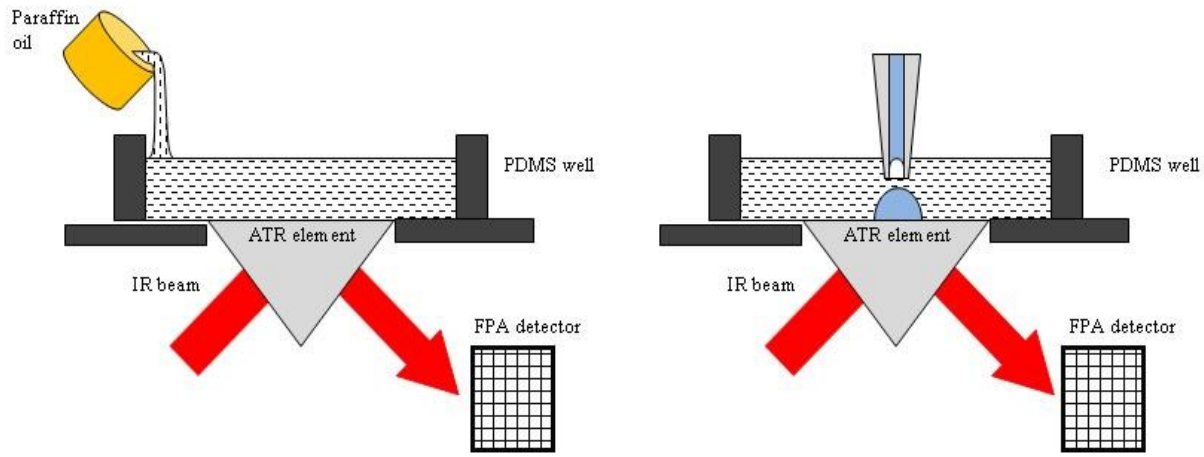

Figure 40 - **Schematic of sample deposition strategy for micro batch protein crystallisation in situ on the ATR element.**

In order to ensure that the samples were deposited in the correct well and to prevent cross contamination, the “live imaging window” of Agilent Resolution Pro software was used, as shown in Figure 41. This allows the position of the wells to be observed whilst depositing multiple samples.

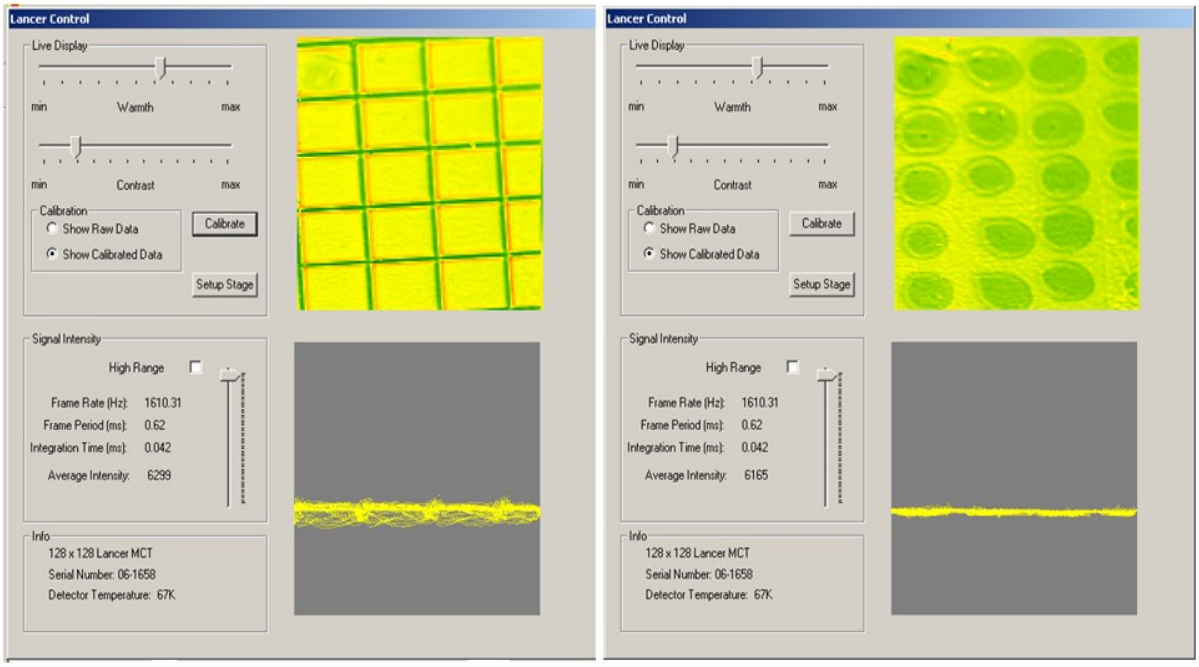

Figure 41 - Live imaging display window in Agilent Resolution Pro software used to aid in sample deposition.

iii. Results and Discussion

Initially the experimental set up was limited to 9 sample wells to be imaged with Macro ATR-FTIR spectroscopic imaging. This was achieved by increasing the size of the focal plane array detector to 128 x 128; this doubled the size of imaging field of view compared with the work carried out by Chan *et al.* (Chan et al., 2009). Figure 42 shows the measurements taken for 9 samples with 2 different Trypsin concentrations of 60 mg/ml and 30 mg/ml and three precipitant solutions: 15 % PEG, 20 % PEG along with the screening solution, deposited according to the sample key presented in the figure.

These conditions were selected as a starting point for the study of microbatch Trypsin crystallisation using ATR-FTIR spectroscopic imaging where the aim, initially was to determine if Trypsin would crystallise in the microbatch setup. It was decided to trial a midrange concentration of 30 mg/ml protein and the 3 different precipitants, depositing two samples of each condition within the imaging area. Then 3 high concentration protein samples, 60 mg/ml Trypsin were deposited but with only the 20 % and 15 % PEG precipitant solutions as it was known that the screen solution would cause protein precipitation at this high protein/PEG concentration. The arrangement of the different samples is shown in Figure 42E.

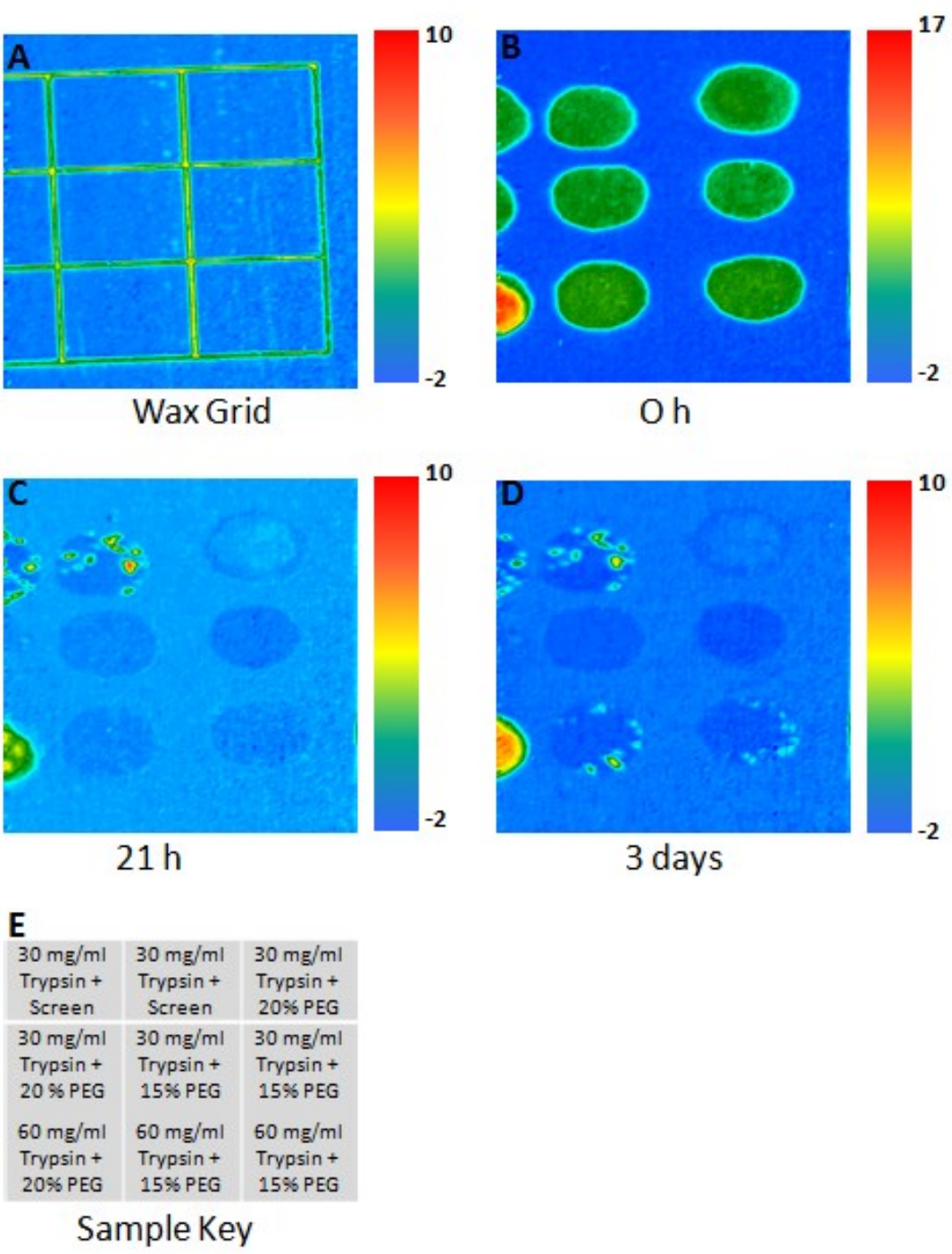

Figure 42 - ATR-FTIR spectroscopic images for 9 well Trypsin crystallisation, A) Wax grid is shown by the distribution of integrated spectral band of wax , B) solution drops generated by plotting distribution of integrated absorbance of the band of water bending mode at 1650 cm^{-1}, C) Trypsin protein crystals discovered by plotting distribution of the integrated absorbance of Amide II band at ca. 1540 cm^{-1} at 21 h, D) Trypsin protein crystals discovered by plotting integrated Amide II band at ca. 1540 cm^{-1} after 3 days, E) Sample Key showing protein and precipitant concentration in each well.

The presence of protein crystals is determined by plotting the distribution of the absorbance of the Amide II band. This is used rather than the Amide I band as this band overlaps with the water bending mode at 1650 cm^{-1}. Immediately after the samples were deposited, Figure 42B shows that from the distribution of the integrated band of bending mode of water, the position of the samples can be seen. Also from the high absorbance of the 60 mg/ml sample with 20 % PEG solution, it would seem that protein instantaneously precipitated out of solution onto the ATR crystal surface suggesting that under these conditions the sample is within the precipitation zone of the crystallisation phase diagram. After 21 h and 3 days, it can be seen that protein crystals have formed at 2 different conditions; 30 mg/ml with the screen solution and 60 mg/ml with 15 % PEG. From the ATR image these crystals are approximately 100 - 200 μm in size. Also within the 60 mg/ml and 20 % PEG sample, it would appear that based on the Amide II absorbance a precipitate of protein has formed.

It was decided to compare the infrared spectra from the precipitated region within the 60 mg/ml Trypsin and 20 % PEG sample (bottom left sample in Figure 42) and that of a protein crystal in the 30 mg/ml and screen sample to determine if any denaturation had occurred as the protein precipitated out of solution, which could prevent crystallisation. These spectra, shown in Figure 43, were generated by averaging a small region with each of the areas and extracting the average spectrum. Water was also subtracted from the spectra of proteinaceous areas to remove interference of the water bending mode in the Amide I region. It can be seen in Figure 43 that there are no noticeable differences in the spectra between the samples suggesting that no denaturation had occurred.

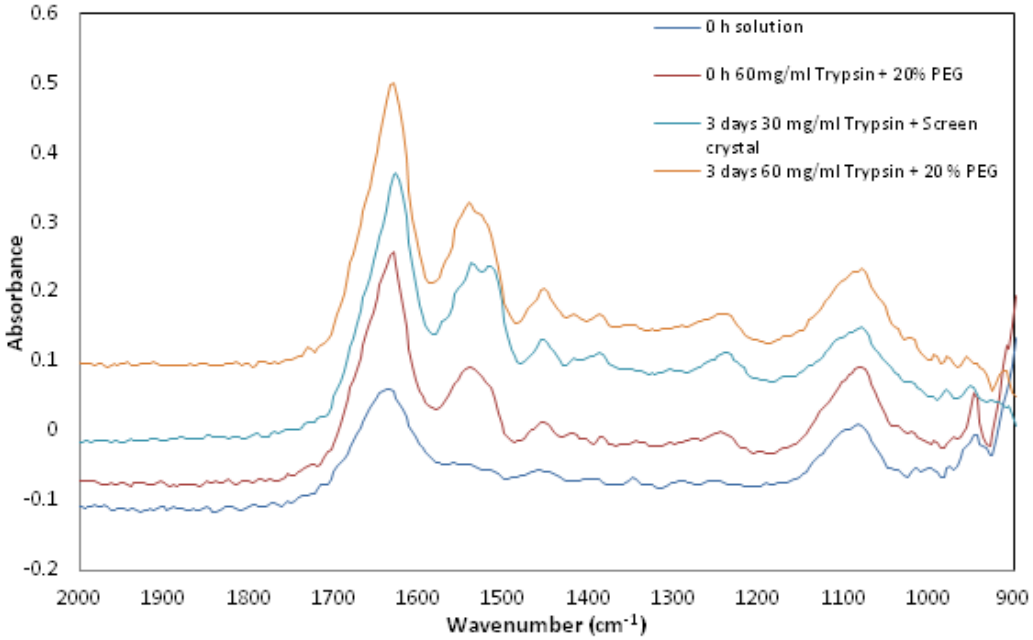

Figure 43 - FTIR spectra extracted from various regions of the crystallisation solutions in the 9 well trial.

Following the partially successful 9 wells crystallisation trial, the number of samples to be studied simultaneously was expanded to 12. The range of protein concentrations studied was broadened to 20 mg/ml, 30 mg/ml and 60 mg/ml. Several samples were repeated in the same experiment. The ATR images generated at different times are shown in Figure 44 and the sample key (Figure 44E) shows the arrangement of samples. Again the presence of crystals was detected by plotting the integrated absorbance of the Amide II band. As per the previous experiment, the samples using the screening solution produced multiple crystals and the two samples with 60 mg/ml Trypsin and 20 % PEG produced a precipitate upon mixing. Also, examination of the average spectra revealed that there is no detectable difference between the regions in the samples containing precipitated and crystalline protein (Figure 45).

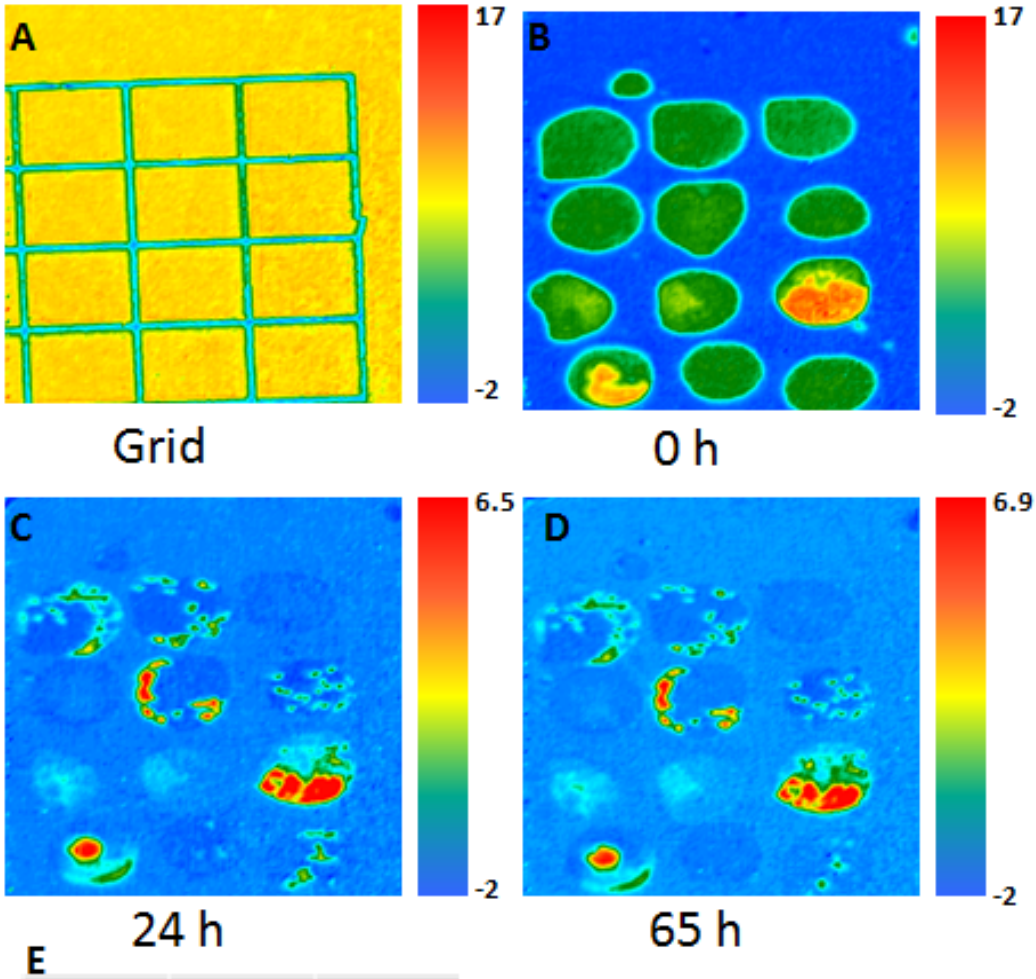

E

20 mg/ml Trypsin + Screen	20 mg/ml Trypsin + Screen	20 mg/ml Trypsin 20% PEG
20 mg/ml Trypsin 20 % PEG	30 mg/ml Trypsin Screen	30 mg/ml Trypsin Screen
30 mg/ml Trypsin 20 % PEG	30 mg/ml Trypsin 15 % PEG	60 mg/ml Trypsin 20 % PEG
60 mg/ml Trypsin 20 % PEG	60 mg/ml Trypsin 15 % PEG	60 mg/ml Trypsin 15 % PEG

Sample Key

Figure 44 - ATR-FTIR spectroscopic images for 12 well Trypsin crystallisation, A) Wax grid shown by distribution of integrated absorbance of band at 2930 cm^{-1} B) solution drops generated by plotting distribution of integrated absorbance of the water bending mode at 1650 cm^{-1}, C) Trypsin protein crystals discovered by plotting integrated absorbance of the Amide II band at ca. 1540 cm^{-1} at 24 h, D) Trypsin protein crystals discovered by plotting the integrated absorbance of the Amide II band at ca. 1540 cm^{-1} after 65 h, E) Sample key showing protein and precipitant concentrations in each well.

In order to confirm that the crystals detected by ATR-FTIR imaging are indeed protein crystals, an optical visible image was taken of each sample at 65 h. This was taken at the end of the experiment to avoid disturbing the sample whilst crystals were forming and also to prevent misalignment with the background spectra taken before the samples were deposited. The visible images are shown in Figure 46 and it can be seen that the location of crystals in visible images do indeed match up with locations of crystals in the ATR images for most of the samples. However, in the case of the 60 mg/ml and 20 % PEG samples the visible images show that the areas considered to be precipitates by looking at the ATR-FTIR images are actually a large number of protein crystals (Figure 46).

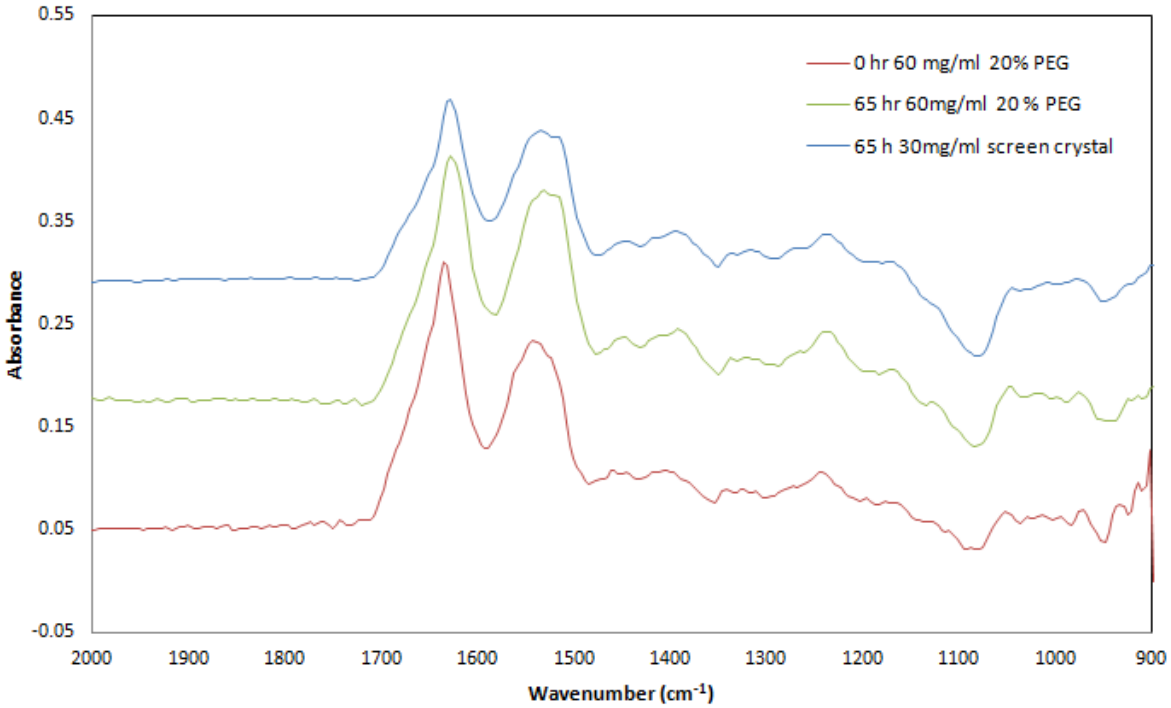

Figure 45 - IR spectra extracted from various regions of the crystallisation solutions in the 12 well trial.

This would explain why there are no significant spectral differences in that region compared with the spectrum of a single crystal. In addition, from both the ATR images and the visible images, it could be concluded that the high protein concentration, high PEG concentration samples follow a slightly different crystallisation pathway to the other lower concentration samples in that the protein seems to precipitate onto the surface of the ATR crystal upon mixing and then go on to form crystals rather than forming discrete nuclei on the surface. Also in this case, the large number of crystals formed within such a small region means that it was not possible to resolve them in the ATR image, hence the larger area corresponding to the distribution of Amide II absorbance.

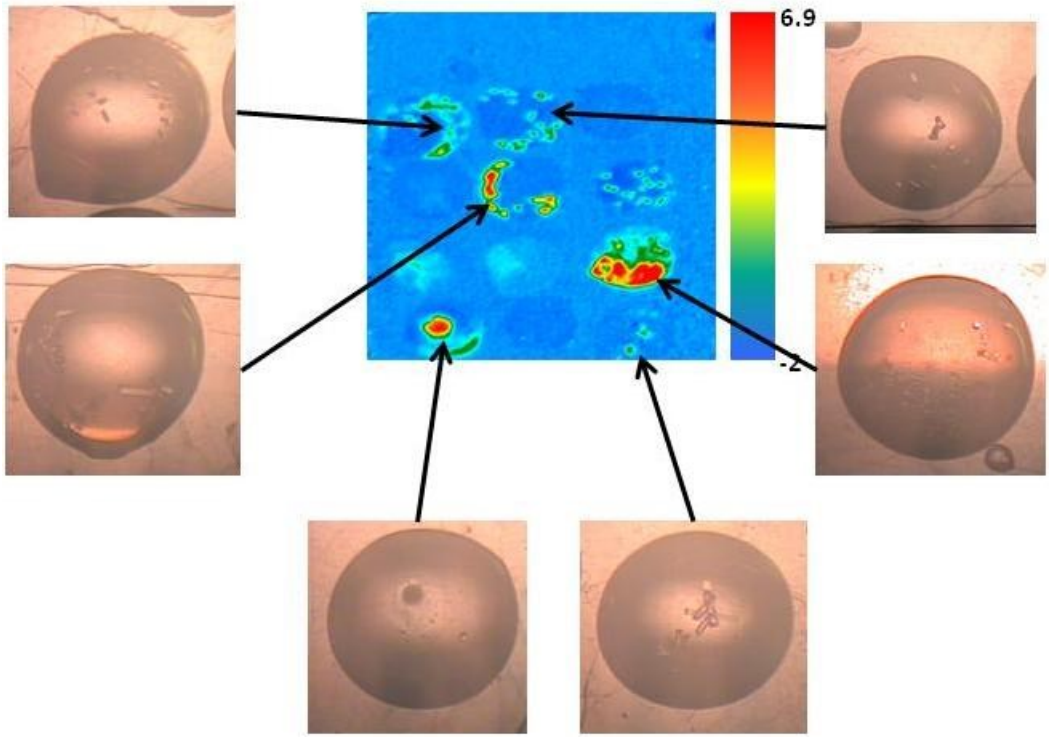

Figure 46 - Visible images of Trypsin crystals from selected sample wells at 65 h showing that the location of crystals within each drop is largely in agreement with the ATR-FTIR images.

From the 12 well images in Figure 44, it can be seen that there was still space to increase the number of samples to 15 although this did require the drop volume to be reduced from 3 µL to 2 µL. In this case, it was decided to decrease the protein concentration further to detect the minimum protein concentration required for the screening solution to produce protein crystals. Therefore, samples of 5 mg/ml, 10 mg/ml, 20 mg/ml, 30 mg/ml and 60 mg/ml were deposited as shown in Figure 47. Again, crystals were detected by plotting the absorbance of the Amide II band. The experiment was stopped after 48 h in this case when it became clear that the minimum concentration required for protein crystals to occur was 10 mg/ml Trypsin. Even with the screening solution, no crystals were formed at 5 mg/ml.

Visible images were also taken after 48 h (Figure 48) and they largely agreed with the ATR images produced. For the 60 mg/ml and 20 % PEG sample, again the visible images shows a large number of crystals on the surface which could not be resolved individually by ATR imaging. This is in agreement with the previous measurements. By increasing the number of samples studied simultaneously in one experiment, the range of conditions analysed is much greater and can allow for the optimum crystallisation conditions to be identified much faster. This is one of the advantages of high throughput studies. Therefore, in this experiment, the range of protein concentrations studied was

increased and the minimum protein concentration required to crystallise Trypsin at these particular microbatch conditions was identified.

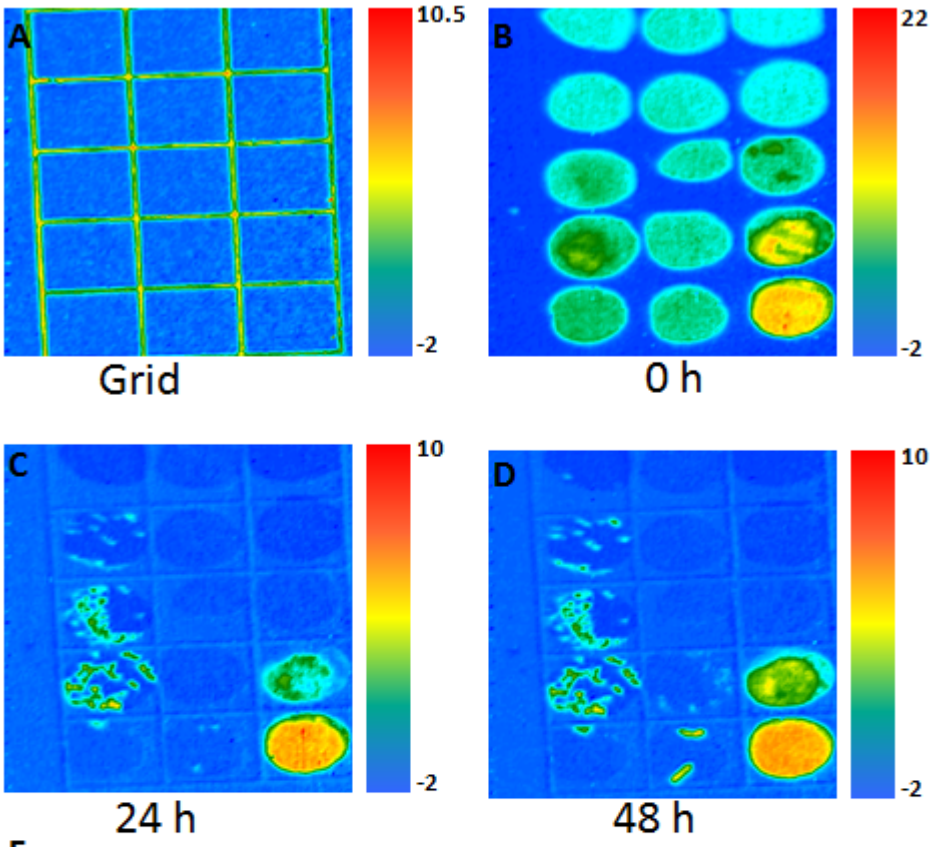

E

5 mg/ml Trypsin Screen	5 mg/ml Trypsin 15 % PEG	5 mg/ml Trypsin 20 % PEG
10 mg/ml Trypsin Screen	10 mg/ml Trypsin 15 % PEG	10 mg/ml Trypsin 20 % PEG
20 mg/ml Trypsin Screen	20 mg/ml Trypsin 15% PEG	20 mg/ml Trypsin 20% PEG
30 mg/ml Trypsin Screen	30 mg/ml Trypsin 15 % PEG	30 mg/ml Trypsin 20 % PEG
60 mg/ml Trypsin 15% PEG	60 mg/ml Trypsin 15 % PEG	60 mg/ml Trypsin 20 % PEG

Sample Key

Figure 47 - ATR-FTIR spectroscopic images for 15 well Trypsin crystallisation, A) Wax grid shown by distribution of integrated absorbance of band at 2930 cm^{-1}, B) solution drops generated by plotting distribution of integrated absorbance of water bending mode at 1650 cm^{-1}, C) Trypsin protein crystals discovered by plotting integrated absorbance of Amide II band at ca. 1540 cm^{-1} at 24 h, D) Trypsin protein crystals discovered by plotting integrated absorbance of Amide II band at ca. 1540 cm^{-1} after 48 h, E) Sample Key showing protein and precipitant concentration in each well.

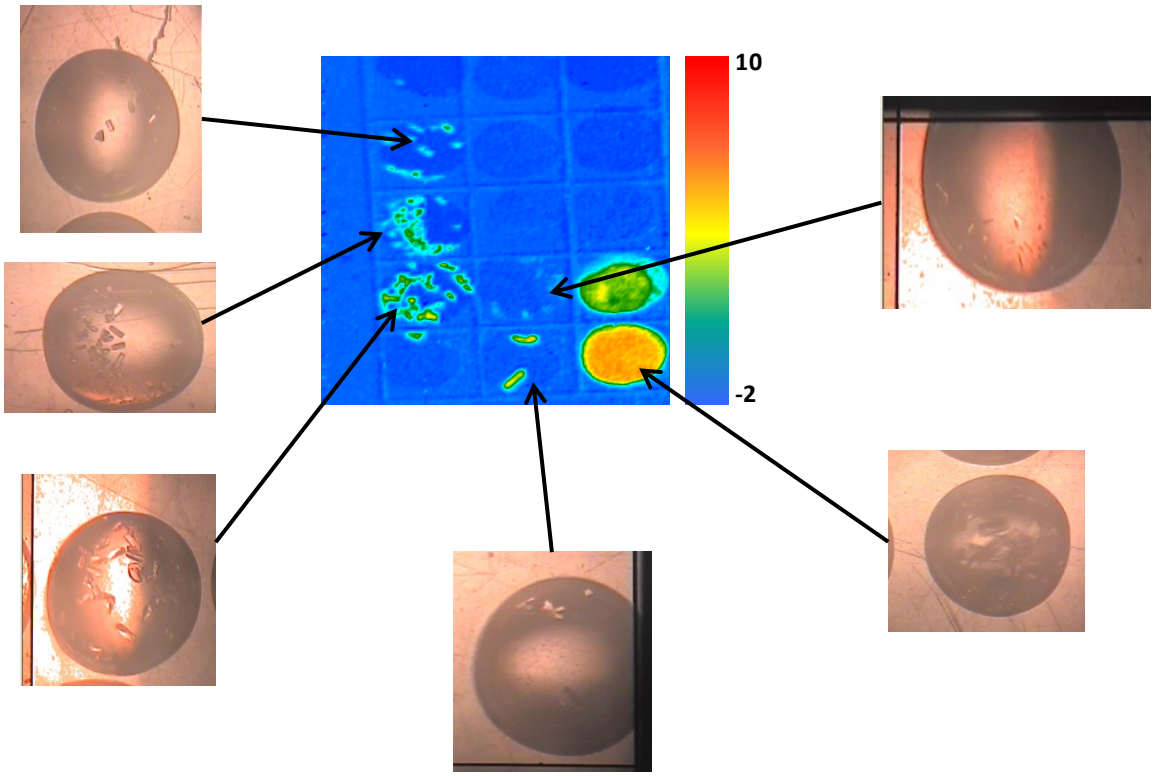

Figure 48 - Visible images of Trypsin crystals from selected sample wells at 48 h from the 15 samples experiment showing the location of crystals in each crystallisation drop.

As previously mentioned, the advantages of high throughout studies are that a large number of samples can be studied simultaneously. This can reduce the time and amount of protein solution required to identify optimum conditions. ATR-FTIR spectroscopic imaging is an inherently suitable method for high throughput studies. As a final stage of this study, the approach was modified further to reduce the droplet volume further to 1.5 µL and increase the number of samples to 20 within one measurement. Another precipitant solution with 32 % PEG was used in addition to the three already studied in previous trials above. The minimum protein concentration that produced crystals was 10 mg/ml, based on the results of the 15 well experiment. Therefore, 20 different samples with a protein concentration ranging from 10 mg/ml to 60 mg/ml and precipitant concentration ranging from 15 – 32 % PEG plus the screen solution were studied simultaneously. The results are shown in Figure 49 with Figure 49E showing the arrangement of samples. It was hoped that this would allow the range of effective precipitant PEG concentration to be determined.

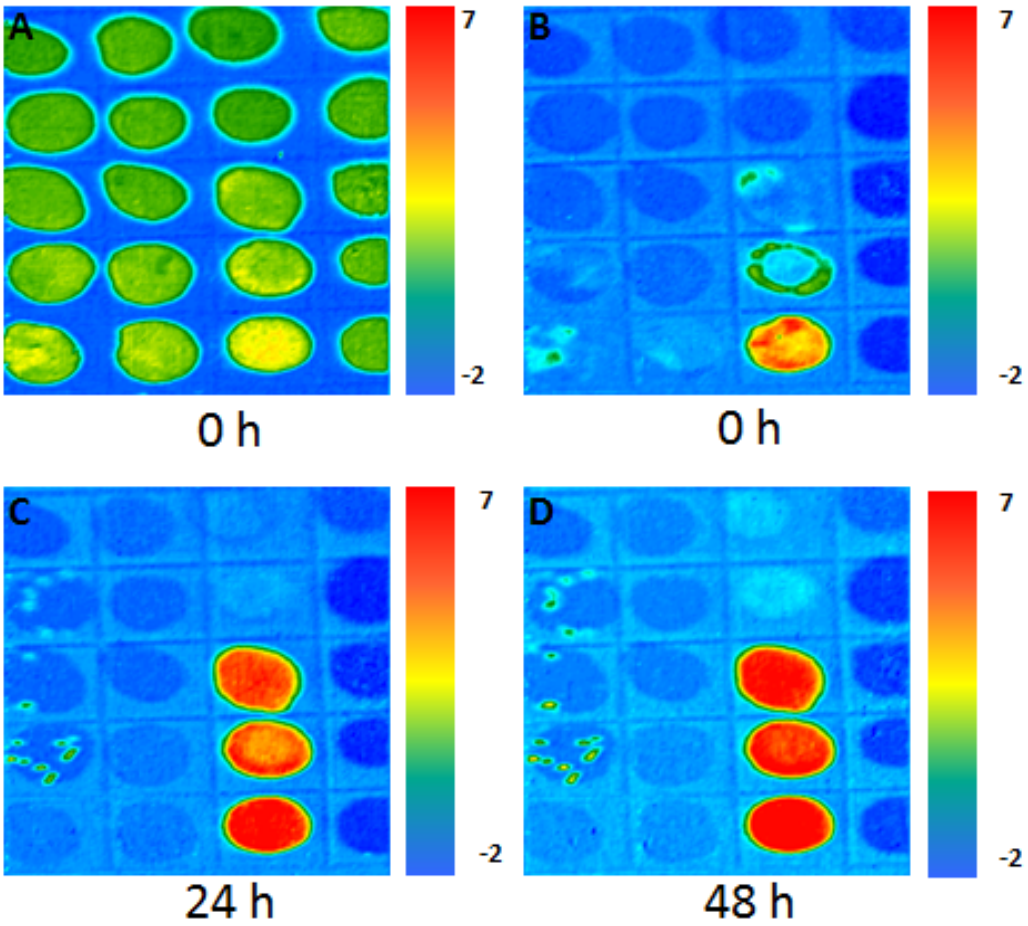

E

10 mg/ml Trypsin Screen	10 mg/ml Trypsin 15 % PEG	10 mg/ml Trypsin 20 % PEG	10 mg/ml Trypsin 32% PEG
15 mg/ml Trypsin Screen	15 mg/ml Trypsin 15 % PEG	15 mg/ml Trypsin 20 % PEG	15 mg/ml Trypsin 32% PEG
20 mg/ml Trypsin Screen	20 mg/ml Trypsin 15% PEG	20 mg/ml Trypsin 20% PEG	20 mg/ml Trypsin 32% PEG
30 mg/ml Trypsin Screen	30 mg/ml Trypsin 15 % PEG	30 mg/ml Trypsin 20 % PEG	60 mg/ml Trypsin 32% PEG
60 mg/ml Trypsin 15% PEG	60 mg/ml Trypsin 15 % PEG	60 mg/ml Trypsin 20 % PEG	30 mg/ml Trypsin 32% PEG

Sample Key

Figure 49 - ATR-FTIR spectroscopic images for 20 well Trypsin crystallisation, A) Solution drops generated by plotting distribution of integrated absorbance of water bending mode at 1650 cm^{-1}, B) Image generated from integrated absorbance of Amide II band at 1540 cm^{-1} C) Trypsin protein crystals discovered by plotting integrated absorbance of Amide II band at ca. 1540 cm^{-1} at 21 h, D) Trypsin protein crystals discovered by plotting integrated absorbance of Amide II band at ca. 1540 cm^{-1} after 3 days, E) Sample Key showing protein and precipitant concentration in each well.

However, from the ATR images in Figure 49, it can be seen that crystallisation was not as successful as in previous experiments. 10 mg/ml protein with the screening solution produced crystals in the previous setup of measurements with a droplet volume of 2 µL (Figure 47); no crystals were observed under the same conditions when the droplet volume was reduced to 1.5 µL. Also the samples containing 20 % PEG at 60 mg/ml, 30 mg/ml and 20 mg/ml seemed to precipitate out of solution and no crystals were formed in any of the solutions, contrary to expectations based on previous results. There could be several reasons for the lack of the formation of protein crystals under these conditions, for example the reduction in drop volume. However, this is unlikely to be the case as proteins are known to form crystals in nanolitre droplets (Santarsiero et al., 2002). Figure 49 does demonstrate the potential to study up to 20 samples simultaneously with Macro ATR-FTIR spectroscopic imaging, which could be applied to the study of different protein systems.

iv. Conclusions

The results presented here show the capability of Macro ATR-FTIR spectroscopic imaging to study the crystallisation of up to 15 different protein samples simultaneously (when samples deposited manually), with potential for this to be increased to 20. The use of high throughput screening of crystallisation conditions established that the minimum concentration required for Trypsin crystallisation was 10 mg/ml and that the optimum precipitant concentration was 30 % PEG, available in the commercially available screening solution. These crystallisation conditions are in agreement with literature (Jancarik and Kim, 1991) and the results here demonstrate the application of ATR-FTIR spectroscopic imaging to study Trypsin crystallisation, a protein that has not previously been studied by ATR-FTIR imaging.

Also, through the inherent chemical specificity of infrared spectroscopy, this method was easily able to demonstrate that the crystals formed were proteinaceous. Comparison with visible images confirmed the accuracy of ATR imaging in the majority of cases, with the main disagreements occurring when a large number of overlapping crystals formed making resolution by ATR imaging impossible. Analysis of spectra from regions containing protein that appeared to have precipitated onto the surface of the ATR crystal revealed that the protein spectra was similar to that extracted from protein crystal regions. This indicated that the precipitation was not the result of denaturation of the protein. Further analysis of visible images showed that the precipitated regions contained a large number of overlapping crystals that could not be resolved individually with ATR-FTIR imaging. In this research, samples have been deposited manually but the opportunity exists for development methodology of automatic deposition (for example, using a mcirodrop system) of much smaller samples into the multiple wells on the surface of ATR crystals. This may significantly increase the number of samples studied simultaneously using ATR-FTIR spectroscopic imaging.

Overall, this chemical imaging methodology could have enormous benefits for structural proteomics projects and help to speed up the crystallisation optimisation process for new target proteins.

III. Micro ATR-FTIR imaging of hanging drop protein crystallisation

i. Introduction

The previous section demonstrated the application of ATR-FTIR imaging to microbatch protein crystallisation. In Macro configuration, the spatial resolution is limited to 40 µm with a ZnSe ATR element. However in many cases, it may not be possible to obtain protein crystals of this size and it would, therefore, be useful to obtain chemical images of in situ protein crystal growth with a higher spatial resolution. This section introduces the use of Micro ATR-FTIR spectroscopic imaging as a method that can be used to study the *in situ* growth of protein crystals in a hanging drop configuration

Micro ATR-FTIR combines a cassegrain type objective and an infrared microscope operating in reflection mode, shown in Figure 50. The angle of incidence of this type of objective is ca. 30° meaning a Germanium ATR element (n = 4) is used to ensure total internal reflection of the IR beam occurs. The high refractive index of the Germanium element combined with the IR microscope objective means that spatial resolution of approximately 4 µm can be achieved (Kazarian and Chan, 2010). This enhanced spatial resolution has enabled the study of many samples previously excluded from FTIR imaging analysis. The field of view with this approach is limited and the size of the imaging area has been measured to be approximately 64 µm x 64 µm (Kazarian and Chan, 2010). Despite this small imaging area, Micro ATR-FTIR spectroscopic imaging has great potential for the studies of polymeric materials (Gupper et al., 2002, Gupper et al., 2004, Nagle et al., 2010, Eder et al., 2012), cross-sections of paintings (Spring et al., 2008), and biomedical materials where it has already been employed to analyse cross sections of hair (Chan et al., 2008b), breast cancer tissue (Kazarian and Chan, 2010), aorta and arteries (Palombo et al., 2009) as well as to chemically image live cancer cells (Kuimova et al., 2009).

The Micro ATR-FTIR set up is particularly amenable to the study of hanging drop protein crystallisation. The Ge ATR crystal is removable, as reported previously by Chan *et al.* (Chan et al., 2008b). Therefore, drops of protein solution and precipitant solution can be deposited directly onto the Ge crystal and a reservoir can then be placed underneath the drop in exactly the same manner as that which is applied in structural biology labs. Confocal Raman microscopy has also been applied to the in situ measurement of hanging drop protein crystallisation to monitor the change in concentration of protein within the crystallisation drop (Noda et al., 2007, Vongsvivut et al., 2008).

Micro ATR-FTIR spectroscopic imaging is an imaging technique and thus requires shorter measurement and sample preparation times to obtain the same number of spectra from a sample in comparison with Confocal Raman microscopy. Also, despite the small imaging area of Micro ATR-FTIR, it is possible to measure the growth of multiple crystals using this approach as demonstrated below.

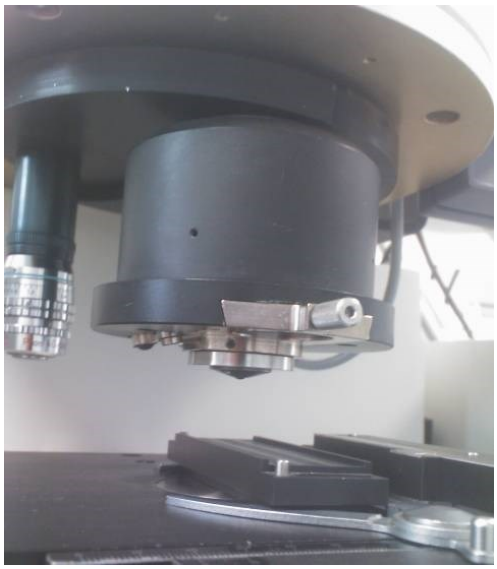

Figure 50 - Removable Germanium ATR objective.

This novel application of Micro ATR-FTIR opens up exciting opportunities for the dynamic study of protein crystallisation by measuring the growth of crystals *in situ*. The high spatial resolution of the technique allows measurement of the early stages of crystal growth through the detection of micro crystals as well as imaging of their growth. This could facilitate the identification of conditions optimal for crystal growth, quickly and easily without need to damage the crystal or move the drop. It has potential to be further developed for the study of protein structure in proteins where it is very hard to obtain X-ray standard crystals, through FTIR spectroscopic analysis of protein secondary structure. This method could also be applied to other areas of research where crystallisation is a key factor, for example within the pharmaceutical industry where crystal engineering plays an important role in understanding the behaviour and role of active pharmaceutical ingredients (Blagden et al., 2007).

This section demonstrates Micro ATR-FTIR spectroscopic imaging of three different proteins. Lysozyme and Thaumatin both crystallise readily and are, therefore, good model proteins with which to develop a new technique. The third protein studied, Lobster α-crustacyanin has previously been structurally characterised with a view to understanding the natural blue colouration of raw lobster shells. This protein is more challenging to crystallise and produces a large number of poorly diffracting crystals (Chayen et al., 2003). The results presented in this section were published by Glassford *et al.* (Glassford et al., 2012b).

ii. Experimental

Materials

Three proteins, Lysozyme, Thaumatin and α-crustacyanin were studied, each with different crystallisation conditions at 20 ^{o}C.

Hen egg-white Lysozyme (L 7651), Thaumatin from *Thaumatococcus danielii* (T 7638) and all the chemicals used in the reservoir solutions were obtained from Sigma-Aldrich. Alpha crustacyanin was provided by Peter Zagalsky of Royal Holloway University of London.

Crystallisation conditions

A solution of 40 mg/ml Lysozyme in 0.1M Sodium Acetate buffer, pH 4.5 was prepared. The corresponding reservoir solution contained 6% w/v NaCl in 0.1 M Sodium Acetate buffer, pH 4.5. Thaumatin solution at 30 mg/ml in 0.8 M Sodium Potassium Tartrate, pH 6.8 was crystallised using a reservoir solution containing 0.1 M BIS-TRIS Propane (BTP) in the same buffer. α-crustacyanin solution at 5 mg/ml in 28% w/v Polyethylene glycol monomethyl ether 2,000 was equilibrated against a reservoir solution of 0.1 M BIS-TRIS pH 6.5.

All crystallisation drops were deposited on the Ge ATR element and equilibrated against 200 µL of the appropriate reservoir solution. 2µL drops each of Lysozyme and Thaumatin were set up in a 1:1 protein to reservoir ratio while α-crustacyanin was set up in a 2:1 ratio.

Micro ATR-FTIR spectroscopic imaging measurements

All ATR-FTIR imaging measurements were carried out on a continuous scan spectrometer (Varian FTS-7000) coupled to an IR microscope equipped with a liquid nitrogen cooled focal plane array detector (FPA). A removable Germanium ATR crystal (Refractive index, n = 4) was attached to a cassegrain objective mounted on the IR microscope. The 64 x 64 pixels FPA detector has a measured imaging area of 64 µm x 64 µm in the Micro mode. Each measurement consists of 250 scans co-added at 8 cm^{-1} spectral resolution and ratioed against a background spectrum measured prior to protein deposition for each new sample. The time taken for each measurement was 7 minutes.

The crystallisation drop was deposited directly onto the measuring surface of the Germanium ATR element which was then mounted onto the IR microscope objective. A small reservoir of solution was placed beneath the crystallisation drop and the system sealed using Silicon grease, in a similar manner to commercially available hanging drop crystallisation plates (Corning Life Sciences). This set up is shown in Figure 51

Optical Images

Optical images for Lysozyme crystals were obtained using the 40 × objective on the IR microscope. In the case of Thaumatin and Lobster α-crustacyanin, optical images were obtained using a Leica optical microscope.

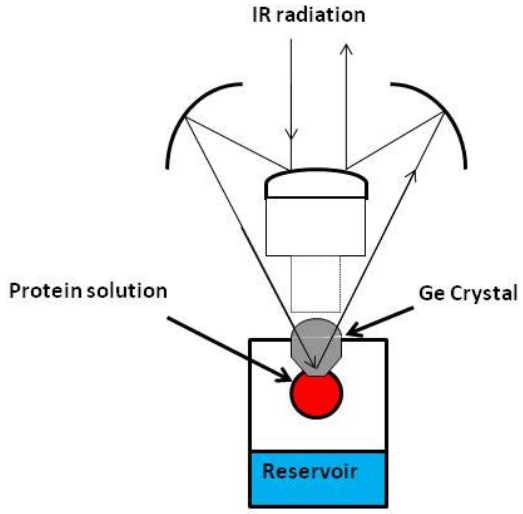

Figure 51 - Schematic of the Micro ATR imaging optics with hanging drop protein crystallisation experiment set-up. The protein crystallisation drop is placed directly onto the Ge ATR element and suspended above a reservoir solution.

iii. Results and discussion

Lysozyme

Lysozyme was used as a model protein for the development of the Micro ATR-FTIR method since it is readily crystallisable. ATR-FTIR imaging measurements were taken as soon as the trial was set up and at subsequent forty minute intervals. Over time the growth of a Lysozyme crystal could be seen in the bottom left corner of the image, shown in Figure 52. Spectra extracted from the region of the protein crystal (Figure 53) show that growth of the protein crystal is marked by the appearance of the characteristic Amide I and II bands. The ATR-FTIR images were generated by plotting the distribution of absorbance of the Amide II band at 1540 cm^{-1} within the imaging area. From the ATR-FTIR images, the maximum size of the crystal measured can be approximated to 29 μm, however it is clear than this is only a part of a crystal as the crystal had partly grown outside the field of view.

Visible images of the measuring surface of the Germanium crystal were taken after 20 hours, shown in Figure 54. Since optical images require the removal of the objective from the IR microscope, only one image was taken during the whole trial in order to minimise disturbance to the crystallisation drop. Moving the Germanium crystal can also affect the ratio with background spectra and hence should be avoided as much as possible. Water vapour can be an issue with IR spectroscopy and removing the objective exposes the spectrometer to the local environment through the gap in equipment where the objective would be. This increases the amount of water vapour within the spectrometer which interferes with the infrared light path, affecting the quality of spectral measurements. Therefore, to minimise the effect of this and allow the system to return to equilibrium, a time interval of 30 minutes was observed before taking a measurement each time the ATR element was moved.

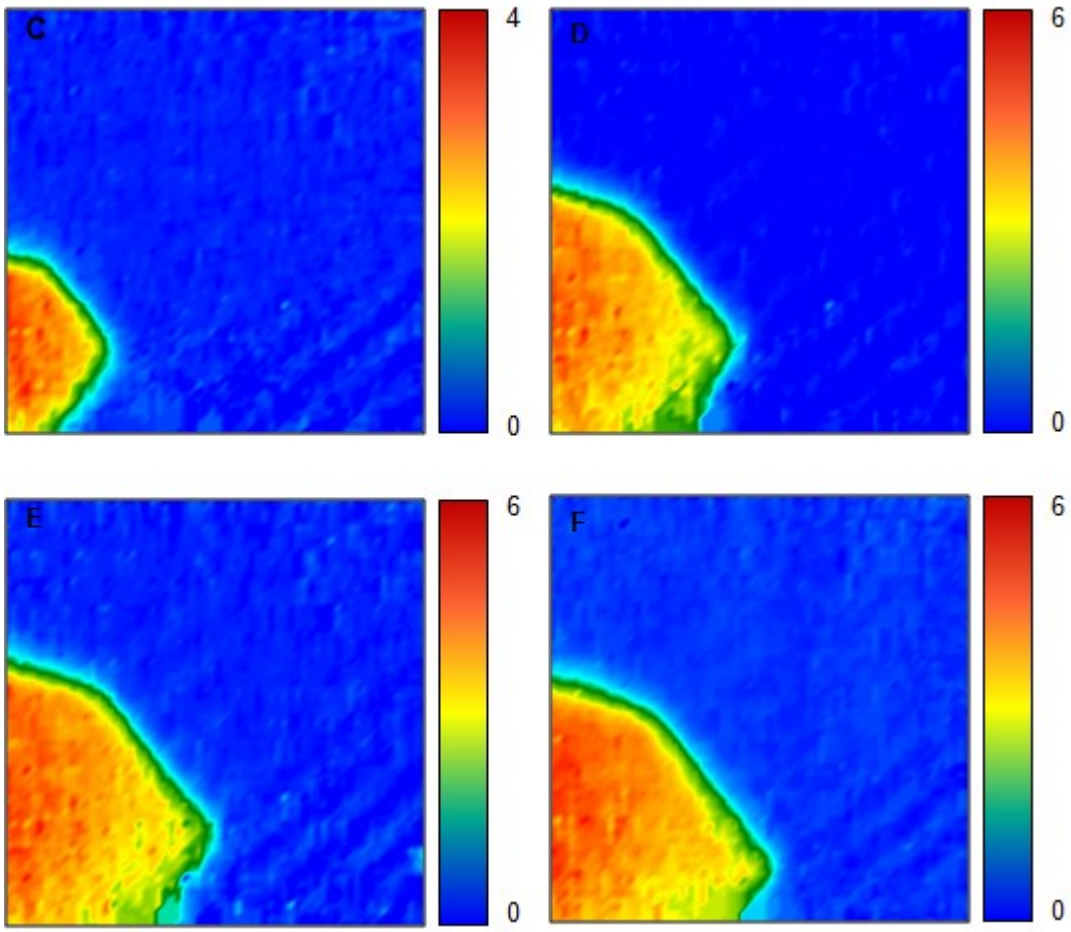

Figure 52 - Micro ATR images of Lysozyme crystal growing on Ge surface. Images show distribution of Amide II band at 1540 cm^{-1}. C = 80 min, D = 110 min, E = 140 min, F = 20 h.

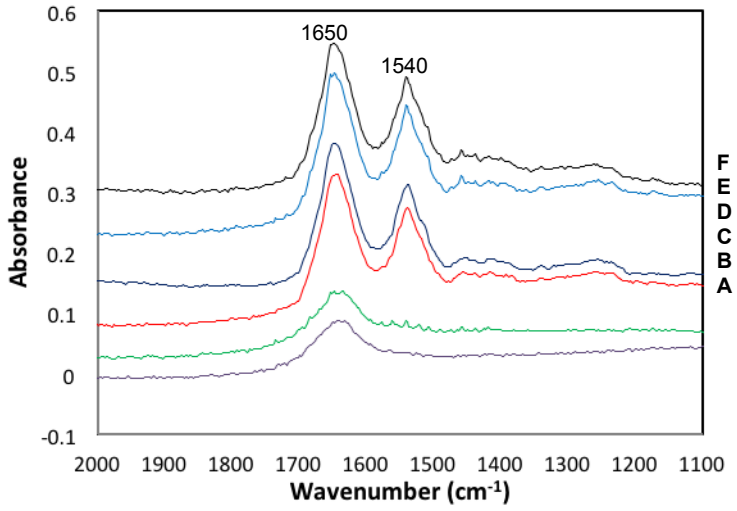

Figure 53 - Spectra extracted from the region of the protein crystal in Figure 52. A = 0 min, B = 40 min, C = 80 min, D = 110 min, E = 140 min, F = 20 h. Spectra A and B show absorption of the crystallisation solution prior to the formation of protein crystals, therefore the main band at ca. 1640 cm^{-1} is from the bending mode of water.

From the visible image (Figure 54), the presence of multiple Lysozyme crystals can be seen, with an approximate size of 50 µm, indicating that half of one of these crystals was captured using Micro ATR-FTIR imaging. This highlights the main limitation of this method; the limited imaging area. Therefore, for proteins that grow rapidly to form big crystals, it may not always be possible to capture their growth using Micro ATR-FTIR imaging. There is no guarantee that a nucleation site will occur within the imaging area and hence there is still a degree of trial and error within this approach. The exact location of the imaging area on the Germanium crystal is also not known precisely, the black dashed box in the visible image shows an estimated position (from the shape and size of the crystal on ATR image). Opportunities exist to overcome this limitation. If the exact location of the ATR imaging area was known then it may be possible to ensure crystal growth in this area through the use of surface modifications or seeding technologies, for example.

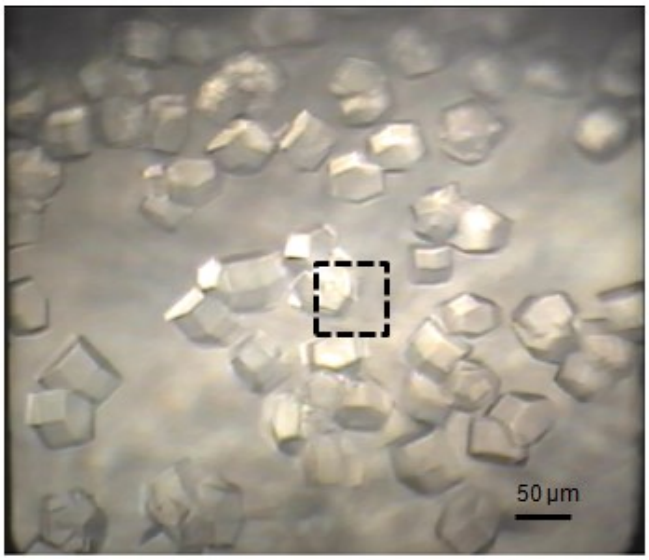

Figure 54 - Visible image of Lysozyme crystals on surface of Ge ATR element. Dashed box shows approximate size of imaging area.

Thaumatin

Thaumatin is another protein that is well characterised and crystallises readily, although crystals take longer to grow than for Lysozyme. ATR-FTIR imaging measurements were taken at time = 0, 24 and 28 h (**Error! Reference source not found.**) where the ATR images were generated by plotting the istribution of the Amide II band at 1525 cm^{-1} within the imaged area. Spectra extracted from the highlighted region are also shown as well as a visible image of the Thaumatin crystals on the Germanium surface. After 24 hours several small crystals have grown within the ATR imaging area, varying between 6 – 15 µm in size. Then at 28 h, the size of these crystals has reduced to a maximum of 6 µm. This could suggest that as the crystals increase in size, the effect of gravity means that the area of crystal in contact with the Ge surface decreases. Again an optical image was taken at the latest stage of the trial to minimise disturbance to the sample. The image shows many protein crystals across the Ge surface; however from the image it is hard to distinguish individual crystals.

Measurements of Thaumatin were repeated and ATR-FTIR images are shown in Figure 56 along with spectra extracted from the highlighted region. The spectra appear to be noisier than the previous measurements due to the presence of a larger amount of water vapour in the system. As before, after 24 h several protein crystals can be observed in the ATR-FTIR image with a maximum size of approximately 15 µm, then after 48 h the number and size of Thaumatin crystals measured has reduced; the biggest one was approximately 6 µm. A visible image (Figure 56iii) of the Germanium surface at 48 h shows Thaumatin crystals of approximately 20 µm. This helps support the postulation that as time increases and the crystals become sufficiently large, they are too heavy and less surface area is in contact with the ATR element, however further investigation is needed to confirm this. The measurements of Thaumatin crystallisation show that Micro ATR can provide information during the initial growth of the crystals meaning that it is a technique suitable for the early stages of crystallisation**.** Further analysis of the protein spectra obtained during this early, critical stage in the process could yield information about crystallisation pathway. Additionally, this analysis has the advantage of differentiation between salt and protein crystals.

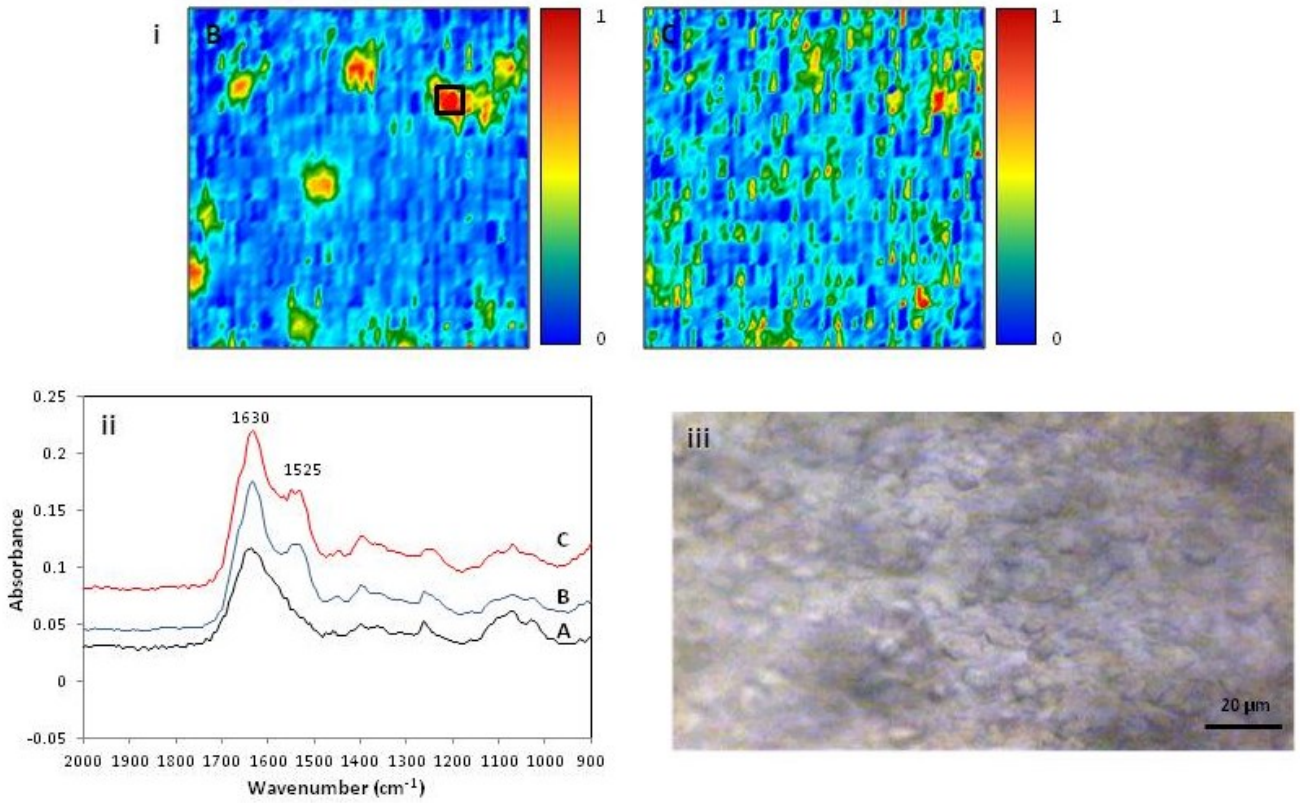

Figure 55 - i) Micro ATR images of Thaumatin crystals showing distribution of Amide II band at 1525 cm^{-1}. ii) Extracted spectra from region marked by box on the image: A = 0 h (spectra only), B = 24 h (crystal size 6 – 15 µm), C = 28 h (crystal size < 6 µm). Spectrum A shows absorption prior to formation of protein crystals. iii) Visible image of Thaumatin crystals on surface of Ge ATR element.

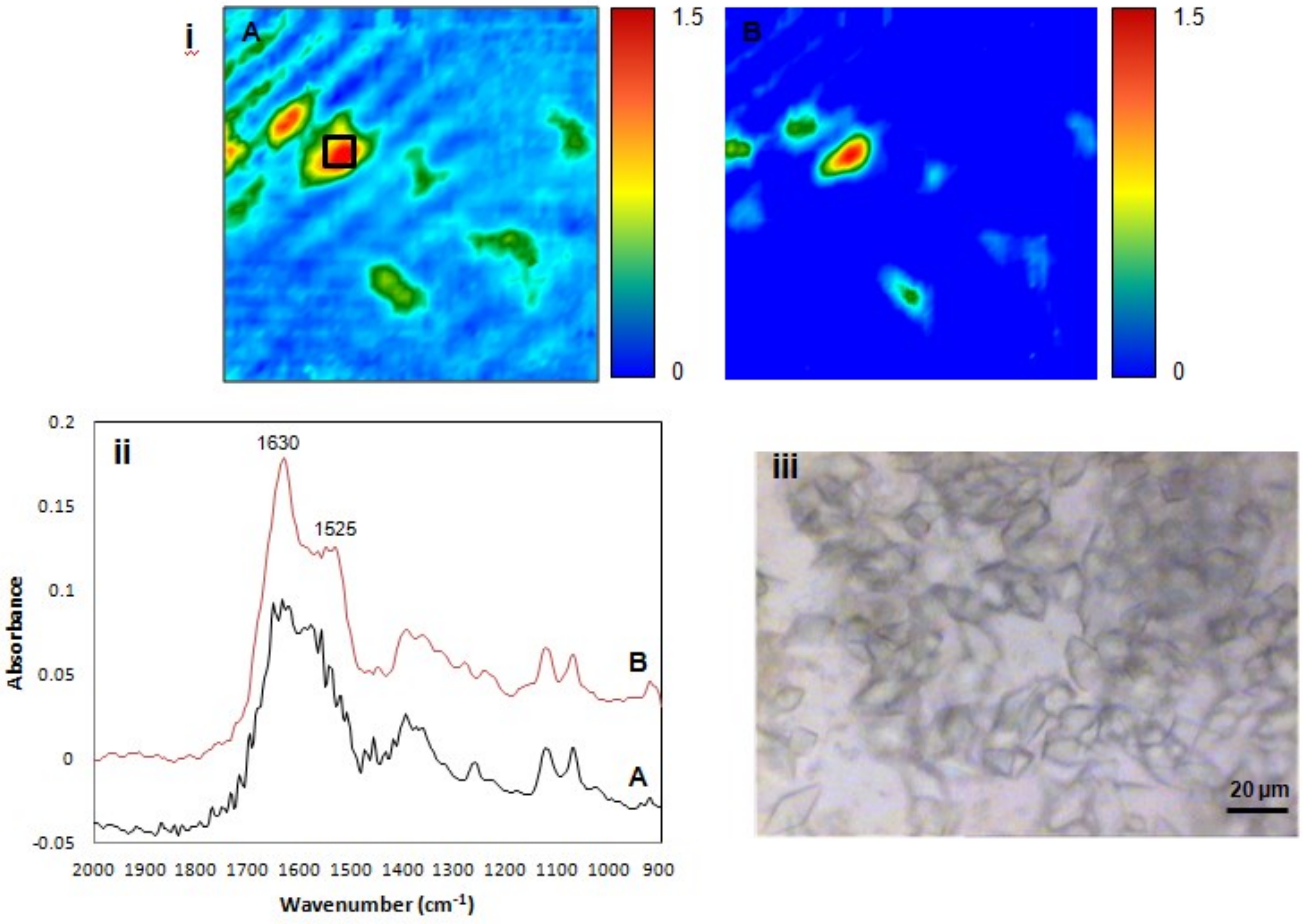

Figure 56 - i) Micro ATR images of Thaumatin crystals showing distribution of Amide II band at ca. 1525 cm^{-1}. ii) Extracted spectra from area marked by box on the image: A = 24 h (crystal size ~ 15 µm), B = 48 h (crystal size ~ 10 µm). iii) Visible image of Thaumatin crystals on Ge ATR element.

Lobster alpha crustacyanin

To determine if Micro ATR imaging could be applied to more challenging proteins, the hanging drop crystallisation of lobster α-crustacyanin was studied**.** Crystallisation drops of lobster α-crustacyanin normally result in the formation of a large number of small blue crystals which in some cases may be too small for use in X-ray studies.

α-Crustacyanin is known to take approximately one day to crystallise under standard laboratory conditions. ATR-FTIR imaging measurements were taken at 0, 48 h and 96 h, with ATR images, generated from plotting the distribution of Amide II band at 1540 cm^{-1}, shown in Figure 57 along with spectra extracted from the highlighted area. After 48 h, a large amount of the protein has aggregated onto the surface of the Ge element although several micro-crystals can also be detected, shown by the small regions of higher protein concentration. A further measurement at 96 h shows several large regions of high protein concentration. From the visible image (Figure 57) it can be seen that the crystals did not grow bigger than 10 μm, therefore these regions are most likely to be several crystals overlapping (largest region from ATR images ~ 15 μm). It should be noted that the optical image obtained shows a larger area of the Ge element surface than the imaging area using ATR-FTIR imaging therefore a direct comparison of crystals is not possible. Measurements were repeated for a new crystallisation drop, at time 1, 21 and 48 h. ATR images and spectra from the highlighted region are shown in Figure 58 along with an optical image of the protein crystals on the Ge surface. These correlate with the previous trial; by 48 h a large amount of protein had aggregated on the surface with several micro crystals present.

The measurement of the crystallisation of α-crustacyanin by this approach demonstrates the applicability to proteins that are more challenging to crystallise and highlights the ability to detect the formation of micro crystals. Previously in Macro ATR imaging studies, the spatial resolution was such that protein crystals had to be much more significant in size before they could be detected. The results presented here demonstrate that the Micro ATR-FTIR technique allows the study of proteins that do not form crystals large enough or of high enough quality for X-ray diffraction studies as well as detection of the crystals in the early stages of growth. The detection and growth of micro crystals may be of increasing importance in the future as more researchers utilise the femtosecond X-ray free-electron laser technique to solve structures of proteins (Chapman et al., 2011).

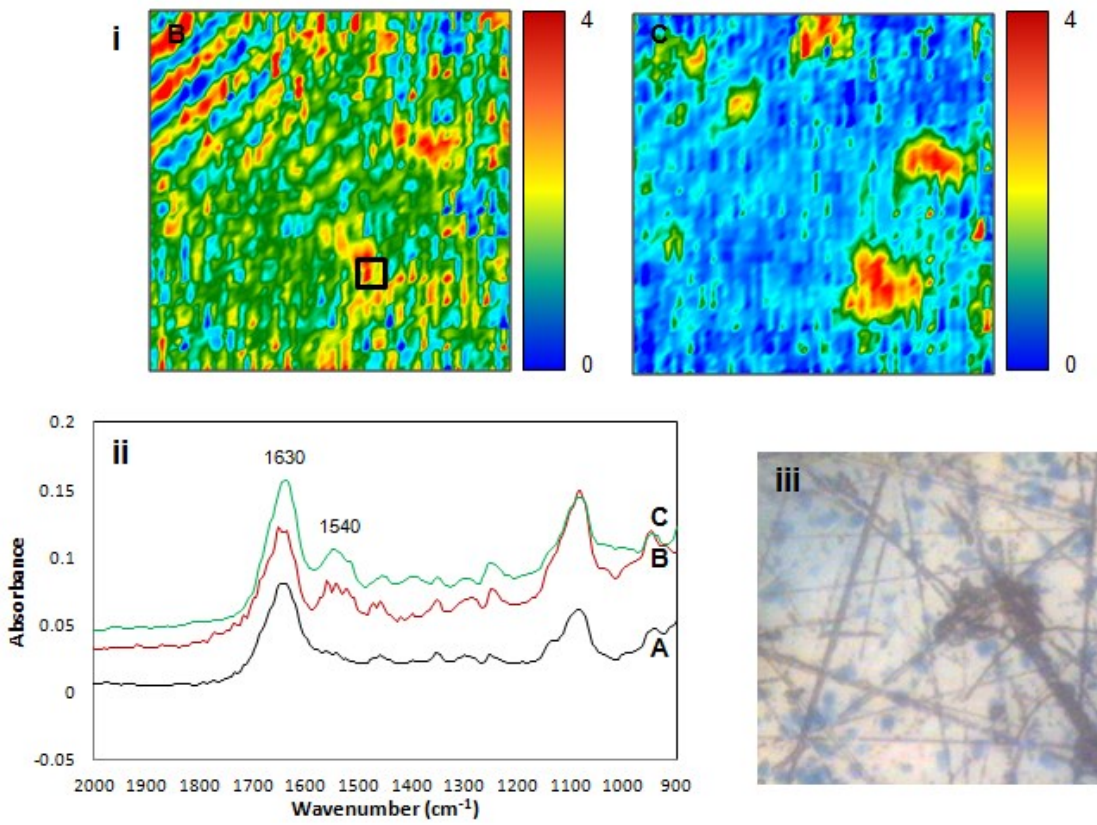

Figure 57 - i) Micro ATR images of Lobster alpha crustacyanin crystallisation. ii) Extracted spectra from boxed area. A = 0 h (spectra only), B = 48 h (Crystal size ~ 6 µm), C = 96 h (Crystal size ~ 15 µm). The ATR images show the distribution of Amide II band at ca. 1540 cm^{-1}. Spectrum A shows absorption prior to formation of protein crystals. iii) Visible image of Lobster alpha crustacyanin crystals on surface of Ge ATR element.

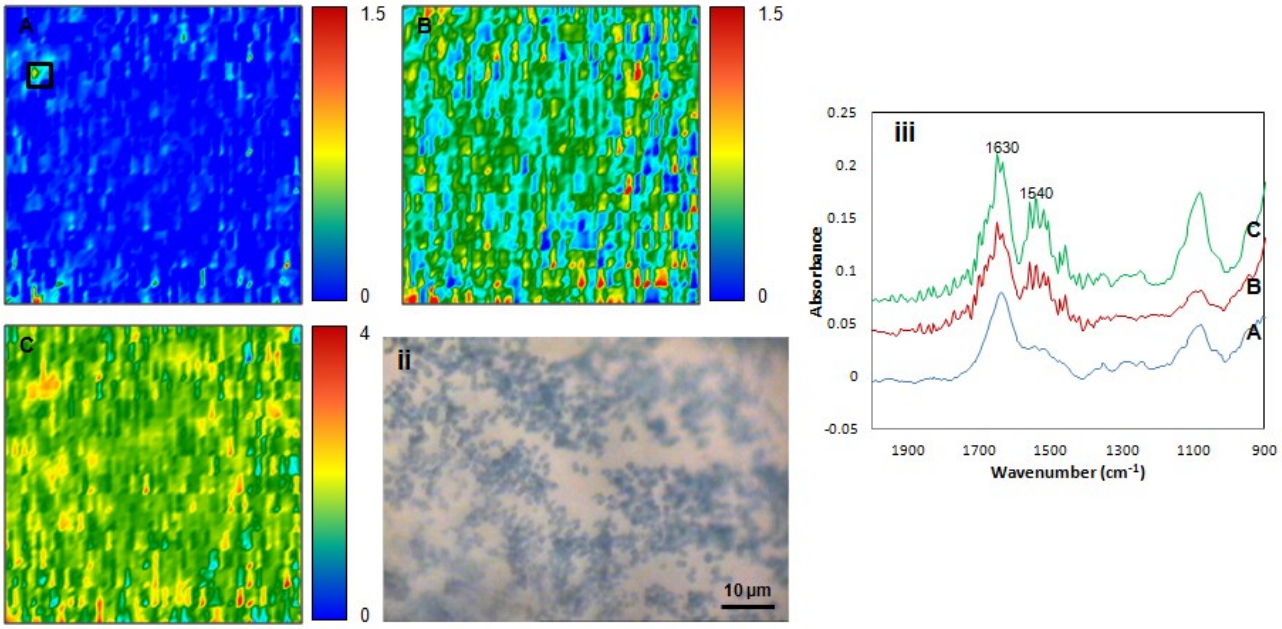

Figure 58 - i) Micro ATR images of Lobster alpha crustacyanin crystallisation. ii) Visible image of Lobster alpha crustacyanin crystals on surface of Ge ATR element. iii) Extracted spectra from boxed area. A = 1 h, B = 21 h, C = 48 h. The ATR images show the distribution of integrated absorbance of band ca. 1540 cm^{-1}. Spectrum A shows absorbance prior to formation of protein crystals.

iv. Conclusions

This section demonstrates the novel application of Micro ATR-FTIR spectroscopic imaging to the study of hanging drop protein crystallisation. The deposition of a protein solution directly onto a Germanium ATR objective means that the growth of protein crystals can be measured *in situ* without the need for additional measures to identify them as actual protein crystals, during the initial stages of crystal growth. The measurement of multiple protein crystals simultaneously has also been shown to be possible. The high spatial resolution of Micro ATR-FTIR images has allowed the detection of protein crystals approximately 6 μm in size. The high spatial resolution measurement of crystal growth *in situ* could offer exciting opportunities for the study of target proteins, especially those which do not produce crystals of the size required for X-ray crystallography. It could also have potential application within other areas of research where the understanding of crystallisation is important such as drug development.

Chapter 6 - ATR-FTIR spectroscopic imaging of proteins on a wettability gradient surface

I. Introduction

Surface property gradients are an important tool in the high-throughput investigation of the effect of surface chemistry on cell and protein adhesion (Mei et al., 2005). There has been great interest in studying the interactions of materials on surfaces as a function of the surface properties, for example the adsorption of protein (Cha et al., 2008, Krishnan et al., 2006, Buijs et al., 1996) and cells (Lee et al., 1994, Ruardy et al., 1997a, Ruardy et al., 1997b, Kennedy et al., 2006) on hydrophilic and hydrophobic surfaces. A widely applied method of modifying the properties of a surface is through the use of self assembled monolayers (SAM) where the desired surface properties can be obtained through the selection of a variety of different "tail groups" of amphiphilic molecules. In addition, it has been shown that a gradient of surface properties can be achieved using SAM (Elwing et al., 1987, Kennedy et al., 2006). The use of polymer brushes is also an established method for preparation of thicker layers with gradient properties surfaces (Morgenthaler et al., 2008, Neuhaus et al., 2011, Pei et al., 2011). However, typically the use of tags or dyes is required in order to detect and quantify the presence of proteins, cells and other biological materials on the surface, independent of the method used to prepare the surface.

Vibrational spectroscopic techniques such as FTIR imaging have a number of advantages for the study of the effects of surface chemistry on cell and protein behaviour. This analytical technique provides detailed chemical information about a sample and offers fast imaging rates (from milliseconds to minutes depending on the spectral quality required) (Chan et al., 2011, Snively and Koenig, 1999), without the need for additional labelling (Salzer et al., 2000, Kazarian and Chan, 2006, Diem et al., 2004). FTIR imaging in ATR mode is particularly flexible in terms of imaging area and spatial resolution as discussed in previous chapters and in numerous review articles (Kazarian et al., 2009, Kazarian and Chan, 2013, Kazarian and Chan, 2010). It requires minimal sample preparations with well defined sampling volumes. Each chemical imaging dataset typically contains ~4,000 to 16,000 spectra providing opportunities to study multiple components in a single set of measurements. Spectra collected simultaneously are spatially resolved which leads to the possibility of using the imaging system as a high throughput platform for parallel measurements of multiple samples (Kazarian, 2007).

This high throughput approach with ATR-FTIR imaging can be achieved by assembling a number of different samples in the imaging field of view on the surface of the ATR element such that each pixel (or a group of pixels) collects infrared spectra from an individual sample. This application has been successfully demonstrated in catalyst studies (Stavitski and Weckhuysen, 2010, Snively et al., 2001), diffusion of chemicals in skin (Andanson et al., 2009), protein crystallisation (Chan et al., 2009), pharmaceutical formulations and dissolution (Chan and Kazarian, 2006). High throughput approaches can reduce the time and cost of research, enabling optimisation of studied systems as well as reducing experimental errors.

As described in section III.viii. of Chapter 2, FTIR spectroscopy is an effective method for studying protein adsorption (Salloum and Schlenoff, 2004), surface effect on protein conformations (Steiner et al., 2007, Green et al., 1999, Ball and Jones, 1995) and protein aggregation (Oberg and Fink, 1998). This chapter presents a new opportunity for high throughput chemical analysis through the combination of ATR-FTIR imaging with chemical gradient surfaces. This will allow high throughput spectroscopic studies of the effect of surface properties on various processes such as protein adsorption and crystallisation. ATR-FTIR spectroscopy is often regarded as a low surface sensitivity technique and thus not well suited for characterising gradient surfaces with limited spatial resolution (Ruardy et al., 1997b, Jeong et al., 1996). However the development of multichannel detectors (e.g. FPA) measuring many thousands of spectra in a short time provides a solution for improvement on spatial resolution as well as sensitivity, by pixel averaging. ATR-FTIR spectroscopic imaging has also been shown to be a suitable technique for studying polymer films with sub micrometer thickness (Frosch, 2010).

The measuring surface of a Silicon (Si) based ATR-FTIR imaging system can be readily modified with SAM such as chlorosilanes or thiols. When using a thiol based system, the measuring surface of the ATR crystal first needs to be coated with a thin layer of gold. While the use of self assembled monolayers is a well established system for protein adsorption studies (Prime and Whitesides, 1991, Krishnan et al., 2006) this chapter describes a significant advance in their application showing that the effect of the surface properties on the samples studied can be characterised *in situ* with relatively high spatial resolution by ATR-FTIR spectroscopic imaging. The wettability was measured, based on the variation in absorbance of the monolayer, across the imaged area and the effects of the gradient surface properties on protein adsorption and protein crystallisation using Lysozyme as a test protein was studied showing the applicability of ATR-FTIR spectroscopic imaging within these types of studies. These results have been published by Glassford *et al.* (Glassford et al., 2012a)

II. Experimental

i. Self assembled monolayer gradient surface

The measuring surface of the Silicon ATR crystal (Pike technology, USA) has a diameter of 20 mm. The imaged area is a rectangle at the centre with dimensions of approximately 7 mm x 9.8 mm. The surface was cleaned by immersing in hot Piranha solution (a 3:1 mixture of H_2SO_4 and H_2O_2 at 100 ^oC, purchased from Sigma Aldrich, UK) for at least 30 minutes and was then thoroughly rinsed with distilled water and air dried. This leaves the surface of the Si crystal terminated with OH groups and with hydrophilic properties. A gradient of hydrophobicity can be created using a modified vapour diffusion approach to prepare a self assembled monolayer on a Silicon surface, similar to that used by Chaudhury and Whitesides (Chaudhury and Whitesides, 1992). In brief, a reservoir was created by placing a rectangular PDMS ring (Sigma Aldrich) at one end of the ATR crystal which was then filled with a solution of 0.5% Octyltrichlorosilane (OTS) (Sigma Aldrich) in hexadecane (Sigma Aldrich) as shown in Figure 59. The surface of the ATR crystal together with the reservoir was then covered and the OTS solution was left to evaporate for 1 hour. The surface of the Si that is closer to the reservoir would be exposed to a higher concentration of OTS vapour and hence becomes more hydrophobic than the areas that are further away. ATR-FTIR imaging measurements were carried out at 15 minute intervals during this time to monitor the growth of the monolayer on the Silicon surface. Following this, the OTS reservoir was removed and the surface was rinsed with hexane to remove non-reacted, excess OTS solution from the Silicon surface.

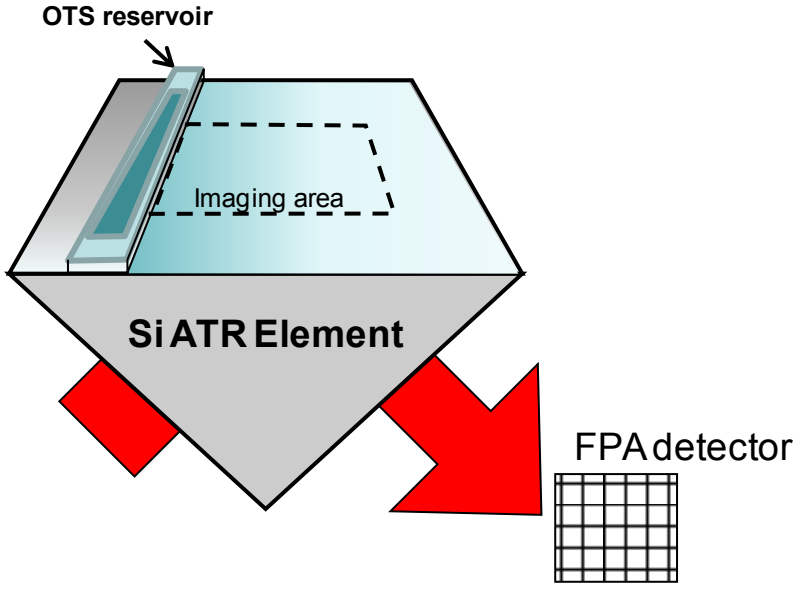

Figure 59 - Schematic diagram showing the experimental set up for creating the surface gradient properties on the Si ATR element.

ii. Contact angle measurements

Contact angle measurements (Easydrop FM40, KRÜSS GmbH) were made along the gradient surface by dropping 1 µl of water at distances of 0 mm, 2.6 mm, 5.3 mm and 8.6 mm from the edge of the reservoir on the Si surface. Contact angles were estimated using the DSA software (version 1.90.0.14) tangent 2 method.

iii. ATR-FTIR imaging measurements

All ATR-FTIR measurements were carried out on a continuous scan spectrometer (IFS66, Bruker Optics, Germany), with a Silicon ATR accessory (VeeMAX II, PIKE technologies, USA) coupled with a 96 x 96 pixels FPA detector. Each pixel of such an array detector collects an infrared spectrum from a specific location of the sample and each image contains 9216 spectra. In this arrangement the imaged area is approximately 7 mm x 9.8 mm with a spatial resolution of ~ 80 µm. For each measurement, 200 scans were co-added at 4 cm^{-1} spectral resolution in the spectral range between 3800 and 1000 cm^{-1}. Measured spectra were ratioed against appropriate backgrounds to give absorption spectra for the monolayer of OTS and adsorbed protein. For the OTS gradient measurements, a freshly cleaned Si ATR element was measured as the background. For the protein adsorption measurements, plain buffer on the OTS gradient was used as background.

iv. Protein adsorption and desorption

Lysozyme solution (Sigma Aldrich, 60 mg/ml and 40 mg/ml) was prepared by dissolving lyophilised Lysozyme in sodium acetate buffer (50 mM, pH 7). A square PDMS boundary (~10 mm x 10 mm x 2 mm) was constructed on the ATR measuring surface to form a well to retain the solution on the ATR surface during the measurement. A background was measured with buffer solution on the gradient of OTS prior to the adsorption of protein. A 0.1 ml aliquot of Lysozyme solution was deposited into the well which was then covered to prevent further evaporation. The solution was incubated at 22 ^{o}C on the ATR measuring surface for 1 hour for Lysozyme to adsorb on to the surface of the ATR element. The Lysozyme solution was then removed and the surface was rinsed twice with buffer solution to remove any non-adsorbed protein molecules. Fresh buffer was deposited on the surface with the adsorbed protein and measurements were taken every 15 min for another hour to assess desorption of protein from the surface. Since buffer solution on a newly prepared OTS gradient was used as the background, any adsorbed protein on the surface would be revealed in the FTIR spectrum.

v. Protein crystallisation

A supersaturated Lysozyme solution (60 mg/ml) was prepared by mixing equal amounts of protein solution and buffer with 7% NaCl. The mixture was deposited on the ATR element surface which had been modified to form a gradient of hydrophobicity. The deposited solution was incubated at 22 ^{o}C for 2 days under oil to allow the protein to crystallise.

III. Results and Discussion

i. Gradient characterisation

Chaudhury and Whitesides used a modified vapour diffusion method to create a gradient of hydrophobicity allowing "water to run uphill" (Chaudhury and Whitesides, 1992). It was decided that this approach could be easily applied to Silicon ATR elements to allow for the *in situ* measurement of the formation and analysis of the gradient SAM formed. Other methods used for SAM preparation would have been difficult to apply directly to the ATR surface, for example solution deposition (known as the diffusion method) where the monolayer is formed by immersing the surface into a SAM solution (Ruardy et al., 1997b). The modified vapour diffusion approach also allowed for the degree of gradient to be controlled by removing the reservoir solution after 45 min, which was shown to be the optimum time from our measurements. The selection of the amphiphilic molecule to be used was also important as it had to be volatile enough to deposit on the surface within a reasonable time frame but not too volatile that no gradient was formed. Initial experiments were carried out using Octadecyltrichlorosilane as it was hoped that the long hydrocarbon chain would allow for easier detection with ATR-FTIR imaging. However, it was not possible to form a gradient using Octadecyltrichlorosilane. It was thought that the long chain hydrocarbon was not volatile enough to deposit effectively in the vapour diffusion method. Therefore, Octyltrichlorosilane was used instead. It has a shorter chain length and is established in surface hydrophobicity studies (Wang et al., 2011, Gnanappa et al., 2011).

The ATR-FTIR imaging data acquired during the exposure of the Si surface to OTS vapour is shown in Figure 60. The image is generated by plotting the integrated absorbance of the OTS $\nu_{as}(CH_2)$ band with integration limits of 2940 cm^{-1} and 2900 cm^{-1}. The formation of the gradient of monolayer can be observed near the OTS reservoir (near top of image). Based on these images, it was difficult to observe the OTS beyond 1 mm from the reservoir. Spectra extracted from these images showed that the average peak to peak noise level of the spectrum from an individual pixel was approximately 0.0017 a.u., similar to the level of absorbance of the $\nu_{as}(CH_2)$ band from an OTS monolayer.

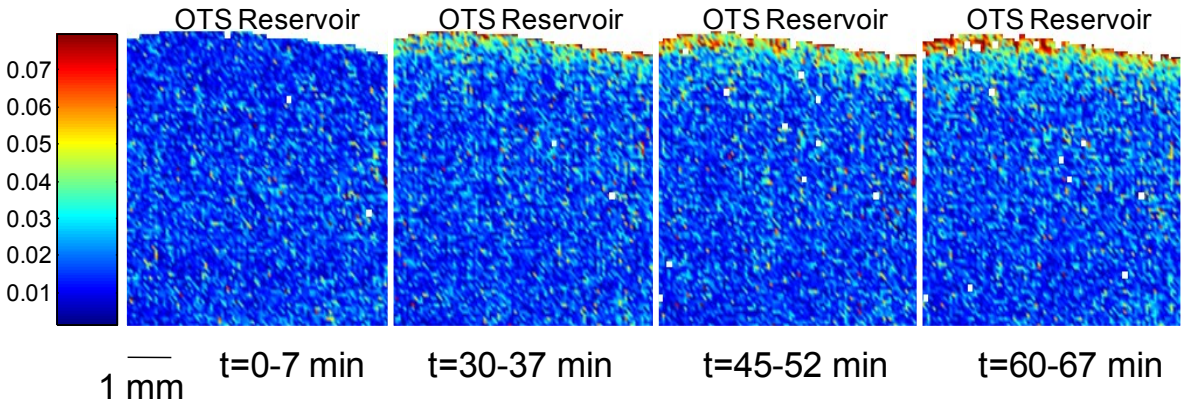

Figure 60 - ATR-FTIR images showing distribution of OTS on the Si surface as a function of exposure time in the OTS vapour. The OTS reservoir is at the top of the image. The integrated absorbance value of the OTS $\nu_{as}(CH_2)$ band is indicated by the colour scale.

An improvement to the signal to noise level of the raw imaging data measured was therefore needed. SAMs are often studied with multiple reflection ATR FT-IR spectroscopic measurements using a single element MCT detector in order to increase sensitivity (Poda et al., 2010). In imaging mode, however, it is not possible to employ multiple reflection ATR because of the degradation of spatial resolution. Furthermore, the noise level from the FPA detector is generally higher than from single element detectors due to the complexity in electronic design. Nevertheless, sensitivity of the imaging measurement can be improved by increasing the number of scans collected with an associated increase in the overall acquisition time.

Alternatively, improvement can be achieved by averaging spectra collected over a number of pixels. Theoretically, the sensitivity (or signal to noise ratio, SNR) of spectral data is improved by the square root of the number of pixels averaged if all spectra averaged have the same SNR. The effect of pixel averaging on the noise level is demonstrated in Figure 61. This shows that the SNR of the spectrum improves remarkably with pixel averaging and the noise level reduced to ~2 e^{-4} a.u. when averaging a 16 x 16 pixel block (256 pixels). However, after averaging pixels in 16 x 16 blocks, the spatial resolution of the image is also reduced by 16 times to ~1 mm x 1.4 mm (each pixel has a projected size of ~60 µm x 84 µm). The pixel dimension is a rectangle because the image is projected from the measuring surface to the detector at an angle of ~45^{o})(Chan and Kazarian, 2003).

Since the gradient was prepared along the vertical direction of the imaging area and the OTS concentration is nearly homogeneous along the horizontal direction of the image, pixel averaging along the horizontal direction enables a gain in sensitivity with minimal loss in spatial resolution. Each line along the horizontal axis has 96 pixels and the averaged spectra have shown a noise level of ~2.9 e^{-4} a.u. It is also possible to average several lines of pixels to further improve on the SNR of spectra with a trade off in spatial resolution.

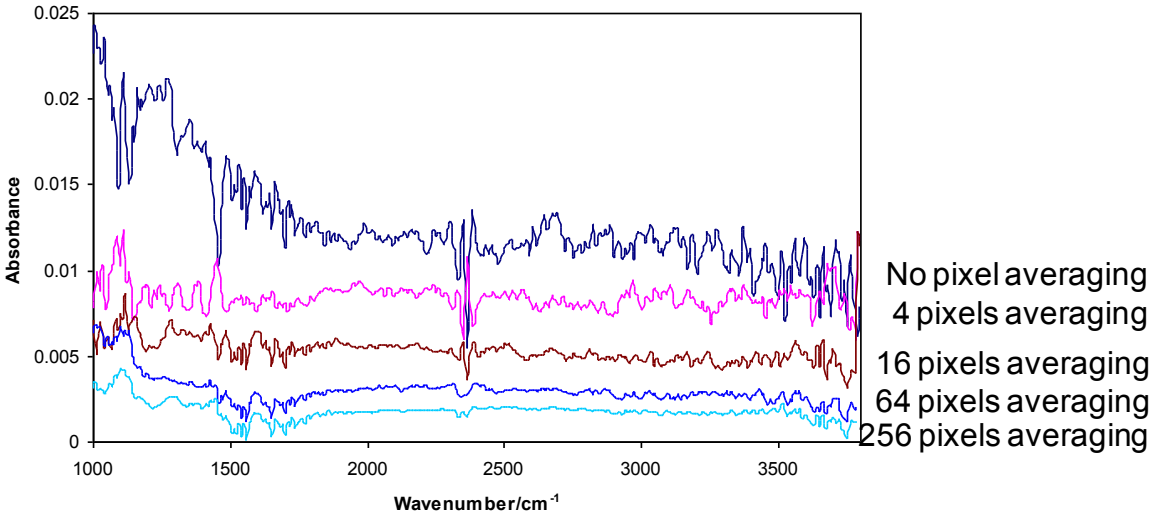

Figure 61 - Extracted spectrum and averaged spectra from the imaging data where the measurement was made with a clean Si ATR element.

By averaging each row of pixels in the imaging data, absorbance profiles of OTS on the surface of the Si element at different times of the exposure can be plotted, as shown in Figure 62a. Representative spectra are shown in Figure 62b. It is clear that the concentration, which is proportional to the absorbance, of OTS on the Si surface increased as a function of time. The area nearer the reservoir recorded a faster increase in OTS concentration than the areas further away resulting in a gradient of concentration of OTS on the surface of Si. The measurements taken when the Si surface was exposed in the OTS vapour for an extended period of time (until the reservoir is completely dried) showed that the OTS monolayer saturates the Si surface up to 1.5 mm from the reservoir and the $\nu_{as}(CH_2)$ band integrated absorbance reached a maximum value of 0.022 cm^{-1} with a peak height of 0.002 a.u. It was also shown that the OTS monolayer reached the saturation point near the reservoir after 45 minutes exposure time and the gradient extends at least 5-6 mm beyond the reservoir (Figure 62). Spatial resolution in the vertical direction is around 84 µm with the optics employed in this study.

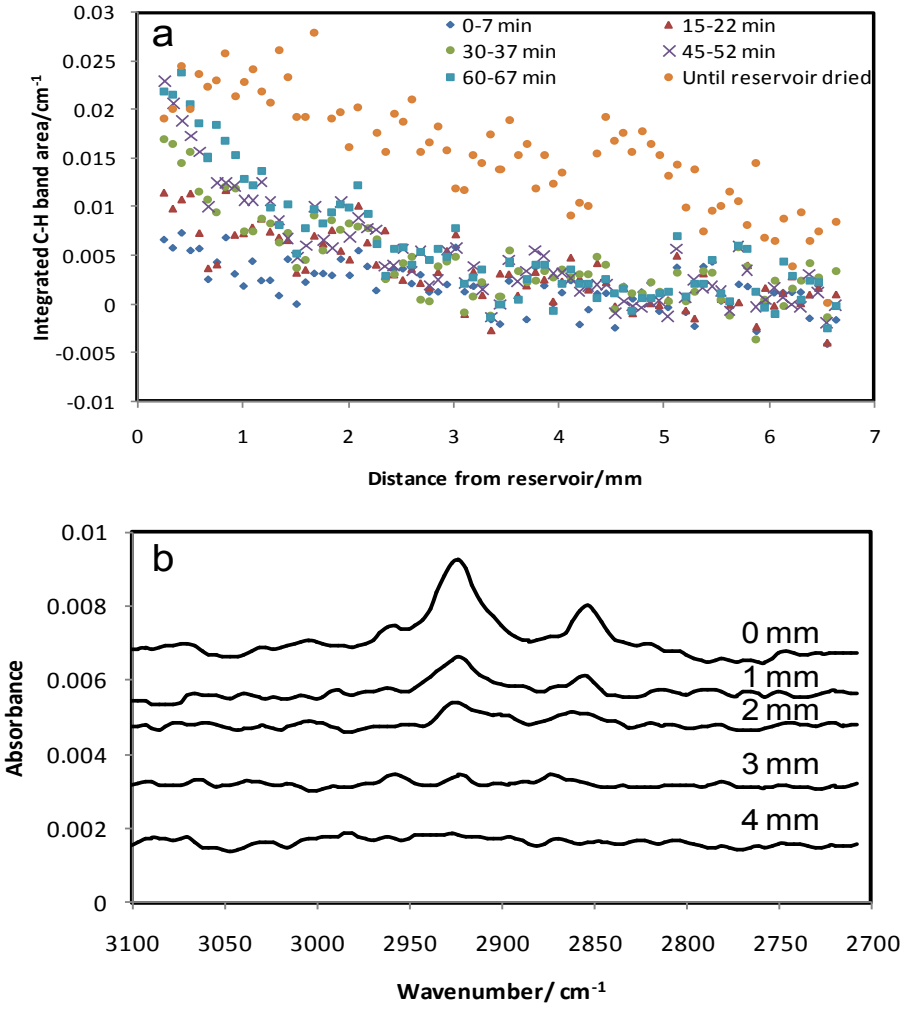

Figure 62 - a) The OTS absorbance profiles along the length perpendicular to the reservoir measured at different times after exposure to OTS vapour. The absorbance is obtained by integrating the ν_{as} (CH_2) band area between 2940 cm^{-1} and 2900 cm^{-1} of the averaged spectrum of each row of the imaged pixels. b) Representative spectra in the ν_{as} (CH_2) region extracted from rows at different distances from the OTS reservoir.

Contact angle measurements were performed to confirm the presence of the gradient property along the treated surface. The contact angles were measured at various distances from the edge of the reservoir by depositing 1 µL of water on the surface (Figure 63). The contact angles at each distance were estimated using the DSA software and are summarised in Table 5. They range from 95.6 ° at the distance nearest the reservoir to 25.5 ° at the furthest location.

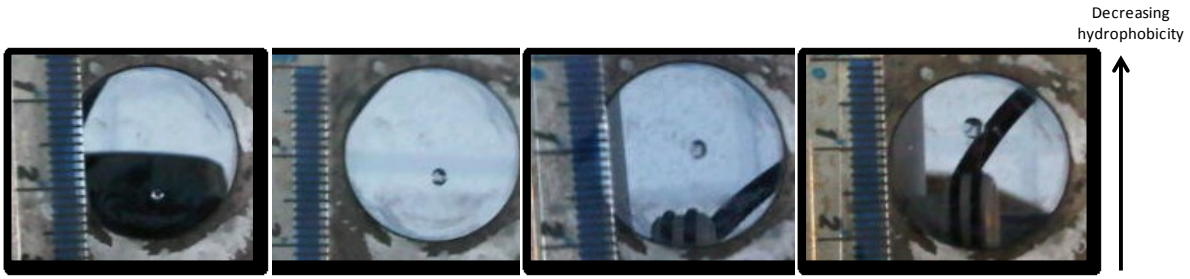

Figure 63 - Images of water droplet on the Si ATR surface with OTS gradient used to calculate contact angles.

Despite the small volume of water used in this measurement, the diameter of the drops span over ~1 - 4 mm on the surface. This demonstrates that the spatial resolution in this contact angle measurement set up is significantly worse than the spatial resolution of FTIR imaging used in the method presented. Nevertheless, the measurement confirms the presence of hydrophobic-hydrophilic gradient along the surface of the Si ATR element. Areas showing a greater absorbance of OTS bands have a higher water contact angle than the area showing a lower absorbance of OTS bands, as seen in Table 5.

Table 5 - Contact angle measurements of 1 µL of water on various positions on the Si ATR surface with OTS gradient.

Distance from the edge of OTS reservoir (mm)	Drop Diameter (mm)	Contact angles ^{o}	*Absorbance of $\nu_{as}(CH_2)$ band (cm^{-1})
0	1.15	95.6	0.018
2.6	1.77	40.0	0.0078
5.3	3.95	29.8	0.0048
8.6	4.19	26.5	-

*Averaged integrated absorbance values within the drop diameter

ii. Protein adsorption on gradient surface

After obtaining and characterising the OTS gradient, Lysozyme solution was deposited onto the gradient surface without moving the ATR element in order to demonstrate the effect of gradient surface properties on protein adsorption. Since the ATR element was not moved, the same area was imaged to facilitate direct overlay of the result from the OTS gradient measurement with the image of adsorbed protein. The protein is characterised using the Amide II band in the spectral region between 1585 cm^{-1} and 1505 cm^{-1}. The Amide II band is used since the Amide I band overlaps with water absorption which may interfere with the result. Although, in this case buffer solution was used as background so the overlap should not be significant. The spectral absorbance measurements of protein solution incubated on the surface of the ATR element were plotted against distance from the reservoir as shown in Figure 64. These initial measurements were a combination of both the dissolved protein in solution as well as the surface adsorbed protein and as such can be seen to be constant along the surface of the ATR element irrespective of the measurement time.

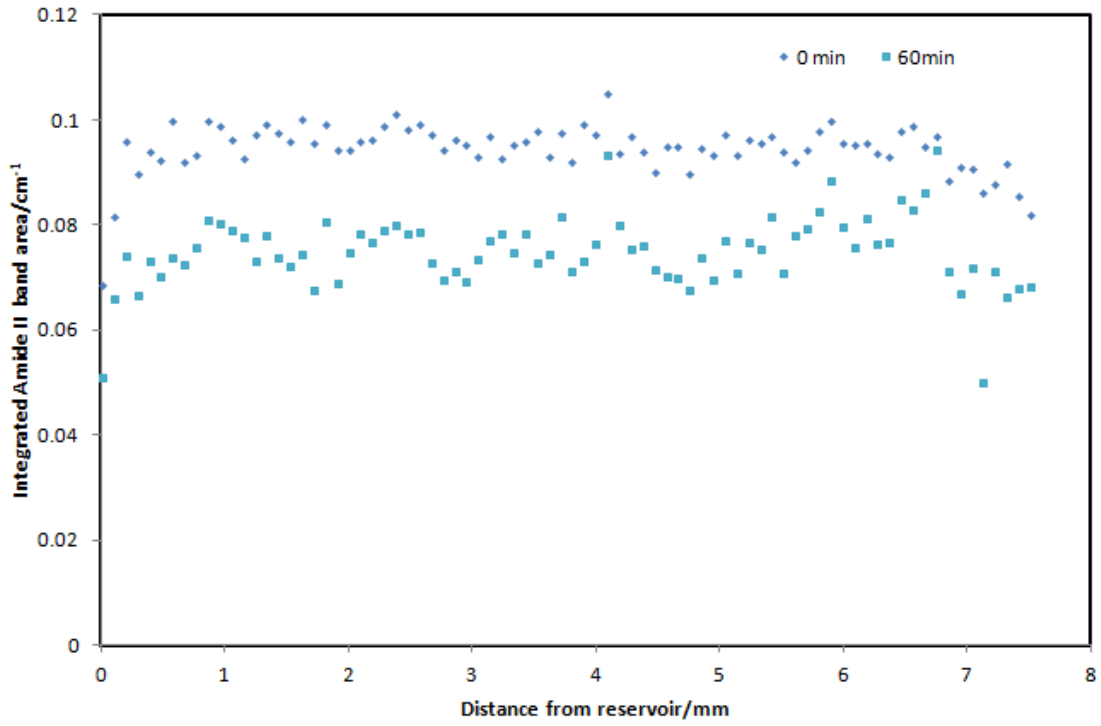

Figure 64 - Integrated Amide II absorbance with distance along Si ATR surface with OTS gradient for Lysozyme solution.

In order to measure only the adsorbed protein, the protein solution is removed and replaced with buffer solution. However there is a possibility that as the protein solution is replaced, the surface adsorbed protein will desorb into the buffer solution. By taking a series of measurements at 15 minute intervals for 1 hour after exchanging the protein solution with plain buffer and plotting the integrated absorbance of the Amide II band against distance along the surface (Figure 65), it was shown that the surface protein concentration remains the same within the measurement time. This suggests that the desorption process is insignificant within the time scale of our measurement. As with the characterisation of OTS concentration on the ATR surface, the pixels along the horizontal line of the imaging data were averaged (96 pixels) such that the imaging data becomes a column of spectra along the line of the OTS gradient.

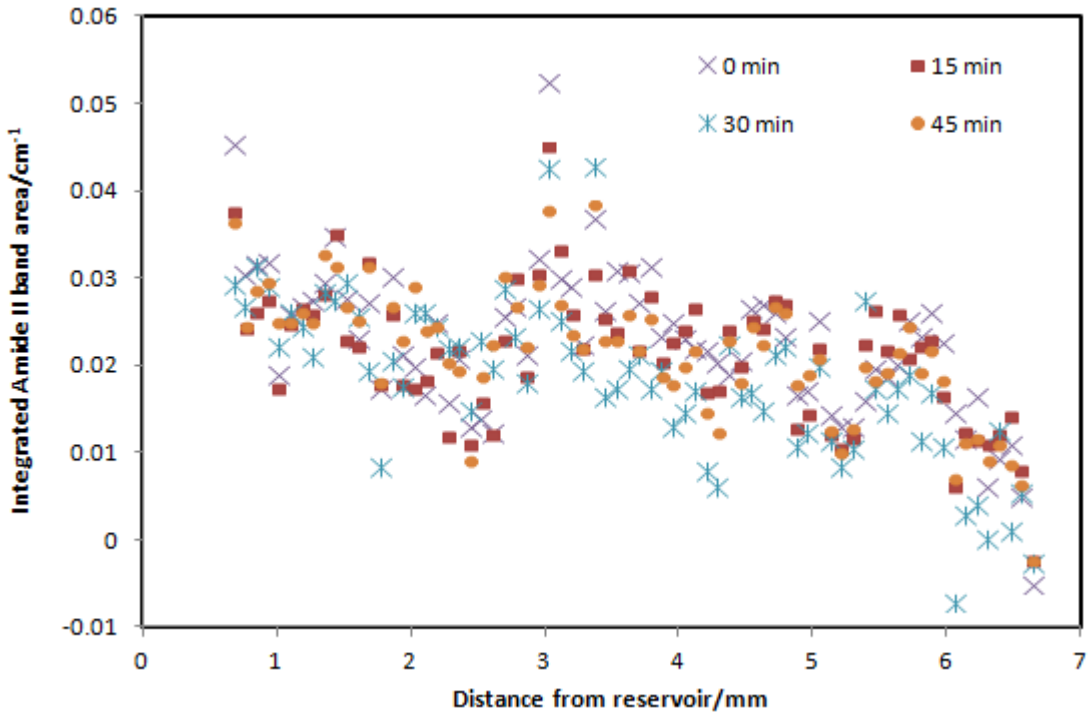

Figure 65 - Integrated Amide II absorbance with distance from reservoir taken at 15 min intervals after adding fresh buffer solution to the surface.

The plot of the Amide II band absorbance (adsorbed protein) together with the surface OTS concentration on the ATR element is shown in Figure 66a with representative spectra shown in Figure 66b. The data indicated that protein concentration decreases with decreasing OTS concentration on the surface of the ATR element. More protein adsorbed to the area where the OTS concentration is higher demonstrating that proteins are more readily adsorbed to hydrophobic surfaces than hydrophilic surfaces. This is in agreement with previous studies on protein adsorption on hydrophobic and hydrophilic surfaces studied by other techniques (Krishnan 2006, Cha 2008) and conventional ATR-FTIR spectroscopy (Jeon et al., 1994). Lysozyme is a known to have hydrophobic regions and therefore it would be expected to adsorb more readily to hydrophobic surfaces (Haynes and Norde, 1995, Prime and Whitesides, 1993). These results demonstrate the suitability of using ATR-FTIR spectroscopic imaging to assess the effects of different surface properties on protein adsorption, *in situ* and in a high throughput manner. This type of work was previously discounted as ATR-FTIR imaging was thought to lack the sensitivity required to carry out such surface analysis.

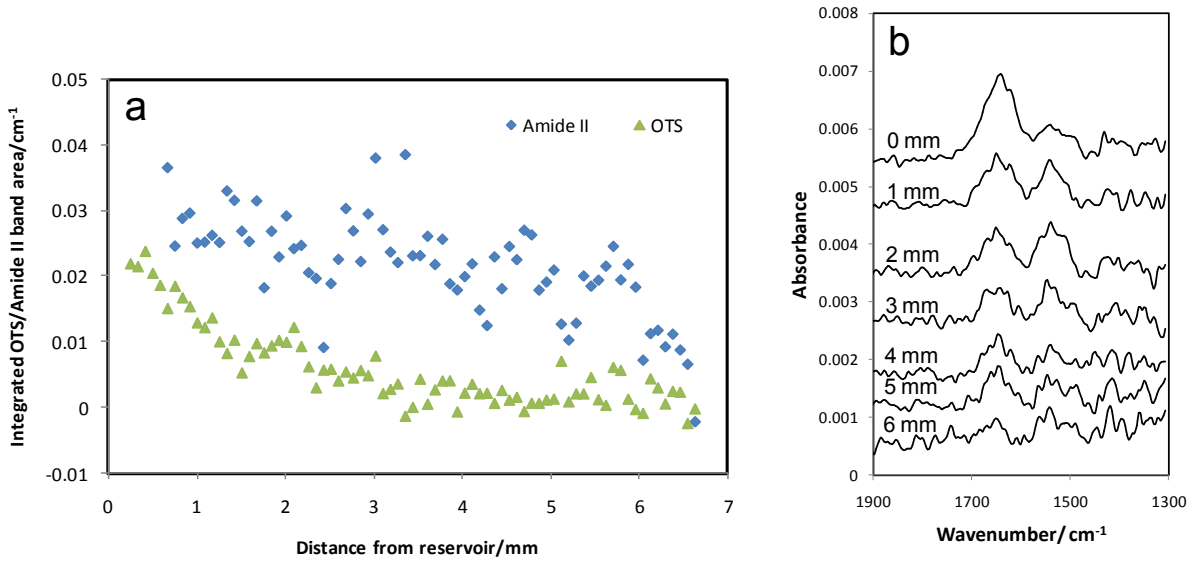

Figure 66 - a) Plot showing the amount of protein adsorbed on the surface of the Si ATR element as a function of distance along the OTS gradient which is shown on the same plot. b) Representative spectra in the Amide I and Amide II region extracted from rows at different distances from the OTS reservoir.

iii. Protein crystallisation

Protein crystallisation is often initiated near the surface of a substrate and the surface properties can play an important role in this process. A change in surface protein adsorption due to the gradient of hydrophobicity may result in a change in protein crystallisation behaviour. The application and advantages of ATR-FTIR spectroscopic imaging to study protein crystallisation has previously been demonstrated by Chan *et al.* (Chan et al., 2009) and in the work of this thesis. The combination of surface gradient and ATR-FTIR imaging provides a new opportunity to study the effects of surface properties on protein crystallisation in a high throughput manner.

A new gradient of OTS with exposure time of 45 minutes was created on the Si surface and characterised following the same procedures as described above. Lysozyme and precipitant solution were then deposited directly onto the prepared gradient and crystallisation was allowed to proceed under oil. The result is shown in Figure 67. The image is rotated and scaled such that it can be compared to the OTS gradient on the surface of the ATR element shown under the FTIR image. The FTIR image is generated by plotting the distribution of the protein-specific Amide II band absorbance across the imaged X-Y plane.

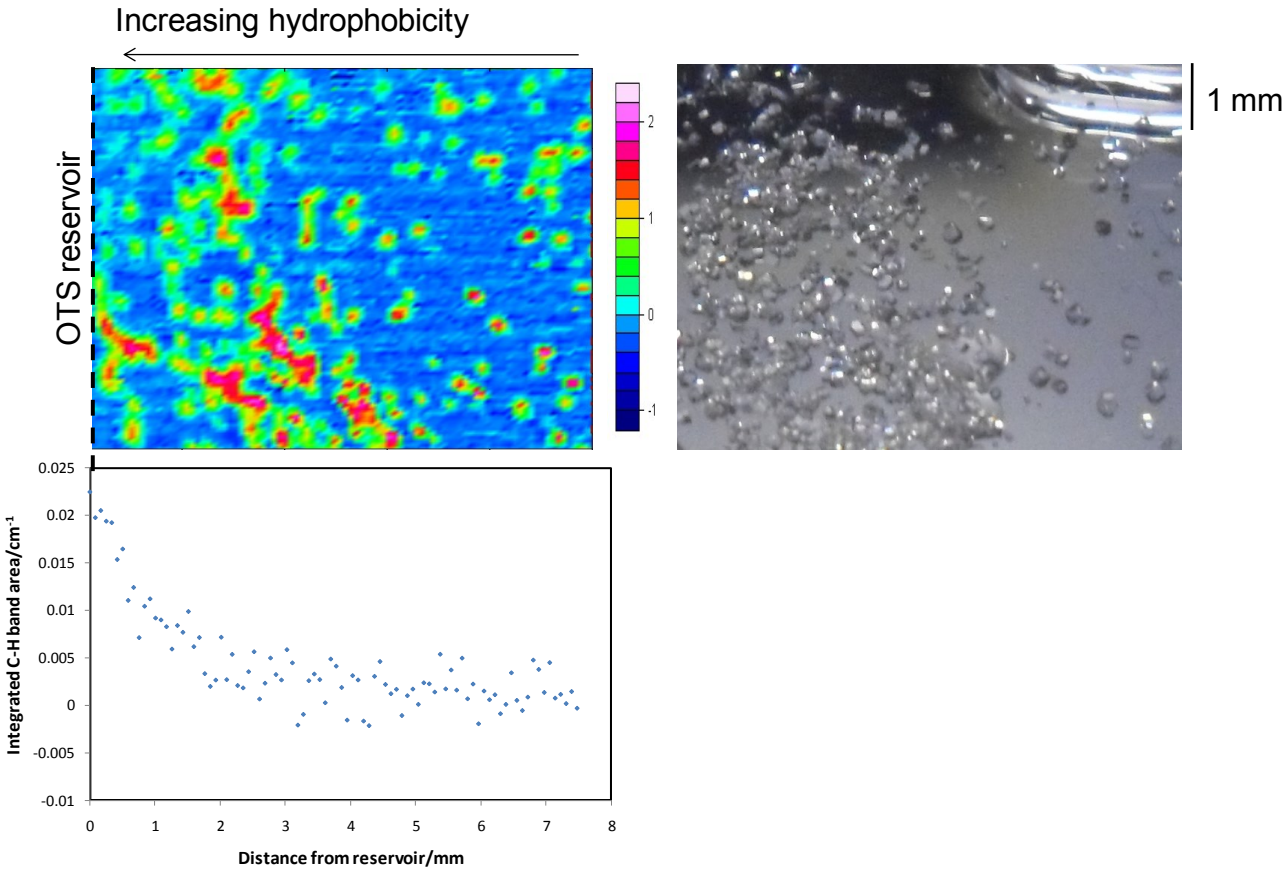

Figure 67 - ATR imaging of Lysozyme protein crystals formed on the Si ATR element. Visible image is shown on the right panel and the OTS gradient along the imaging surface is shown as a plot below the FTIR image.

The advantage of ATR-FTIR imaging is that crystals are detected and identified as proteinaceous in one single step. The protein crystals are shown by locations of highly localised Amide II absorbance on the image which removes any ambiguity that these crystals may have been salt crystals.

The result shows that after 2 days of incubation, many Lysozyme protein crystals are formed on the surface of the ATR element. The sizes of the protein crystal were similar across the imaged area; however, some protein crystals grew very close to each other and formed clusters. According to the imaging result, more protein crystals were formed on the hydrophobic side of the gradient and relatively few scattered protein crystals were formed on the hydrophilic side. This result suggests that surface hydrophobicity does have an effect on Lysozyme protein crystallisation and was demonstrated here by in situ ATR-FTIR imaging approach. Based on the protein adsorption result shown in Figure 8, there is also the indication that higher protein adsorption on the surface may facilitate protein crystallisation. As more protein is adsorbed onto the hydrophobic regions the increase in protein concentration may increase the likelihood of the nucleation of protein crystals. However, no significant effect on the protein crystal size is observed.

These findings provide more information on key biophysical properties which are advantageous to protein crystallisation and it will be interesting to explore the application of this technique to crystallisation of other more challenging proteins. It should be noted that Lysozyme was used as a model protein in this study to demonstrate the feasibility of this ATR-FTIR imaging approach to the study of the effect of surfaces on protein crystallisation.

IV. **Conclusions**

The combination of ATR-FTIR imaging with gradient concentration of self assembled monolayers (SAM) has shown to be a powerful method to study the effect of surface properties on protein adsorption and protein crystallisation. The concentration of SAM on the surface of the ATR element and the effects of this on both the amount of protein adsorbed and the number of protein crystals formed have been characterised and spatially resolved information obtained using the imaging system. More Lysozyme adsorbed to the hydrophobic side of the ATR element and more protein crystals formed in the same region suggesting a correlation exists between surface protein adsorption and protein crystallisation.

The spatial resolution achieved along the gradient is approximately 84 micrometers which could be further improved by using different optical arrangements. The sensitivity of the measurement was effectively enhanced by 6 fold by averaging the spectra measured in each row of the imaged pixels (96 pixels). Further improvement in sensitivity by averaging more rows of pixels can be achieved; this, however, would result in sacrificing the spatial resolution.

The purpose of this study was to demonstrate the development of a new technique to study SAMs using ATR-FTIR imaging and how this technique may be applied for the study of the effect of surfaces with gradient properties on biological materials simultaneously in one experiment, as shown using Lysozyme as a model protein. The use of this approach to study other proteins may reveal different behaviours depending on the properties of the protein.

It is anticipated that this technique can be applied to the high-throughput study of the effect of gradient properties on adhesion of live cells, having the advantage of characterisation of both the gradient materials and the cells without disturbing the natural environment of the system.

Chapter 7 - Conclusions and Future Work

ATR-FTIR spectroscopic imaging is a powerful and versatile analytical technique which has great potential to aid in protein studies, particularly protein crystallisation. Some of this potential has been demonstrated and developed by the work carried out in this thesis. A detailed discussion of the outcomes from each area of work has been included at the end of each chapter; therefore, the overall conclusions are presented in this chapter along with future perspectives for the application of ATR-FTIR spectroscopic imaging to study proteins.

I. Overall Conclusions

The key objective of this thesis was to develop the application of ATR-FTIR spectroscopic imaging to protein studies. This has been achieved in three core areas; further development of the application of Macro ATR-FTIR imaging to study microbatch protein crystallisation, the design and implementation of Micro ATR-FTIR imaging as a new approach to study hanging drop protein crystallisation and the development of a method combining wettability gradient surfaces with Macro ATR-FTIR imaging to study the effect of different surface properties on protein behaviour in a high-throughput manner.

Initially, a study was carried out to determine if the effects of anomalous dispersion on the bands in ATR spectra could be countered by increasing the angle of incidence of IR light to a sample. The angle of incidence was varied by fitting apertures to the lens in a diamond Golden Gate ATR accessory and the position of the Amide I band at each different angle was compared with the Amide I band position for a sample measured in transmission. Although some band shift towards the transmission peak position was observed as the angle of incidence was increased, the use of variable angle apertures did not completely negate the shift in band position caused by anomalous dispersion. It was, therefore, concluded from this useful investigation that for protein measurements, the use of a high refractive index internal reflection element should be used, for example Germanium or Silicon, which was implemented in the research presented here. This is particularly valid if one wishes to compare spectra measured in transmission with that measured in ATR mode for secondary structure analysis.

Significant progress was made in the application of ATR-FTIR imaging to protein crystallisation by expanding the number of samples studies simultaneously in Macro imaging as well through the development of Micro ATR-FTIR imaging to study hanging drop protein crystallisation. This presents the use of the imaging technique for studies using two of the most common crystallisation methods, hanging drop crystallisation and microbatch crystallisation, and could have exciting benefits for

structural proteomics projects as it allows for the identification of crystals as proteinaceous without the need for additional dyes or labels. The high spatial resolution of Micro ATR-FTIR spectroscopic imaging allowed for crystals approximately 6 µm in size to be detected and allowed their growth to be measured *in situ*. This could be particularly useful for the study of target proteins that do not produce crystals of the size required for X-ray crystallography as well as within other areas of crystallisation research, such as pharmaceuticals.

One of the key outcomes from the work in this thesis is the demonstration of the high throughput capabilities of ATR-FTIR spectroscopic imaging to protein studies. This was shown through the study of up to 20 different samples simultaneously to screen for Trypsin crystallisation conditions as well as through the combination of gradient wettability surface with Macro ATR-FTIR spectroscopic imaging. This presents good progress as high throughput studies have a range of advantages, namely savings in time and money, especially within protein research and importantly, making such measurements more reliable. Although, it should be noted that in terms of application to protein crystallisation experiments, the use of Macro ATR-FTIR imaging should be viewed as an complementary method of screening for crystallisation conditions, providing chemical information *in situ*, in addition to the conventional high throughput capabilities in the structural biology field, where thousands of samples can be screened simultaneously based on UV and visible light. It also has potential application to other screening experiments outside protein crystallisation studies such as within pharmaceutical studies for example, which has also been demonstrated within Kazarian's research group (Chan and Kazarian, 2005).

The use of Macro ATR-FTIR spectroscopic imaging to study the effect of gradient surfaces on protein adsorption and crystallisation represents a significant advance in the application of this imaging technology within the field of protein studies. Pixel averaging effectively enhanced the sensitivity of the measurements by 6 times, demonstrating that ATR-FTIR imaging with a FPA detector can be used for such sensitive surface analysis. This also represents the development of a new methodology to study self-assembled monolayers (SAMs) and demonstrates the application of such surfaces to studies of protein behaviour. It has potential to be expanded to other systems, where the effect of surface properties is important, such as adhesion of cells or understanding different stages of protein interactions with surfaces during bioprocessing of biopharmaceuticals.

In general, the work presented in this thesis demonstrates the applicability of ATR-FTIR spectroscopic imaging to a range of different protein systems and presents new and interesting applications of ATR-FTIR imaging within this field. This could be built upon and expanded to the study of different systems to provide chemically specific information, *in situ* and in a high throughput

manner. Overall, this chemical imaging methodology could have benefits for structural proteomics projects and continue to help speed up the crystallisation conditions optimisation process for new target proteins as well as within the fields of biopharmaceuticals and bioprocessing.

II. Future work

The methodologies developed in this thesis have introduced a platform for new research opportunities to use ATR-FTIR spectroscopic imaging within the field of protein studies. This could have exciting opportunities to further the understanding of protein behaviour in different environments by providing chemically specific spatial information measured *in situ*. Recommendations for future research can be split into two main areas – the application of the methodologies developed in this thesis to different protein systems and the further development of ATR-FTIR spectroscopic imaging for use within this field of studies. These recommendations are outlined below.

- The high throughput capabilities of ATR-FTIR spectroscopic imaging are clearly beneficial and these present significant opportunities. Within the area of protein crystallisation, the Macro ATR-FTIR imaging of microbatch crystallisation could be applied to the study of target proteins within proteomics studies, with the aim of reducing the time it takes to find optimum crystallisation conditions for a protein of interest, in conjunction with techniques already applied within structural biology labs.

- The potential to expand the number of samples studied simultaneously for microbatch crystallisation studies could be explored further. For example, the use of the microdrop system has previously been used for the deposition of pharmaceutical samples of different concentrations directly onto the ATR crystal within Professor Kazarian's group (Kazarian, 2007). This could be adapted for the deposition of multiple protein crystallisation samples. Although, a limitation in this case may be the spatial resolution of the Macro imaging system (spatial resolution for Macro imaging in high throughput is typically 40 µm) as reducing the drop volume is known to reduce the size of crystals grown (Bodenstaff et al., 2002) .

- The application of ATR-FTIR spectroscopic imaging to the study of protein aggregation is evolving and could represent a significant advancement in the use of imaging to study protein behaviour. The ability to study multiple samples simultaneously could allow for conditions which promote or prevent protein aggregation, such as the effect of pH and concentration, to be screened efficiently. Within the field of biopharmaceuticals to

understand the effect of exposure to different conditions during processing or to screen for the propensity of different protein variants to aggregation under similar processing conditions would also be very useful.

- The application of Micro ATR-FTIR imaging of hanging drop protein crystallisation represented an exciting new use for this imaging technique. However, some advancements could be made to further its use for protein crystallisation studies. One of the main limitations of the methodology was that the location of crystal growth on the surface of the Ge ATR element could not be controlled and this meant it was hard to ensure growth of a protein crystal was captured within the imaging field of view, especially for quick forming, large crystals. Such a limitation could be overcome through the use of surface modification or protein crystallisation seeding technologies but first the location of the imaging field of view on the Ge objective needs to be identified. Also the quality of some spectral data obtained from the initial work presented in this thesis was not sufficiently high to allow for further analysis of the Amide I band, which could yield secondary structural information. This could be improved by making adjustments to the purge or sealing of the spectrometer to reduce water vapour in the system, or by increasing the number of scans (although this would increase time of measurement which would reduce applicability to fast dynamic systems). The use of Micro ATR-FTIR imaging to study the formation of crystals with high spatial resolution could also have a range of applications beyond protein crystallisation studies, for example within the field of pharmaceuticals. The high spatial resolution and infrared spectra obtained could provide more and valuable insight into the kinetics of crystal formation by observing spectral changes in the system during the formation of crystals.

- The combination of gradient surface properties with ATR-FTIR spectroscopic imaging for *in situ* analysis of the effect of surface properties represents an exciting development and there are lots of potential avenues for future research utilising this methodology. For example, the study of competitive binding of antibodies and other proteins could be investigated for immunoassay application. This has already been investigated with traditional FTIR spectroscopy and with surface enhanced infrared spectroscopy (SEIRAS) but the spatial information available from ATR-FTIR imaging provides additional insights into these processes. It could also be applied to understanding the effect of surfaces on antibodies during bioproccesing, such as how the proteins behave in contact with chromatographic fixed bed adsorbers which are a key isolation process within the industry.

Better understanding of what is happening as antibodies interact with the internal beads of the columns could allow for more efficient use and design of such columns. Both of these examples would require further analysis of the Amide bands to provide more information about the effect of the surface on protein conformation. It is also expected that this methodology could have applications to study the effect of different surface properties on other biological materials such as cells, which is particularly relevant for the design of biomaterials.

- One potential limitation of ATR-FTIR imaging is the sensitivity, particularly for the study of SAMs and their effect of protein behaviours. This is particularly important if secondary structure analysis is to be carried out on the protein spectra. SEIRAS offers the potential to increase sensitivity through coating the surface of the ATR element with gold nanoparticles and could be combined with ATR-FTIR imaging. As discussed in section III.ix. of Chapter 2, SEIRAS is increasing being applied to protein studies, particularly for the understanding of antibody binding and for the study of membrane proteins. Preliminary results of surface enhanced ATR-FTIR spectroscopic imaging were reported by Kazarian and Chan (Kazarian and Chan, 2010) and it would be interesting to further develop this for applications to protein systems. Another established surface modification methodology used Thiols chemisorbed to gold surfaces, meaning the study of Thiol SAMs could be achieved with the enhanced sensitivity of ATR elements coated with gold nanoparticles.

- The advancements in the field of microfluidics combined with FTIR imaging (Chan et al., 2010, Chan and Kazarian, 2012, Chan and Kazarian, 2013) present some exciting opportunities for the study of proteins. This has potential to be used to gain greater understanding of protein conformation under flow as well as to replicate conditions proteins may be exposed to during processing.

References

AAMOUCHE, A. & GOORMAGHTIGH, E. 2008. FTIR-ATR biosensor based on self-assembled phospholipids surface: Haemophilia factor VIII diagnosis. *Spectroscopy-an International Journal,* 22**,** 223-234.

ALGUEL, Y., LEUNG, J., SINGH, S., RANA, R., CIVIERO, L., ALVES, C. & BYRNE, B. 2010. New Tools for Membrane Protein Research. *Current Protein & Peptide Science,* 11**,** 156-165.

ANDANSON, J. M., CHAN, K. L. A. & KAZARIAN, S. G. 2009. High-Throughput Spectroscopic Imaging Applied to Permeation Through the Skin. *Applied Spectroscopy,* 63**,** 512-517.

AROCA, R. F., ROSS, D. J. & DOMINGO, C. 2004. Surface-enhanced infrared spectroscopy. *Applied Spectroscopy,* 58**,** 324A-338A.

AROSIO, P., BAROLO, G., MULLER-SPATH, T., WU, H. & MORBIDELLI, M. 2011. Aggregation Stability of a Monoclonal Antibody During Downstream Processing. *Pharmaceutical Research,* 28**,** 1884-1894.

ATAKA, K., GIESS, F., KNOLL, W., NAUMANN, R., HABER-POHLMEIER, S., RICHTER, B. & HEBERLE, J. 2004. Oriented attachment and membrane reconstitution of his-tagged cytochrome c oxidase to a gold electrode: In situ monitoring by surface-enhanced infrared absorption spectroscopy. *Journal of the American Chemical Society,* 126**,** 16199-16206.

ATAKA, K. & HEBERLE, J. 2003. Electrochemically induced surface-enhanced infrared difference absorption (SEIDA) spectroscopy of a protein monolayer. *Journal of the American Chemical Society,* 125**,** 4986-4987.

ATAKA, K. & HEBERLE, J. 2006. Use of surface enhanced infrared absorption spectroscopy (SEIRA) to probe the functionality of a protein monolayer. *Biopolymers,* 82**,** 415-419.

ATAKA, K. & HEBERLE, J. 2007. Biochemical applications of surface-enhanced infrared absorption spectroscopy. *Analytical and Bioanalytical Chemistry,* 388**,** 47-54.

ATAKA, K. & HEBERLE, J. 2008. Bioenergetics at the gold surface: SEIRAS probes photosynthetic and respiratory reactions at the monolayer level. *Biochemical Society Transactions,* 36**,** 986-991.

ATAKA, K., KOTTKE, T. & HEBERLE, J. 2010. Thinner, Smaller, Faster: IR Techniques To Probe the Functionality of Biological and Biomimetic Systems. *Angewandte Chemie-International Edition,* 49**,** 5416-5424.

ATKINS, P. & DE PAULA, J. 2002. *Atkin's Physical Chemistry* New York: Oxford University Press.

AVERETT, L. A., GRIFFITHS, P. R. & HISHIKIDA, K. 2008. Effective path length in attenuated total reflection spectroscopy. *Analytical chemistry,* 80**,** 3045-3049.

BALL, A. & JONES, R. A. L. 1995. Conformational-changes in adsorbed proteins. *Langmuir,* 11**,** 3542-3548.

BARTH, A. & ZSCHERP, C. 2002. What vibrations tell us about proteins. *Quarterly reviews of biophysics,* 35**,** 369-430.

BERGFORS, T. 2003. Seeds to crystals. *Journal of Structural Biology,* 142**,** 66-76.

BERTHELEME, N., CHAE, P. S., SINGH, S., MOSSAKOWSKA, D., HANN, M. M., SMITH, K. J., HUBBARD, J. A., DOWELL, S. J. & BYRNE, B. 2013. Unlocking the secrets of the gatekeeper: Methods for stabilizing and crystallizing GPCRs. *Biochimica et Biophysica Acta (BBA) - Biomembranes,* 1828**,** 2583-2591.

BILL, R. M., HENDERSON, P. J. F., IWATA, S., KUNJI, E. R. S., MICHEL, H., NEUTZE, R., NEWSTEAD, S., POOLMAN, B., TATE, C. G. & VOGEL, H. 2011. Overcoming barriers to membrane protein structure determination. *Nature Biotechnology,* 29**,** 335-340.

BLAGDEN, N., DE MATAS, M., GAVAN, P. T. & YORK, P. 2007. Crystal engineering of active pharmaceutical ingredients to improve solubility and dissolution rates. *Advanced drug delivery reviews,* 59**,** 617-30.

BODENSTAFF, E. R., HOEDEMAEKER, F. J., KUIL, M. E., DE VRIND, H. P. M. & ABRAHAMS, J. P. 2002. The prospects of protein nanocrystallography. *Acta Crystallographica Section D-Biological Crystallography,* 58**,** 1901-1906.

BOLANOS GARCIA, V., CHAYEN, N. & CHAYEN, N. 2009. New directions in conventional methods of protein crystallization. *Progress in Biophysics and Molecular Biology,* 101**,** 3-12.

BOUHEKKA, A. & BURGI, T. 2012. In situ ATR-IR spectroscopy study of adsorbed protein: Visible light denaturation of bovine serum albumin on TiO2. *Applied Surface Science,* 261**,** 369-374.

BOULET-AUDET, M., BUFFETEAU, T., BOUDREAULT, S., DAUGEY, N. & PEZOLET, M. 2010. Quantitative Determination of Band Distortions in Diamond Attenuated Total Reflectance Infrared Spectra. *Journal of Physical Chemistry B,* 114**,** 8255-8261.

BRANDEN, C. & TOOZE, J. 1991. *Introduction to protein structure*, Garland Publishing.

BROWN, C. W., LI, Y., SEELENBINDER, J. A., PIVARNIK, P., RAND, A. G., LETCHER, S. V., GREGORY, O. J. & PLATEK, M. J. 1998. Immunoassays based on surface enhanced infrared absorption spectroscopy. *Analytical Chemistry,* 70**,** 2991-2996.

BUIJS, J., NORDE, W. & LICHTENBELT, J. W. T. 1996. Changes in the secondary structure of adsorbed IgG and F(ab')(2) studied by FTIR spectroscopy. *Langmuir,* 12**,** 1605-1613.

BYLER, D. M. & SUSI, H. 1986. Examination of the secondary structure of proteins by deconvolved FTIR spectra. *Biopolymers,* 25**,** 469-487.

CARPENTER, E. P., BEIS, K., CAMERON, A. D. & IWATA, S. 2008. Overcoming the challenges of membrane protein crystallography. *Current opinion in structural biology,* 18**,** 581-586.

CARPENTER, J. F., RANDOLPH, T. W., JISKOOT, W., CROMMELIN, D. J. A., MIDDAUGH, C. R. & WINTER, G. 2010. Potential Inaccurate Quantitation and Sizing of Protein Aggregates by Size Exclusion Chromatography: Essential Need to Use Orthogonal Methods to Assure the Quality of Therapeutic Protein Products. *Journal of Pharmaceutical Sciences,* 99**,** 2200-2208.

CHA, P., KRISHNAN, A., FIORE, V. F. & VOGLER, E. A. 2008. Interfacial energetics of protein adsorption from aqueous buffer to surface with varying hydrophilicity. *Langmuir,* 24**,** 2553-2563.

CHAN, K. L. A., GOVADA, L., BILL, R. M., CHAYEN, N. E. & KAZARIAN, S. G. 2009. Attenuated Total Reflection-FT-IR Spectroscopic Imaging of Protein Crystallization. *Analytical Chemistry,* 81**,** 3769-3775.

CHAN, K. L. A. & KAZARIAN, S. 2008. Attenuated total reflection-Fourier transform infrared imaging of large areas using inverted prism crystals and combining imaging and mapping. *Applied Spectroscopy,* 62**,** 1095-101.

CHAN, K. L. A. & KAZARIAN, S. G. 2003. New opportunities in micro- and macro-attenuated total reflection infrared spectroscopic imaging: Spatial resolution and sampling versatility. *Applied Spectroscopy,* 57**,** 381-389.

CHAN, K. L. A. & KAZARIAN, S. G. 2005. Fourier transform infrared imaging for high-throughput analysis of pharmaceutical formulations. *Journal of combinatorial chemistry,* 7**,** 185-189.

CHAN, K. L. A. & KAZARIAN, S. G. 2006. ATR-FTIR spectroscopic imaging with expanded field of view to study formulations and dissolution *Lab on a Chip,* 6**,** 864-870.

CHAN, K. L. A. & KAZARIAN, S. G. 2007. Attenuated total reflection Fourier transform infrared imaging with variable angles of incidence: A three-dimensional profiling of heterogeneous materials. *Applied Spectroscopy,* 61**,** 48-54.

CHAN, K. L. A. & KAZARIAN, S. G. 2012. FT-IR Spectroscopic Imaging of Reactions in Multiphase Flow in Microfluidic Channels. *Analytical Chemistry,* 84**,** 4052-4056.

CHAN, K. L. A. & KAZARIAN, S. G. 2013. Aberration-free FTIR spectroscopic imaging of live cells in microfluidic devices. *Analyst*.

CHAN, K. L. A., KAZARIAN, S. G., MAVRAKI, A. & WILLIAMS, D. R. 2005. Fourier transform infrared imaging of human hair with a high spatial resolution without the use of a synchrotron. *Applied Spectroscopy,* 59**,** 149-155.

CHAN, K. L. A., KAZARIAN, S. G., VASSOU, D., GIONIS, V. & CHRYSSIKOS, G. D. 2007. In situ high-throughput study of drug polymorphism under controlled temperature and humidity using FT-IR spectroscopic imaging. *Vibrational Spectroscopy,* 43**,** 221-226.

CHAN, K. L. A., NIU, X., DEMELLO, A. J. & KAZARIAN, S. G. 2011. Generation of Chemical Movies: FT-IR Spectroscopic Imaging of Segmented Flows. *Analytical Chemistry,* 83**,** 3606-3609.

CHAN, K. L. A., NIU, X. Z., DE MELLO, A. J. & KAZARIAN, S. G. 2010. Rapid prototyping of microfluidic devices for integrating with FT-IR spectroscopic imaging. *Lab on a Chip,* 10**,** 2170-2174.

CHAN, K. L. A., TAY, F. H., POULTER, G. & KAZARIAN, S. G. 2008a. Chemical Imaging with Variable Angles of Incidence Using a Diamond Attenuated Total Reflection Accessory. *Applied Spectroscopy,* 62**,** 1102-1107.

CHAN, K. L. A., TAY, F. H., TAYLOR, C. & KAZARIAN, S. G. 2008b. A novel approach for study of in situ diffusion in human hair using Fourier transform infrared spectroscopic imaging. *Applied Spectroscopy,* 62**,** 1041-1044.

CHANDONIA, J. M. & BRENNER, S. E. 2006. The impact of structural genomics: Expectations and outcomes. *Science,* 311**,** 347-351.

CHAPMAN, H., FROMME, P., BARTY, A., WHITE, T., KIRIAN, R., AQUILA, A., HUNTER, M., SCHULZ, J., DEPONTE, D., WEIERSTALL, U., DOAK, R. B., SHOEMAN, R. L., MARTIN, A., SCHLICHTING, I., LOMB, L., COPPOLA, N., EPP, S., HARTMANN, R., ROLLES, D., RUDENKO, A., FOUCAR, L., KIMMEL, N., WEIDENSPOINTNER, G., HOLL, P., LIANG, M., BARTHELMESS, M., CALEMAN, C., BOUTET, S., BOGAN, M., KRZYWINSKI, J., BOSTEDT, C., HÃ¶MKE, A., GUMPRECHT, L., RUDEK, B., ERK, B., SCHMIDT, C., HÃ¶MKE, A., REICH, C., PIETSCHNER, D., STRÃ¼DER, L., HAUSER, G., GORKE, H., ULLRICH, J., HERRMANN, S., SCHALLER, G., SCHOPPER, F., SOLTAU, H., KÃ¼HNEL, K.-U., MESSERSCHMIDT, M., BOZEK, J., HAU RIEGE, S., FRANK, M., HAMPTON, C., SIERRA, R., STARODUB, D., WILLIAMS, G., HAJDU, J., TIMNEANU, N., SEIBERT, M. M., ANDREASSON, J., ROCKER, A., JÃ¶NSSON, O., SVENDA, M., STERN, S., NASS, K., ANDRITSCHKE, R., SCHRÃ¶TER, C.-D., KRASNIQI, F., BOTT, M., SCHMIDT, K., WANG, X., GROTJOHANN, I., HOLTON, J., RUPP, D., NEUTZE, R., MARCHESINI, S., FROMME, R., SCHORB, S., ADOLPH, M., GORKHOVER, T., ANDERSSON, I., HIRSEMANN, H., POTDEVIN, G., GRAAFSMA, H. & NILSSON, B. 2011. Femtosecond X-ray protein nanocrystallography. *Nature,* 470**,** 73-7.

CHAUDHURY, M. K. & WHITESIDES, G. M. 1992. How to Make Water Run Uphill. *Science,* 256**,** 1539-1541.

CHAYEN, N. E. 2004. Turning protein crystallisation from an art into a science. *Current Opinion in Structural Biology,* 14**,** 577-583.

CHAYEN, N. E., CIANCI, M., GROSSMANN, J. G., HABASH, J., HELLIWELL, J. R., NNEJI, G. A., RAFTERY, J., RIZKALLAH, P. J. & ZAGALSKY, P. F. 2003. Unravelling the structural chemistry of the colouration mechanism in lobster shell. *Acta Crystallographica Section D-Biological Crystallography,* 59**,** 2072-2082.

CHAYEN, N. E. & SARIDAKIS, E. 2008. Protein crystallization: from purified protein to diffraction-quality crystal. *Nature Methods,* 5**,** 147-153.

CHAYEN, N. E., SARIDAKIS, E., EL-BAHAR, R. & NEMIROVSKY, Y. 2001. Porous silicon: an effective nucleation-inducing material for protein crystallization. *Journal of Molecular Biology,* 312**,** 591-595.

CHEREZOV, V. 2011. Lipidic cubic phase technologies for membrane protein structural studies. *Current Opinion in Structural Biology,* 21**,** 559-566.

CHEREZOV, V. & CAFFREY, M. 2006. Picolitre-scale crystallization of membrane proteins. *Journal of Applied Crystallography,* 39**,** 604-606.

CHITTUR, K. K. 1998. FTIR/ATR for protein adsorption to biomaterial surfaces. *Biomaterials,* 19**,** 357-369.

CLARK, A., SAUNDERSON, D. & SUGGETT, A. 1981. Infrared and Laser-Raman spectroscopic studies of thermally induced globular protein gels. *International journal of peptide & protein research,* 17**,** 353-364.

CORNUT, I., DESBAT, B., TURIET, J. M. & DUFOURCQ, J. 1996. In situ study by polarization modulated Fourier transform infrared spectroscopy of the structure and orientation of lipids and amphipathic peptides at the air-water interface. *Biophysical Journal,* 70**,** 305-312.

CROMWELL, M. E. M., HILARIO, E. & JACOBSON, F. 2006. Protein aggregation and bioprocessing. *Aaps Journal,* 8**,** E572-E579.

DAMALIO, J. C. P., NOBRE, T. M., LOPES, J. L., OLIVEIRA, O. N. & ARAUJO, A. P. U. 2013. Lipid interaction triggering Septin2 to assembly into beta-sheet structures investigated by Langmuir monolayers and PM-IRRAS. *Biochimica Et Biophysica Acta-Biomembranes,* 1828**,** 1441-1448.

DENGL, S., WEHMER, M., HESSE, F., LIPSMEIER, F., POPP, O. & LANG, K. 2013. Aggregation and Chemical Modification of Monoclonal Antibodies under Upstream Processing Conditions. *Pharmaceutical Research,* 30**,** 1380-1399.

DIEM, M., ROMEO, M., BOYDSTON-WHITE, S., MILJKOVIC, M. & MATTHAUS, C. 2004. A decade of vibrational micro-spectroscopy of human cells and tissue (1994-2004). *Analyst,* 129**,** 880-885.

DOBSON, C. M. 2003. Protein folding and misfolding. *Nature,* 426**,** 884-890.

DOLAMIC, I. & BURGI, T. 2011. In Situ ATR-IR Study on the Photocatalytic Decomposition of Amino Acids over Au/TiO2 and TiO2. *Journal of Physical Chemistry C,* 115**,** 2228-2234.

DONG, A., HUANG, P. & CAUGHEY, W. S. 1990. Protein secondary structures in water from 2nd-derivative Amide I Infrared spectra. *Biochemistry,* 29**,** 3303-3308.

DRENTH, J. 1999. *Principles of Protein X-Ray Crystallography*, Springer.

EDER, G. C., SPOLJARIC-LUKACIC, L. & CHERNEV, B. S. 2012. Visualisation and characterisation of ageing induced changes of polymeric surfaces by spectroscopic imaging methods. *Analytical and Bioanalytical Chemistry,* 403**,** 683-695.

ELWING, H., WELIN, S., ASKENDAL, A., NILSSON, U. & LUNDSTROM, I. 1987. A Wettability Gradient-Method for Studies of Macromolecular Interactions at the Liquid Solid Interface. *Journal of Colloid and Interface Science,* 119**,** 203-210.

FAHAM, S. & BOWIE, J. U. 2002. Bicelle crystallization: a new method for crystallizing membrane proteins yields a monomeric bacteriorhodopsin structure. *Journal of Molecular Biology,* 316**,** 1-6.

FERRER, J. L., LARIVE, N. A., BOWLER, M. W. & NURIZZO, D. 2013. Recent progress in robot-based systems for crystallography and their contribution to drug discovery. *Expert Opinion on Drug Discovery,* 8**,** 835-847.

FINK, A. L. 1998. Protein aggregation: folding aggregates, inclusion bodies and amyloid. *Folding & Design,* 3**,** R9-R23.

FROSCH 2010. Nondestructive Three-Dimensional Analysis of Layered Polymer Structures with Chemical Imaging. *Langmuir,* 26**,** 19027-19032.

GARCIA-RUIZ, J. M. 2003. Nucleation of protein crystals. *Journal of Structural Biology,* 142**,** 22-31.

GAUTIER, A., MOTT, H. R., BOSTOCK, M. J., KIRKPATRICK, J. P. & NIETLISPACH, D. 2010. Structure determination of the seven-helix transmembrane receptor sensory rhodopsin II by solution NMR spectroscopy. *Nature Structural & Molecular Biology,* 17**,** 768-774.

GERONTAS, S., SHAPIRO, M. S. & BRACEWELL, D. G. 2013. Chromatography modelling to describe protein adsorption at bead level. *Journal of Chromatography A,* 1284**,** 44-52.

GLASSFORD, S., CHAN, K. L. A., BYRNE, B. & KAZARIAN, S. G. 2012a. Chemical Imaging of Protein Adsorption and Crystallization on a Wettability Gradient Surface. *Langmuir,* 28**,** 3174-3179.

GLASSFORD, S. E., GOVADA, L., CHAYEN, N. E., BYRNE, B. & KAZARIAN, S. G. 2012b. Micro ATR FTIR imaging of hanging drop protein crystallisation. *Vibrational Spectroscopy,* 63**,** 492-498.

GNANAPPA, A. K., O'MURCHU, C., SLATTERY, O., PETERS, F., O'HARA, T., ASZALOS-KISS, B. & TOFAIL, S. A. M. 2011. Improved aging performance of vapor phase deposited hydrophobic self-assembled monolayers. *Applied Surface Science,* 257**,** 4331-4338.

GOORMAGHTIGH, E., RUYSSCHAERT, J. M. & RAUSSENS, V. 2006. Evaluation of the information content in infrared spectra for protein secondary structure determination. *Biophysical Journal,* 90**,** 2946-2957.

GRAY, J. J. 2004. The interaction of proteins with solid surfaces. *Current opinion in structural biology,* 14**,** 110-115.

GREEN, R. J., HOPKINSON, I. & JONES, R. A. L. 1999. Unfolding and intermolecular association in globular proteins adsorbed at interfaces. *Langmuir,* 15**,** 5102-5110.

GRIFFITHS, P. R. & DE HASETH, J. A. 1986. *Fourier transform infrared spectrometry*, John Wiley & Sons, Inc.

GUPPER, A., WILHELM, P., KOTHLEITNER, G., EICHHORN, K. J. & POMPE, G. 2004. Spectroscopic imaging techniques for characterization of polymer morphologies: A combination of infrared and electron microscopy. *Macromolecular Symposia,* 205**,** 171-180.

GUPPER, A., WILHELM, P., SCHMIED, M., KAZARIAN, S. G., CHAN, K. L. A. & REUSSNER, J. 2002. Combined application of imaging methods for the characterization of a polymer blend. *Applied Spectroscopy,* 56**,** 1515-1523.

GUTMANN, D. A. P., MIZOHATA, E., NEWSTEAD, S., FERRANDON, S., HENDERSON, P. J. F., VAN VEEN, H. W. & BYRNE, B. 2007. A high-throughput method for membrane protein solubility screening: The ultracentrifugation dispersity sedimentation assay. *Protein Science,* 16**,** 1422-1428.

HAMES, D. & HOOPER, N. 2005. *Biochemistry*, Taylor & Francis Group.

HANCER, M., SPERLINE, R. P. & MILLER, J. D. 2000. Anomalous dispersion effects in the IR-ATR spectroscopy of water. *Applied Spectroscopy,* 54**,** 138-143.

HARIS, P. I. & SEVERCAN, F. 1999. FTIR spectroscopic characterization of protein structure in aqueous and non-aqueous media. *Journal of Molecular Catalysis B-Enzymatic,* 7**,** 207-221.

HARRICK, N. J. 1967. *Internal reflection spectroscopy*, John Wiley & Sons, Inc.

HARTSTEIN, A., KIRTLEY, J. R. & TSANG, J. C. 1980. Enhancement of the infrared-absorption from molecular monolayers with thin metal overlayers. *Physical Review Letters,* 45**,** 201-204.

HAYNES, C. A. & NORDE, W. 1995. STRUCTURES AND STABILITIES OF ADSORBED PROTEINS. *Journal of Colloid and Interface Science,* 169**,** 313-328.

HEAPS, D. A. & GRIFFITHS, P. R. 2006. Band shapes in the infrared spectra of thin organic films on metal nanoparticles. *Vibrational Spectroscopy,* 42**,** 45-50.

HIRANO-IWATA, A., YAMAGUCHI, R., MIYAMOTO, K., KIMURA, Y. & NIWANO, M. 2009. In situ real-time monitoring of biomolecular interactions by using surface infrared spectroscopy. *Journal of Applied Physics,* 105.

HTTP://ACADEMIC.BROOKLYN.CUNY.EDU/BIOLOGY/BIO4FV/PAGE/3D_PROT.HTM. [Accessed].

HTTP://BLANCO.BIOMOL.UCI.EDU/MPSTRUC/. [Accessed].

HTTP://TARGETDB.PDB.ORG. [Accessed].

HTTP://WWW.PDB.ORG/PDB/HOME/HOME.DO. [Accessed].

HTTP://WWW.PIKETECH.COM/TECHNICAL/CRYSTAL-SELECTION-ATR.HTML. [Accessed].

JANCARIK, J. & KIM, S. H. 1991. SPARSE-MATRIX SAMPLING - A SCREENING METHOD FOR CRYSTALLIZATION OF PROTEINS. *Journal of Applied Crystallography,* 24**,** 409-411.

JENKINS, N., MURPHY, L. & TYTHER, R. 2008. Post-translational modifications of recombinant proteins: Significance for biopharmaceuticals. *Molecular Biotechnology,* 39**,** 113-118.

JEON, J. S., RAGHAVAN, S. & SPERLINE, R. P. 1994. Quatitative-analysis of albumin adsorption onto uncoated and poly(ether)urethane-coated ZnSe surfaces using the attentuated total-reflection FTIR technique *Colloids and Surfaces a-Physicochemical and Engineering Aspects,* 92**,** 255-265.

JEONG, B. J., LEE, J. H. & LEE, H. B. 1996. Preparation and characterization of comb-like PEO gradient surfaces. *Journal of Colloid and Interface Science,* 178**,** 757-763.

JIANG, X., ZUBER, A., HEBERLE, J. & ATAKA, K. 2008. In situ monitoring of the orientated assembly of strep-tagged membrane proteins on the gold surface by surface enhanced infrared absorption spectroscopy. *Physical Chemistry Chemical Physics,* 10**,** 6381-6387.

JOSEPH, E., RICCI, C., KAZARIAN, S. G., MAZZEO, R., PRATI, S. & IOELE, M. 2010. Macro-ATR-FT-IR spectroscopic imaging analysis of paint cross-sections. *Vibrational Spectroscopy,* 53**,** 274-278.

KAZARIAN, S. G. 2007. Enhancing high-throughput technology and microfluidics with FTIR spectroscopic imaging. *Analytical and Bioanalytical Chemistry,* 388**,** 529-532.

KAZARIAN, S. G. & CHAN, K. L. A. 2006. Applications of ATR-FTIR spectroscopic imaging to biomedical samples. *Biochimica Et Biophysica Acta-Biomembranes,* 1758**,** 858-867.

KAZARIAN, S. G. & CHAN, K. L. A. 2010. Micro- and Macro-Attenuated Total Reflection Fourier Transform Infrared Spectroscopic Imaging. *Applied Spectroscopy,* 64**,** 135A-152A.

KAZARIAN, S. G. & CHAN, K. L. A. 2013. ATR-FTIR spectroscopic imaging: recent advances and applications to biological systems. *Analyst,* 138**,** 1940-1951.

KAZARIAN, S. G., CHAN, K. L. A. & TAY, F. H. 2009. ATR-FT-IR imaging for pharmaceutical and polymeric materials: From micro to macro approaches. *In:* SALZER, R. & SIESLER, H. W. (eds.) *Infrared and Raman spectroscopic imaging.* Weinheim: Wiley-VCH.

KAZARIAN, S. G., EWING, A.V. 2013. Applications of Fourier transform infrared spectroscopic imaging to tablet dissolution and drug release. *Expert Opinion on Drug Delivery,* 10**,** 1207-1221.

KENNEDY, S. B., WASHBURN, N. R., SIMON, C. G. & AMIS, E. J. 2006. Combinatorial screen of the effect of surface energy on fibronectin-mediated osteoblast adhesion, spreading and proliferation. *Biomaterials,* 27**,** 3817-3824.

KIM, M. S., KHANG, G. & LEE, H. B. 2008. Gradient polymer surfaces for biomedical applications. *Progress in Polymer Science,* 33**,** 138-164.

KIMBER, J. A., KAZARIAN, S. G. & STEPANEK, F. 2011. Microstructure-based mathematical modelling and spectroscopic imaging of tablet dissolution. *Computers & Chemical Engineering,* 35**,** 1328-1339.

KONG, J. & YU, S. 2007. Fourier transform infrared spectroscopic analysis of protein secondary structures. *Acta Biochimica Et Biophysica Sinica,* 39**,** 549-559.

KRIMM, S. 1962. Infrared spectra and chain conformation of proteins. *Journal of Molecular Biology,* 4**,** 528-540.

KRISHNAN, A., CHA, P., LIU, Y. H., ALLARA, D. & VOGLER, E. A. 2006. Interfacial energetics of blood plasma and serum adsorption to a hydrophobic self-assembled monolayer surface. *Biomaterials,* 27**,** 3187-3194.

KUIMOVA, M. K., CHAN, K. L. A. & KAZARIAN, S. G. 2009. Chemical Imaging of Live Cancer Cells in the Natural Aqueous Environment. *Applied Spectroscopy,* 63**,** 164-171.

LANE, R. & SEO, S. S. 2012. Attenuated Total Reflectance Fourier Transform Infrared Spectroscopy Method to Differentiate Between Normal and Cancerous Breast Cells. *Journal of Nanoscience and Nanotechnology,* 12**,** 7395-7400.

LEE, J. H., JUNG, H. W., KANG, I. K. & LEE, H. B. 1994. Cell behaviour on polymer surfaces with different functional-groups *Biomaterials,* 15**,** 705-711.

LI, L. & ISMAGILOV, R. F. 2010. Protein Crystallization Using Microfluidic Technologies Based on Valves, Droplets and SlipChip. *In:* REES, D. C., DILL, K. A. & WILLIAMSON, J. R. (eds.) *Annual Review of Biophysics, Vol 39.* Palo Alto: Annual Reviews.

MA, Z. W., MAO, Z. W. & GAO, C. Y. 2007. Surface modification and property analysis of biomedical polymers used for tissue engineering. *Colloids and Surfaces B-Biointerfaces,* 60**,** 137-157.

MATHEUS, S., FRIESS, W. & MAHLER, H. C. 2006. FTIR and nDSC as analytical tools for high-concentration protein formulations. *Pharmaceutical Research,* 23**,** 1350-1363.

MCPHERSON, A. 2004. Introduction to protein crystallization. *Methods,* 34**,** 254-265.

MEI, Y., WU, T., XU, C., LANGENBACH, K. J., ELLIOTT, J. T., VOGT, B. D., BEERS, K. L., AMIS, E. J. & WASHBURN, N. R. 2005. Tuning cell adhesion on gradient poly(2-hydroxyethyl methacrylate)-grafted surfaces. *Langmuir,* 21**,** 12309-12314.

MERKLIN, G. T. & GRIFFITHS, P. R. 1997a. Effect of microscopic surface roughness in surface-enhanced infrared absorption spectrometry. *Journal of Physical Chemistry B,* 101**,** 5810-5813.

MERKLIN, G. T. & GRIFFITHS, P. R. 1997b. Influence of chemical interactions on the surface-enhanced infrared absorption spectrometry of nitrophenols on copper and silver films. *Langmuir,* 13**,** 6159-6163.

MILLER, L. M., BOURASSA, M. W. & SMITH, R. J. 2013. FTIR spectroscopic imaging of protein aggregation in living cells. *Biochimica et Biophysica Acta (BBA) - Biomembranes*.

MIYAZAWA, T. & BLOUT, E. R. 1961. The Infrared Spectra of Polypeptides in Various Conformations: Amide I and II Bands1. *Journal of the American Chemical Society,* 83**,** 712-719.

MORGENTHALER, S., ZINK, C. & SPENCER, N. D. 2008. Surface-chemical and -morphological gradients. *Soft Matter,* 4**,** 419-434.

MRKSICH, M. & WHITESIDES, G. M. 1996. Using self-assembled monolayers to understand the interactions of man-made surfaces with proteins and cells. *Annual Review of Biophysics and Biomolecular Structure,* 25**,** 55-78.

NAGLE, D. J., GEORGE, G. A., RINTOUL, L. & FREDERICKS, P. M. 2010. Use of micro-ATR/FTIR imaging to study heterogeneous polymer oxidation by direct solvent casting onto the ATR IRE. *Vibrational Spectroscopy,* 53**,** 24-27.

NAKANISHI, K., SAKIYAMA, T. & IMAMURA, K. 2001. On the adsorption of proteins on solid surfaces, a common but very complicated phenomenon. *Journal of Bioscience and Bioengineering,* 91**,** 233-244.

NASSE, M. J., WALSH, M. J., MATTSON, E. C., REININGER, R., KAJDACSY-BALLA, A., MACIAS, V., BHARGAVA, R. & HIRSCHMUGL, C. J. 2011. High-resolution Fourier-transform infrared chemical imaging with multiple synchrotron beams. *Nature Methods,* 8**,** 413-U58.

NATH, N., HYUN, J., MA, H. & CHILKOTI, A. 2004. Surface engineering strategies for control of protein and cell interactions. *Surface Science,* 570**,** 98-110.

NEUHAUS, S., PADESTE, C. & SPENCER, N. D. 2011. Versatile Wettability Gradients Prepared by Chemical Modification of Polymer Brushes on Polymer Foils. *Langmuir,* 27**,** 6855-6861.

NISHIKAWA, Y., NAGASAWA, T., FUJIWARA, K. & OSAWA, M. 1993. Silver island films for surface-enhanced infrared-absorption spectroscopy - Effect of island morphology on the absorption enhancement. . *Vibrational Spectroscopy,* 6**,** 43-53.

NODA, K., SATO, H., WATANABE, S., YOKOYAMA, S. & TASHIRO, H. 2007. Efficient characterization for protein crystals using confocal Raman spectroscopy. *Applied Spectroscopy,* 61**,** 11-18.

OBERG, K. A. & FINK, A. L. 1998. A new attenuated total reflectance Fourier transform infrared spectroscopy method for the study of proteins in solution. *Analytical Biochemistry,* 256**,** 92-106.

ONODERA, K., HIRANO-IWATA, A., MIYAMOTO, K. I., KIMURA, Y., KATAOKA, M., SHINOHARA, Y. & NIWANO, M. 2007. Label-free detection of protein-protein interactions at the GaAs/Water interface through surface infrared spectroscopy: Discrimination between specific and nonspecific interactions by using secondary structure analysis. *Langmuir,* 23**,** 12287-12292.

OSAWA, M., ATAKA, K., YOSHII, K. & NISHIKAWA, Y. 1993. Surface-enhanced infrared spectroscopy - The origin of the absorption enhancement and band selection rule in the infrared-spectra of molecules adsorbed on fine metal particles *Applied Spectroscopy,* 47**,** 1497-1502.

OSAWA, M. & IKEDA, M. 1991. Surface enhanced infrared-absorption of para-nitrobenzoic acid deposited on silver island films - contributions of eletromagnetic and chemical mechanisms *Journal of Physical Chemistry,* 95**,** 9914-9919.

OSAWA, M., KURAMITSU, M., HATTA, A. & SUETAKA, W. 1986. Electricmagnetic effect in enhanced infrared-absorption of adsorbed molecules on thin metal-films. *Surface Science,* 175**,** L787-L793.

P. SCHWINTÉ, J. C. V., C. PICART, Y. HAIKEL, P. SCHAAF, B. SZALONTAI 2001. Stabilizing Effects of Various Polyelectrolyte Multilayer Films on the Structure of Adsorbed/Embedded Fibrinogen Molecules: An ATR−FTIR Study†. *The journal of physical chemistry. B,* 105**,** 11906-11916.

PALOMBO, F., CREMERS, S. G., WEINBERG, P. D. & KAZARIAN, S. G. 2009. Application of Fourier transform infrared spectroscopic imaging to the study of effects of age and dietary L-arginine on aortic lesion composition in cholesterol-fed rabbits. *Journal of the Royal Society Interface,* 6**,** 669-680.

PEI, J., HALL, H. & SPENCER, N. D. 2011. The role of plasma proteins in cell adhesion to PEG surface-density-gradient-modified titanium oxide. *Biomaterials,* 32**,** 8968-8978.

PERRY, S. L., GUHA, S., PAWATE, A. S., BHASKARLA, A., AGARWAL, V., NAIR, S. K. & KENIS, P. J. A. 2013. A microfluidic approach for protein structure determination at room temperature via on-chip anomalous diffraction. *Lab on a Chip,* 13**,** 3183-3187.

PINKERNEIL, P., GULDENHAUPT, J., GERWERT, K. & KOTTING, C. 2012. Surface-Attached Polyhistidine-Tag Proteins Characterized by FTIR Difference Spectroscopy. *Chemphyschem,* 13**,** 2649-2653.

PODA, A., ANDERSON, A. & ASHURST, W. R. 2010. Self-assembled octadecyltrichlorosilane monolayer formation on a highly hydrated silica film. *Applied Surface Science,* 256**,** 6805-6813.

PRIM, D., CRELIER, S. & SEGURA, J. M. 2011. Coupling of a Microfluidic Mixer to a Fourier-transform Infrared Spectrometer for Protein-Conformation Studies. *Chimia,* 65**,** 815-816.

PRIME, K. & WHITESIDES, G. 1991. Self-assembles organic monolayers - Model systems for studying adsorption of proteins at surfaces *Science,* 252**,** 1164-1167.

PRIME, K. L. & WHITESIDES, G. M. 1993. ADSORPTION OF PROTEINS ONTO SURFACES CONTAINING END-ATTACHED OLIGO(ETHYLENE OXIDE) - A MODEL SYSTEM USING SELF-ASSEMBLED MONOLAYERS. *Journal of the American Chemical Society,* 115**,** 10714-10721.

PRIVE, G. G. 2007. Detergents for the stabilization and crystallization of membrane proteins. *Methods,* 41**,** 388-397.

RASK-ANDERSEN, M., ALMEN, M. S. & SCHIOTH, H. B. 2011. Trends in the exploitation of novel drug targets. *Nature Reviews Drug Discovery,* 10**,** 579-590.

REYNOLDS, P. M., PEDERSEN, R. H., STORMONTH-DARLING, J., DALBY, M. J., RIEHLE, M. O. & GADEGAARD, N. 2013. Label-Free Segmentation of Co-cultured Cells on a Nanotopographical Gradient. *Nano Letters,* 13**,** 570-576.

RICH, P. R. & IWAKI, M. 2007. Methods to probe protein transitions with ATR infrared spectroscopy. *Molecular Biosystems,* 3**,** 398-407.

RIGLER, P., ULRICH, W. P., HOFFMANN, P., MAYER, M. & VOGEL, H. 2003. Reversible immobilization of peptides: Surface modification and in situ detection by attenuated total reflection FTIR Spectroscopy. *Chemphyschem,* 4**,** 268-275.

ROSENBERG, A. S. 2006. Effects of protein aggregates: An immunologic perspective. *The AAPS Journal,* 8**,** E501-E507.

RUARDY, T. G., MOORLAG, H. E., SCHAKENRAAD, J. M., VANDERMEI, H. C. & BUSSCHER, H. J. 1997a. Growth of fibroblasts and endothelial cells on wettability gradient surfaces. *Journal of Colloid and Interface Science,* 188**,** 209-217.

RUARDY, T. G., SCHAKENRAAD, J. M., VANDERMEI, H. C. & BUSSCHER, H. J. 1997b. Preparation and characterization of chemical gradient surfaces and their application for the study of cellular interaction phenomena. *Surface Science Reports,* 29**,** 3-30.

SALLOUM, D. S. & SCHLENOFF, J. B. 2004. Protein adsorption modalities on polyelectrolyte multilayers. *Biomacromolecules,* 5**,** 1089-1096.

SALZER, R., STEINER, G., MANTSCH, H. H., MANSFIELD, J. & LEWIS, E. N. 2000. Infrared and Raman imaging of biological and biomimetic samples. *Fresenius' Journal of Analytical Chemistry,* 366**,** 712-726.

SANTARSIERO, B. D., YEGIAN, D. T., LEE, C. C., SPRAGGON, G., GU, J., SCHEIBE, D., UBER, D. C., CORNELL, E. W., NORDMEYER, R. A., KOLBE, W. F., JIN, J., JONES, A. L., JAKLEVIC, J. M., SCHULTZ, P. G. & STEVENS, R. C. 2002. An approach to rapid protein crystallization using nanodroplets. *Journal of Applied Crystallography,* 35**,** 278-281.

SARIDAKIS, E. 2012. Perspectives on High-Throughput Technologies Applied to Protein Crystallization. *Protein and Peptide Letters,* 19**,** 778-783.

SARVER JR, R. W. & KRUEGER, W. C. 1991. Protein secondary structure from fourier transform infrared spectroscopy: A data base analysis. *Analytical Biochemistry,* 194**,** 89-100.

SCHARTNER, J., GULDENHAUPT, J., MEI, B., ROGNER, M., MUHLER, M., GERWERT, K. & KOTTING, C. 2013. Universal Method for Protein Immobilization on Chemically Functionalized Germanium Investigated by ATR-FTIR Difference Spectroscopy. *Journal of the American Chemical Society,* 135**,** 4079-4087.

SETHURAMAN, A. & BELFORT, G. 2005. Protein structural perturbation and aggregation on homogeneous surfaces. *Biophysical Journal,* 88**,** 1322-1333.

SETHURAMAN, A., VEDANTHAM, G., IMOTO, T., PRZYBYCIEN, T. & BELFORT, G. 2004. Protein unfolding at interfaces: Slow dynamics of alpha-helix to beta-sheet transition. *Proteins-Structure Function and Bioinformatics,* 56**,** 669-678.

SHASHILOV, V. A. & LEDNEV, I. K. 2010. Advanced Statistical and Numerical Methods for Spectroscopic Characterization of Protein Structural Evolution. *Chemical Reviews,* 110**,** 5692-5713.

SHUKLA, A. A. H., P.; GUPTA, P.; YIGZAW, Y.; HUBBARD, B 2005. Strategies to address aggregation during Protein A chromatography. *Bioprocess International* 3**,** 36 - 45

SMITH, B. C. 1996. *Fundamentals of Fourier transform infrared spectroscopy*, CRC Press, Inc.

SNIVELY, C. M. & KOENIG, J. L. 1999. Characterizing the performance of a fast FT-IR imaging spectrometer. *Applied Spectroscopy,* 53**,** 170-177.

SNIVELY, C. M., OSKARSDOTTIR, G. & LAUTERBACH, J. 2001. Chemically sensitive parallel analysis of combinatorial catalyst libraries. *Catalysis Today,* 67**,** 357-368.

SPRING, M., RICCI, C., PEGGIE, D. A. & KAZARIAN, S. G. 2008. ATR-FTIR imaging for the analysis of organic materials in paint cross sections: case studies on paint samples from the National Gallery, London. *Analytical and Bioanalytical Chemistry,* 392**,** 37-45.

STAVITSKI, E. & WECKHUYSEN, B. M. 2010. Infrared and Raman imaging of heterogeneous catalysts. *Chemical Society Reviews,* 39**,** 4615-4625.

STEFANI, M. 2008. Protein Folding and Misfolding on Surfaces. *International Journal of Molecular Sciences,* 9**,** 2515-2542.

STEINER, G. & KOCH, E. 2009. Trends in Fourier transform infrared spectroscopic imaging. *Analytical and Bioanalytical Chemistry,* 394**,** 671-678.

STEINER, G., TUNC, S., MAITZ, M. & SALZER, R. 2007. Conformational Changes during Protein Adsorption. FT-IR Spectroscopic Imaging of Adsorbed Fibrinogen Layers. *Analytical Chemistry,* 79**,** 1311-1316.

SUREWICZ, W. K., MANTSCH, H. H. & CHAPMAN, D. 1993. Determination of protein secondary structure by Fourier-Transform Infrared spectroscopy - A critical assessment *Biochemistry,* 32**,** 389-394.

TAMM, L. K., ABILDGAARD, F., ARORA, A., BLAD, H. & BUSHWELLER, J. H. 2003. Structure, dynamics and function of the outer membrane protein A (OmpA) and influenza hemagglutinin fusion domain in detergent micelles by solution NMR. *Febs Letters,* 555**,** 139-143.

TAY, F. H. & KAZARIAN, S. G. 2009. Study of Petroleum Heat-exchanger Deposits with ATR-FTIR Spectroscopic Imaging. *Energy & Fuels,* 23**,** 4059-4067.

TREVISAN, J., ANGELOV, P. P., CARMICHAEL, P. L., SCOTT, A. D. & MARTIN, F. L. 2012. Extracting biological information with computational analysis of Fourier-transform infrared (FTIR) biospectroscopy datasets: current practices to future perspectives. *Analyst,* 137**,** 3202-3215.

TSAI, D. H., DAVILA-MORRIS, M., DELRIO, F. W., GUHA, S., ZACHARIAH, M. R. & HACKLEY, V. A. 2011. Quantitative Determination of Competitive Molecular Adsorption on Gold Nanoparticles Using Attenuated Total Reflectance-Fourier Transform Infrared Spectroscopy. *Langmuir,* 27**,** 9302-9313.

UVERSKY, V. N. 2002. Natively unfolded proteins: A point where biology waits for physics. *Protein Science,* 11**,** 739-756.

VAN DER WEERT, M., VAN'T HOF, R., VAN DER WEERD, J., HEEREN, R. M. A., POSTHUMA, G., HENNINK, W. E. & CROMMELIN, D. J. A. 2000. Lysozyme distribution and conformation in a biodegradable polymer matrix as determined by FTIR techniques. *Journal of Controlled Release,* 68**,** 31-40.

VERGIS, J. M., PURDY, M. D. & WIENER, M. C. 2010. A high-throughput differential filtration assay to screen and select detergents for membrane proteins. *Analytical Biochemistry,* 407**,** 1-11.

VONGSVIVUT, J., WATANABE, S., NODA, K., SATO, H. & TASHIRO, H. 2008. In-situ confocal Raman monitoring of evaporation process during protein crystallization. *Scienceasia,* 34**,** 400-408.

WAGNER, S., KLEPSCH, M. M., SCHLEGEL, S., APPEL, A., DRAHEIM, R., TARRY, M., HÖGBOM, M., VAN WIJK, K. J., SLOTBOOM, D. J., PERSSON, J. O. & DE GIER, J.-W. 2008. Tuning Escherichia coli for membrane protein overexpression. *Proceedings of the National Academy of Sciences,* 105**,** 14371-14376.

WANG, L.-X. & JIANG, X.-E. 2012. Bioanalytical Applications of Surface-enhanced Infrared Absorption Spectroscopy. *Chinese Journal of Analytical Chemistry,* 40**,** 975-982.

WANG, L., LIN, C. G., YANG, L. H., ZHANG, J. W. & ZHENG, J. Y. 2011. Preparation of nano/micro-scale column-like topography on PDMS surfaces via vapor deposition: Dependence on volatility solvents. *Applied Surface Science,* 258**,** 265-269.

WHITBECK, M. R. 1981. 2ND DERIVATIVE INFRARED-SPECTROSCOPY. *Applied Spectroscopy,* 35**,** 93-95.

WHITMORE, L. & WALLACE, B. A. 2008. Protein secondary structure analyses from circular dichroism spectroscopy: Methods and reference databases. *Biopolymers,* 89**,** 392-400.

WRAY, P., CHAN, K. L. A., KIMBER, J. & KAZARIAN, S. G. 2008. Compaction of pharmaceutical tablets with different polymer matrices studied by FTIR imaging and X-ray microtomography. *Journal of Pharmaceutical Sciences,* 97**,** 4269-4277.

WROBEL, T. P., MARZEC, K. M., MAJZNER, K., KOCHAN, K., BARTUS, M., CHLOPICKI, S. & BARANSKA, M. 2012. Attenuated total reflection Fourier transform infrared (ATR-FTIR) spectroscopy of a single endothelial cell. *Analyst,* 137**,** 4135-4139.

XU, J., CHEN, T., BAO, W., WANG, K. & XIA, X. 2012. Label-Free Strategy for In-Situ Analysis of Protein Binding Interaction Based on Attenuated Total Reflection Surface Enhanced Infrared Absorption Spectroscopy (ATR-SEIRAS). *Langmuir,* 28**,** 17564-17570.

YANG, W. J., GRIFFITHS, P. R., BYLER, D. M. & SUSI, H. 1985. Protein conformation by infrared-spectroscopy - Resolution enhancement by Fourier Self Deconvolution *Applied Spectroscopy,* 39**,** 282-287.

YU, Y., WANG, X., OBERTHUR, D., MEYER, A., PERBANDT, M., DUAN, L. & KANG, Q. 2012. Design and application of a microfluidic device for protein crystallization using an evaporation-based crystallization technique. *Journal of Applied Crystallography,* 45**,** 53-60.